

## Intercomparison Study of Numerical Models for Long-Range Atmospheric Transport of Mercury

Stage II. Comparison of modeling results with observations  
obtained during short-term measuring campaigns

Technical Report 1/2003

A. Ryaboshapko, R. Artz,  
R. Bullock, J. Christensen,  
M. Cohen, A. Dastoor,  
D. Davignon, R. Draxler,  
R. Ebinghaus, I. Ilyin,  
J. Munthe, G. Petersen,  
D. Syrakov









**MSC-E Technical Report 1/2003**

**June 2003**

# **Intercomparison Study of Numerical Models for Long-Range Atmospheric Transport of Mercury**

## **Stage II. Comparison of modeling results with observations obtained during short-term measuring campaigns**

Alexey Ryaboshapko, Richard Artz, Russell Bullock,  
Jesper Christensen, Mark Cohen, Ashu Dastoor, Didier Davignon, Roland Draxler,  
Ralf Ebinghaus, Ilia Ilyin, John Munthe,  
Gerhard Petersen, Dimitar Syrakov

**METEOROLOGICAL SYNTHESIZING CENTRE - EAST**

Ul. Arhitektor Vlasov, 51, Moscow 117393 Russia

tel.: 7 095 128 90 98

fax: 7 095 125 24 09

e-mail: [msce@msceast.org](mailto:msce@msceast.org)







## The authors (the models):

### Richard S. ARTZ (HYSPLIT)

NOAA Air Resources Laboratory  
1315 East West Highway  
SSMC3, R/ARL, Room 3316  
Silver Spring MD 20910  
tel: 301-713-0972  
fax: 301-713-0119  
e-mail: richard.artz@noaa.gov

### Jesper CHRISTENSEN (DEHM)

National Environmental Research Institute  
Department of Atmospheric Environment  
P.O.Box 358  
DK-Roskilde DENMARK  
tel: 45 46 30 11 75  
fax: 45 46 30 11 14  
e-mail: jc@dmu.dk

### Ashu DASTOOR (GRAHM)

Modelling and Integration Research Division AES,  
Environment Canada  
2121 Trans-Canada Highway, 5th Floor  
Dorval, H9P 1J3 Quebec CANADA  
tel. 514 421 4766  
fax: 514 421 2106  
e-mail: ashu.dastoor@ec.gc.ca

### Roland R. DRAXLER (HYSPLIT)

NOAA Air Research Laboratory  
1315 East West Highway SSMC 3  
Room 3316, R/ARL Silver Spring  
MD 20910 USA  
tel: 301-713-0295 x117  
fax: 301-713-0119  
e-mail: roland.draxler@noaa.gov

### Iliia ILYIN (MSCE-Hg)

Meteorological Synthesizing Center "East"  
Ul. Arhitektor Vlasov, 51,  
Moscow 117393 Russia  
tel.: +7 095 128 96 21  
fax: +7 095 125 24 09  
e-mail: ilia.ilyin@msceast.org

### Gerhard PETERSEN (ADOM)

GKSS - Research Centre, Institute of Hydrophysics  
Max-Planck-Strasse 1  
D-21502 Geesthacht GERMANY  
tel: 49 41 52 87 18 47  
fax: 49 41 52 87 18 88  
e-mail: Petersen@gkss.de

### Dimiter SYRAKOV (EMAP)

National Institute of Meteorology and Hydrology  
Tzarigradsko chaussee 66  
1784 Sofia BULGARIA  
tel: 3592 975 39 86  
fax: 3592 988 03 80  
e-mail: Dimiter.Syrakov@meteo.bg

### O. Russell BULLOCK, Jr. (CMAQ)

U.S. Department of Commerce, NOAA,  
Air Resources Laboratory (on assignment to the U.S. EPA  
Office of Research and Development), Mail Drop  
E243-03 Research Triangle Park NC 27711 USA  
tel: 919 541 13 49  
fax: 919 541 13 79  
e-mail: bro@hpcc.epa.gov

### Mark COHEN (HYSPLIT)

NOAA Air Research Laboratory  
1315 East West Highway SSMC 3  
Room 3316, R/ARL Silver Spring  
MD 20910 USA  
tel: 301 713 0295 x122  
fax: 301 713 0119  
e-mail: mark.cohen@noaa.gov

### Didier DAVIGNON (GRAHM)

Modelling and Integration Research Division  
Air Quality Research Branch  
Meteorological Service of Canada, Environment Canada  
2121 Trans Canada Highway, 5<sup>th</sup> Floor  
Dorval, Quebec H9P 1J3 Canada  
tel. 514 421 4766  
fax: 514 421 2106

### Ralf EBINGHAUS (Observations)

GKSS - Research Centre, Institute of Physical and  
Chemical Analysis, Max-Planck-Strasse 1,  
D-21502 Geesthacht  
Germany  
fax: 49 41 52 87 23 66  
e-mail: ebinghaus@dvmc10.gkss.de

### John MUNTHE (Hg Chemistry)

Swedish Environmental Research Institute  
Dagjammingsgatan 1, P.O. Box 47086  
S-40758 Goteborg SWEDEN  
tel: 46 31 725 62 00  
fax: 46 31 725 62 90  
e-mail: john.munthe@ivl.se

### Alexey RYABOSHAPKO (MSCE-Hg)

Meteorological Synthesizing Center "East"  
Ul. Arhitektor Vlasov, 51,  
Moscow 117393 Russia  
tel.: +7 095 128 96 21  
fax: +7 095 125 24 09  
e-mail: alexey.ryaboshapko@msceast.org



## **SUMMARY**

In accordance with the recommendation of the Executive Body for the Convention on Long-Range Transboundary Air Pollution (CLRTAP) an intercomparison study of atmospheric long-range transport models for heavy metals was initiated by (Cooperative Programme for Monitoring and Evaluation of the LRTAP) EMEP in 1994. The intercomparison study is considered to be one of essential prerequisites for the development and application of operational heavy metal models. This report presents data on the model comparison carried out as the 2<sup>nd</sup> stage of the multi-stage program of the intercomparison of numerical models for the long-range atmospheric transport of mercury. The stage is focussed on the comparison of modelling results with observations obtained during short-term measuring campaigns. Seven regional and global models developed in Canada, Bulgaria, Denmark, Germany, Russia and the USA participated in this stage of the study. The measurements were carried out during two field campaigns each of two-week duration. Three main atmospheric mercury forms were measured – Total Gaseous Mercury (TGM), Reactive Gaseous Mercury (RGM) and Total Particulate Mercury (TPM). The measurements were done at the five monitoring stations in Germany, Sweden and Ireland in 1995 and 1999.

The comparison demonstrates that the models currently used for the assessment of regional and global pollution by mercury can provide satisfactory agreement between the modelling and observational data on mean TGM concentrations. The models can catch short-term concentration peaks but often underestimate the peak amplitudes. The comparison of RGM data reveals large differences between the modelling and observational results: for individual samples the difference can exceed an order of magnitude. On the average, the models can generally predict RGM values within a factor of 4. For TPM all models have achieved rather good agreement with observations. The models can well reproduce elevated TPM concentrations. Generally, the agreement between models and measurements for TPM results is on the level of the factor of 2. On the base of the results of this intercomparison, some recommendations for future work have been formulated.



## CONTENTS

INTRODUCTION	7
<i>Chapter 1.</i> PROGRAM OF THE SECOND STAGE AND WORKING PLAN	9
<i>Chapter 2.</i> THE MEASUREMENT DATA	11
<i>Chapter 3.</i> THE EMISSION DATA	17
<i>Chapter 4.</i> ANALYSIS OF AIR MASS TRANSPORT	20
<i>Chapter 5.</i> DESCRIPTIONS OF THE PARTICIPATING MODELS	23
5.1. The CMAQ model	23
5.2. The ADOM model	28
5.3. The MSCE-Hg model	29
5.4. The GRAHM model	31
5.5. The DEHM model	32
5.6. The HYSPLIT model	33
5.7. The EMAP model	36
5.8. Similarities and distinctions	37
<i>Chapter 6.</i> COMPARISON OF INDIVIDUAL MODEL RESULTS AGAINST OBSERVATIONS	39
6.1. The CMAQ model	40
6.2. The ADOM model	44
6.3. The MSCE-Hg model	48
6.4. The GRAHM model	52
6.5. The DEHM model	56
6.6. The HYSPLIT model	60
6.7. The EMAP model	64
<i>Chapter 7.</i> ANALYSIS OF THE COMPARISONS	68
<i>Chapter 8.</i> NEW ASPECTS OF ATMOSPHERIC MERCURY DYNAMICS	71
CONCLUSIONS AND RECOMMENDATIONS	77
ACKNOWLEDGEMENTS	80
REFERENCES	81



## INTRODUCTION

The Protocol to the 1979 Convention on Long-Range Transboundary Air Pollution on Heavy Metals (signed currently by 36 countries) determined the main task for EMEP in this field: "EMEP shall, using appropriate models ....., provide to the Executive Body for the Convention calculations of transboundary fluxes and depositions of heavy metals within the geographical scope of EMEP". The Meteorological Synthesizing Centre East (MSC-E) of EMEP has a responsibility to perform model calculations of transboundary transport and deposition of heavy metals over Europe. The Steering Body to EMEP at its 18<sup>th</sup> session decided (EB.AIR/GE.1/24, 1994) that MSC-E was authorised to organize an intercomparison study of atmospheric long-range transport models for lead, cadmium and mercury. Such a study is considered by the Steering Body to be one of essential prerequisites for the development and application of operational models for heavy metals.

The intercomparison studies for lead and cadmium were carried out in 1996 (EMEP/MSC-E report 2/96, 1996) and in 1998 (EMEP/MSC-E report 2/2000, 2000), respectively. As a follow-up activity and in accordance with recommendations of EMEP/WMO/UNEP workshops in Moscow 1996 and in Geneva 1999, the mercury model intercomparison study was initiated in 1999. The Scientific Advisory Team of EMEP/MSC-E noted that this task would be far more complex, since unlike lead and cadmium, mercury exists in ambient air in different physical-chemical forms and is subjected to a variety of physical and/or chemical or photochemical processes and interactions.

The mercury intercomparison study is focused on:

- an evaluation of model parameterization of the main physical-chemical processes of mercury transformations in the gaseous and the liquid phase;
- comparison of modeling results with measurements obtained from both short-term campaigns and from the EMEP monitoring network and other international and national programs;
- comparison of the main features of the long-range transport of different mercury forms.

The mercury model intercomparison study involves four stages:

**Stage I.** Comparison of modules for the physico-chemical transformations of mercury species in a cloud/fog environment with prescribed initial mercury concentrations in ambient air and other physical and chemical parameters relevant for atmospheric mercury transformations.

**Stage II.** Comparison of model results with observations during 1-2 weeks episodes. Hourly and daily averages and event-based averages of mercury concentrations in air and in precipitation, respectively, obtained from the joint Swedish/Canadian/German field campaign TRANSECT 1995 and from the European Union Environment & Climate project Mercury Species Over Europe (MOE-1999) will be used.

**Stage III.** Comparison of model results with observed monthly and annual means of mercury concentrations in air and precipitation and deposition fluxes available from European monitoring stations in 1998.

**Stage IV.** Comparison of model predicted atmospheric budgets of mercury species in the entire EMEP domain and for selected European countries (UK, Poland and Italy), including dry and wet deposition within and outside the area of the countries.

At the first stage of the model intercomparison study (1999 – 2001) scientific groups from Germany, Sweden, the USA and MSC-East took part. The results were presented in a MSCE technical report (MSC-E 2/2001, [www.emep.int](http://www.emep.int)) and published in “Atmospheric Environment” Journal (Vol. 36, No 24, 2002, 3881-3898).

The second stage (started in 2001) is focused on the comparison of modeling results against observational data. The observations were performed at five measurement sites in Europe during two short-term campaigns in 1995 and 1999. In the first episode, only total gaseous mercury was considered (or mercury in elemental form). In the second episode (1999) reactive gaseous and aerosol mercury were measured in addition to total gaseous mercury.

The following scientific groups (and models) involved in atmospheric mercury modeling participated in this second stage:

- GKSS-Forschungszentrum Geesthacht GmbH (Germany): the European mercury version of the Acid Deposition and Oxidants Model (ADOM).
- U.S. Environmental Protection Agency (USA): the Community Multi-Scale Air Quality (CMAQ) model.
- Environment Canada (Canada): Global/Regional Atmospheric Heavy Metals model (GRAHM).
- National Oceanic and Atmospheric Administration (USA): Hybrid Single Particle Lagrangian Integrated Trajectory model (HYSPLIT).
- National Institute of Meteorology and Hydrology (Bulgaria): Eulerian Model for Air Pollution (EMAP).
- National Environmental Research Institute (Denmark): Danish Eulerian Hemispheric Model (DEHM).
- Meteorological Synthesizing Centre-East (Russia): MSCE Heavy Metal model, Hg version (MSCE-Hg).

This report presents the measurement data used for the intercomparison, the anthropogenic emission data for Europe used as input to the models, a description of physical-chemical schemes of the participating models, and the results of the comparison. In addition, a preliminary analysis of air mass transport is given to distinguish some episodes when the measurement stations may have been under the influence of known emission sources. Potential future model extensions and improvements in terms of implementation of recent findings in atmospheric mercury chemistry and mercury speciation are discussed separately in chapter 8 “New aspects of atmospheric mercury dynamics”. Finally, some conclusions and recommendations for modellers and users of modelling results are given in the report.

## Chapter 1

### PROGRAM OF THE SECOND STAGE AND WORKING PLAN

The program of the second stage of the Hg model intercomparison study was finally approved by the involved experts (workshop in Moscow in February 2002). The second stage is devoted to modeling the short-term episodes of mercury atmospheric transport and deposition in Northern Europe and comparison them with observations carried out during two measuring campaigns. In addition, the data of continuous measurements at Mace Head station (Ireland) were also used, mainly for the hemispheric and global models.

Analysis of the first episode covering the fortnight period of summer-95 is focused on total gaseous mercury concentrations (TGM) as the main parameter for the comparison with the observations. Modelling of the second episode included concentrations of reactive gaseous mercury (RGM) and total particulate mercury (TPM) in addition to TGM as parameters for comparison with observations. The agreed temporal resolution and units to be used are presented in Table 1.1.

**Table 1.1.** Calculating parameters, temporal resolution and units

Output parameter	Temporal resolution	Units
TGM (or $\text{Hg}^0 + \text{RGM}$ )	1 hr	$\text{ng/m}^3$
RGM (or $\text{Hg}^{2+}_{\text{gas}}$ )	According to sampling periods	$\text{pg/m}^3$
TPM (or $\text{Hg}^{2+}_{\text{part}}$ )	According to sampling periods	$\text{pg/m}^3$

Modelling of mercury chemical transformations in the atmosphere requires the knowledge of concentrations of several reactants and of a number of geophysical parameters [Ryaboshapko *et al.*, 2001]. The following values were agreed to be commonly used in the calculations:

- sulfur dioxide – daily mean values calculated by EMEP/MSC-W (the period from 19.06.1996 to 07.07.1996 for the first episode and the period from 23.10.1999 to 14.11.1999 for the second episode); data for 1995 are not available;
- ozone – 6-hr mean ozone values calculated by EMEP/MSC-W from 19.06.1996 to 07.07.1996 (to be used for the first episode) and from 23.10.1996 to 14.11.1996 (to be used for the second episode); data for 1995 and for 1999 are not available;
- soot – the modelled values of soot concentrations kindly presented by Dr. Trond Iversen; the data are given for HIRLAM domain at 7 vertical levels up to 4 km height; it is assumed that soot concentration in EMEP cells outside the HIRLAM domain is equal to the minimum value within HIRLAM area (at corresponding vertical levels);
- chlorine in the gas phase - 100 ppt – within the lowest hundred meters over the ocean at night; zero above 100 m over the ocean at night; zero - during daytime; zero - over the continents;
- value of pH of cloud water – 4.5;
- chloride concentration in cloud water – 2.5 mg/l;
- OH radical in cloud water - midday (maximum) concentration of OH radical –  $10^{-12}$  M; at night-time the radical concentration is zero;

- HO<sub>2</sub> radical in cloud water - midday (maximum) concentration of HO<sub>2</sub> radical – 5·10<sup>-9</sup> M; at night-time the radical concentration is zero.

Some input parameters were adopted by the participants in accordance with their modelling schemes. These included: (a) individual meteorological data sets are used by each participant: and (b) - boundary conditions (concentrations of modelled species at domain boundaries) for the regional models. For the global model, there was no need to estimate boundary conditions.

It was agreed to focus on five exact geographical points (measurement sites), and each participation team was free to use its own modelling domain in order to estimate the concentrations at these sites. Some models are of a regional character and adopted the EMEP modelling domain with 50\*50 km resolution. One model is global with coarser resolution. One model uses a zooming effect. To provide uniformity of measuring and modelling data the participants agreed to present all results in Greenwich time (GMT).

The participants agreed that for the first episode the main attention is paid to TGM values measured at two German and two Swedish stations. For the second episode, attention was also given to gaseous oxidized mercury compounds (RGM) and to particulate mercury (TPM). Total gaseous mercury was measured at the stations in accordance with different sampling protocols: 5 minutes averaging, 15 minutes averaging and 30 minutes averaging. It was agreed to use in the comparison hourly mean values both for measurements and calculations. Sampling periods for RGM and TPM were different – 7, 20.5 and 21 hours. In this case each sample was considered and compared individually.

Some statistical parameters were agreed to be used for quantitative characterization of the comparison. These included the mean arithmetic value, correlation coefficient (measurements against calculations) and fractional bias. A separate task was to evaluate the ability of the different models to follow the short-term peaks in the measurements. This characteristic of the models is considered on a qualitative base (e.g., the coincidence or divergence for periods of each peak).

The participants of the modelling campaign accepted a timetable of preparation of the second stage final report and a possible publication in scientific literature. The timetable is presented in Table 1.2.

**Table 1.2.** *Timetable for the second stage fulfilment*

Actions	Time period
Preparation for calculations in full agreed volume	February – March, 2002
Calculations	April, 2002
Sending the results in agreed formats to EMEP/MSC-E	May, 2002
Processing of the results	May-June, 2002
Preparation of a draft of a joint report	June-Sept., 2002
Preparation of the final version of the report	Oct.-Dec., 2002
Preparation of the first version of a joint scientific article	Jan.-April, 2003
Submission of the manuscript to a journal	April-June, 2003

## Chapter 2

### MEASUREMENT DATA

Measurements of concentrations of different mercury species were carried out at two German, two Swedish and one Irish monitoring station. Locations of the stations and characteristics of surrounding areas are presented in Table 2.1. The data of the table show that Neuglobsow station is situated in the north-eastern part of Germany and can be under the influence of industrial emission sources of Central Europe. The Zingst station is on the shore of the Baltic Sea where no immediately local (major) emission sources are believed to be situated. However, the station can also be influenced by Central European emission sources. Swedish stations are more or less remote and reflect air pollution levels over relatively clean Scandinavia. The station at Mace Head is located in the most western part of Europe. It can characterise air composition over the North Atlantic.

*Table 2.1. Locations and characteristics of the monitoring stations*

Station/country	Coordinates		Elevation, m	Characteristic of surrounding area
	Lat	Lon		
Neuglobsow, Germany	53.2N	13.0E	62	Forested area
Zingst, Germany	54.4N	12.7E	1	Sandy sea shore of the Baltic
Rörvik, Sweden	57.4N	11.9E	10	Western forested shore of Sweden
Aspvreten, Sweden	58.8N	17.4E	20	Eastern forested shore of Sweden
Mace Head, Ireland	53.3N	9.9W	20	Atlantic shore, grassland

The latest sampling and analytical methods were used for these measurements. The first measurement campaign (the first episode of the model intercomparison study) was in summer 1995. Total gaseous mercury concentrations were measured simultaneously at German and Swedish stations. The second campaign (episode) took place in November 1999. Three mercury forms – total gaseous mercury (TGM), reactive gaseous mercury (RGM) and total particulate mercury (TPM) - were measured in this second episode.

Total Gaseous Mercury (TGM) refers to gaseous elemental Hg ( $\text{Hg}^0$ ) and small contributions from other gaseous species that also may be trapped by the solid gold sampler and detected as  $\text{Hg}^0$ . To measure TGM, the TEKRAN method was used, which utilises the gold-amalgamation principle during accumulative sampling cycles. The Tekran Mercury Vapour Analyser (Model 2537A) is an automatic semi-continuous instrument. The pre-filtered sample air stream is pulled through gold cartridges where the Hg is quantitatively retained. The Hg is then thermally desorbed in an argon carrier gas stream and detected in an integrated atomic fluorescence spectrometer (AFS). The instrument utilises two cartridges in parallel, with alternating operation modes (sampling and desorbing/analysing) on a pre-defined time base of 5 minutes. A 47-mm diameter Teflon pre-filter protects the sampling cartridges against contamination by particulate matter. A sampling flow-rate of  $1.5 \text{ L min}^{-1}$  was used. Under these conditions the detection limit has been calculated to be  $0.15 \text{ ng/m}^{-3}$  and the precision with a measurement uncertainty of 10 %. The accuracy and precision of this instrument has been recently assessed in measurement intercomparisons performed at various locations [Schroeder *et al.*, 1995, Ebinghaus *et al.*, 1999, Munthe *et al.*, 2001].

A new method for sampling and analysis of total particulate-phase Mercury (TPM) was used. The method is based on the AES mini-trap developed by *Lu et al.* [1998]. A quartz micro-fibre filter of 7 mm diameter is housed in a quartz glass tube of 140 mm length. The filter is supported by a pure nickel (Ni) screen grid. The sampling device serves as both particulate trap and pyrolyser for airborne particulate species. Air is pulled through the quartz tube at a flow-rate of 4 – 6 L min<sup>-1</sup>. After sampling the mercury content on the traps is analysed via pyrolysis where the trap is heated to 900°C in a stream of argon or nitrogen. In this step, the Hg is reduced to Hg<sup>0</sup> and is subsequently transferred to the gas-phase and detected by conventional amalgamation – thermal desorption – atomic fluorescence spectrometric detection. To bring down blanks to a minimum, the TPM traps were cleaned by pyrolysis at the sampling site prior to sampling.

Reactive gaseous mercury (RGM) is an operationally defined gaseous Hg fraction present in ambient air. However, it can be assumed that RGM to the most part consists of mercuric chloride (HgCl<sub>2</sub>), but other divalent species are also possible. These species adsorb to solid KCl matrices and RGM can therefore be sampled using KCl-coated denuders. The analysis of RGM trapped on denuders is achieved by heating to 500°C, which converts RGM to Hg<sup>0</sup>, and subsequent detection and quantification using the standard CVAFS procedure. Automated sampling techniques with annular denuders and thermo-reduction are also in use. Mist chambers, containing a KCl/HCl solution may also be used to trap RGM. With this approach air is drawn through a glass chamber containing fine dispersed liquid aerosol that continuously is formed from the refluxing KCl/HCl solution. The solution is then analysed using SnCl<sub>2</sub> reduction and CVAFS. During the campaigns, both automated and manual denuder techniques were used as well as mist chambers.

A detailed description of all methods applied for the sampling and analysis of different atmospheric mercury species during the field measurement campaigns can be found in *Munthe et al.* [2001].

Two measurement campaigns were organised to assess spatial distribution and temporal variations of mercury species. Sampling and analytical methodology as well as the results were described in detail in [*Schmolke et al.*, 1999; *Ebinghaus et al.*, 2002; *Munthe et al.*, 2003]. The measurement uncertainty of TGM measurement is less than 10 %. [*Ebinghaus et al.*, 1999]. Uncertainty of RGM and TPM measurement data was much higher – as much as a factor of 2 or even higher.

To provide comparability of the results the sampling periods at all stations are expressed below in Greenwich time. TGM concentrations during the second episode were measured at 3 stations: Neuglobsow, Zingst and Mace Head. The initial averaging protocol was different: every 5 minutes at Neuglobsow, every 15 minutes at Mace Head and every 30 minutes at Zingst. To provide comparability with the calculation data the following procedure of obtaining the hourly mean value was used:

- for Neuglobsow – from 35 min of previous hour to 30 min of next hour;
- for Mace Head – from 45 min of previous hour to 30 min of next hour;
- for Zingst – from 45 min of previous hour to 15 min of next hour.

The variability of TGM concentrations during the first episode is demonstrated in Fig. 2.1 drawn on the base of hourly means. One can see from the figures that German sites are characterised by short-term but high peaks up to 4 ng/m<sup>3</sup>. Such peaks are much higher than the mean values and obviously exceed possible measurement errors. The variability of the data of Swedish stations is much lower.

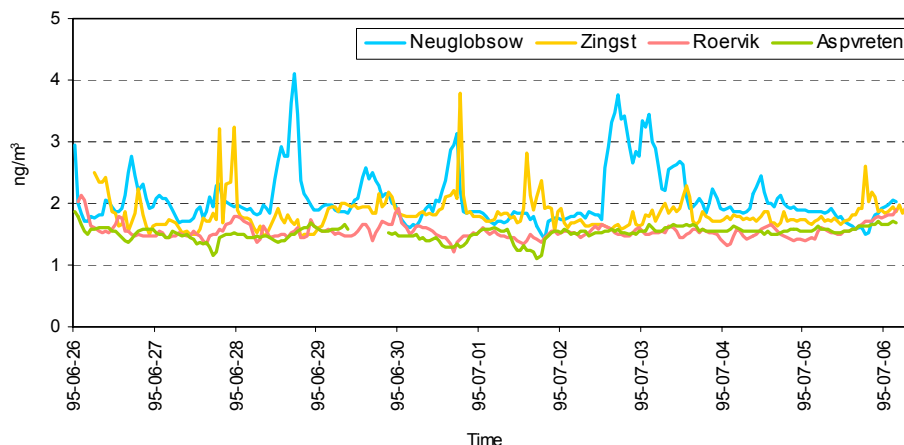


**Figure 2.1.** Observed TGM concentrations at the monitoring stations during the 1-st episode

Table 2.2 presents the daily mean TGM concentrations measured during 11 days of the first episode. One can see that there is an obvious concentration gradient from the south to the north (from central Germany to central Sweden). Besides, the data obtained at German stations are more variable – standard deviation value is the highest at Neuglobsow station and the lowest at Aspvreten station. This fact points to a possibility of recurrent influence of a strong anthropogenic source on mercury concentrations measured at German stations.

**Table 2.2.** Daily mean TGM concentrations measured at the monitoring stations during the 1<sup>st</sup> episode, ng/m<sup>3</sup>

Date	Neuglobsow	Zingst	Rörvik	Aspvreten
95-06-26	1.95	2.24	1.73	1.63
95-06-27	2.03	1.67	1.53	1.50
95-06-28	1.98	1.89	1.56	1.42
95-06-29	2.33	1.79	1.53	1.55
95-06-30	2.02	1.93	1.62	1.46
95-07-01	2.01	1.96	1.46	1.44
95-07-02	1.76	1.75	1.49	1.43
95-07-03	2.88	1.82	1.54	1.57
95-07-04	2.03	1.76	1.49	1.58
95-07-05	1.93	1.74	1.51	1.55
95-07-06	1.76	2.00	1.71	1.64
<b>Mean (± S.D.)</b>	<b>2.08 ± 0.45</b>	<b>1.85 ± 0.33</b>	<b>1.55 ± 0.12</b>	<b>1.52 ± 0.11</b>

During the second episode in addition to continuous measurements of TGM at three stations (Neuglobsow, Zingst and Mace Head) several samples of RGM and TPM were collected at each of 5 monitoring stations. The measured TGM concentrations during the second episode are showed in Fig. 2.2. One can see from the figure that German sites are characterised by short-term but high peaks (up to 4 ng/m<sup>3</sup> at Neuglobsow). The curve for the Mace Head data is much smoother. However, the baseline<sup>1</sup> of the concentration values measured at Mace Head is noticeably higher than in the case of German stations. This observation was not expected; however, its explanation is beyond the framework of this report.

<sup>1</sup> A value which is the main mode of frequency distribution of the results

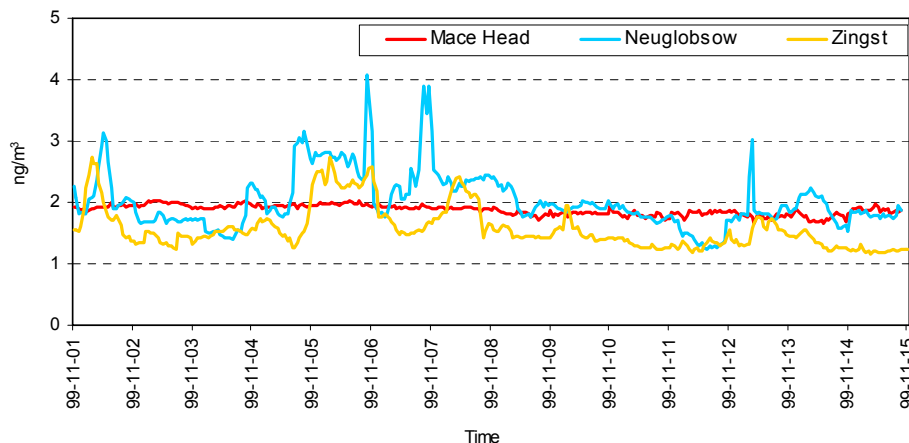


**Figure 2.2.** Observed TGM concentrations at the monitoring stations during the 2<sup>nd</sup> episode

The daily mean TGM concentrations are presented in Table 2.3. Again, the German stations exhibit the highest variability of concentration values.

**Table 2.3.** Daily mean TGM concentrations measured at the monitoring stations during the 2<sup>nd</sup> episode, ng/m<sup>3</sup>

Date	Neuglobsow	Zingst	Mace Head
99-11-01 (12:00-24:00)	2.21	2.12	1.90
99-11-02	1.96	1.52	1.97
99-11-03	1.66	1.41	1.94
99-11-04	1.83	1.59	1.95
99-11-05	2.70	1.99	1.96
99-11-06	2.45	2.07	1.95
99-11-07	2.60	1.78	1.91
99-11-08	2.30	1.75	1.87
99-11-09	1.90	1.54	1.80
99-11-10	1.93	1.39	1.82
99-11-11	1.63	1.27	1.79
99-11-12	1.64	1.39	1.81
99-11-13	1.95	1.54	1.76
99-11-14	1.80	1.24	1.83
99-11-15 (00:00-08:00)	1.78	1.20	1.86
<b>Mean (± S.D.)</b>	<b>2.02 ± 0.46</b>	<b>1.58 ± 0.35</b>	<b>1.88 ± 0.08</b>

During the second episode samples of RGM and TPM were collected during different time intervals. For RGM the sampling periods covered only several hours. During two weeks of the experiment, 6-7 samples were collected at each site. The protocol for TPM provided sampling during 21 hours a day (representing almost continuous measurements). During this second episode, 8 to 14 TPM samples were collected at each station.

The results of RGM measurements are presented in Figs 2.3-2.6. Here the width of the bars corresponds to the duration of sampling. Surprisingly, the highest concentrations (up to 25 pg/m<sup>3</sup>) were measured at Mace Head station, which was considered to represent the background. This

suggests that RGM can be generated in the oceanic atmosphere. Over continental Europe a pattern can be observed: RGM concentrations drop from German stations northward to Swedish stations. At Neuglobsow the mean concentration value is on the level of 10  $\text{pg}/\text{m}^3$ , while at Aspvreten – on the level of 5  $\text{pg}/\text{m}^3$ .

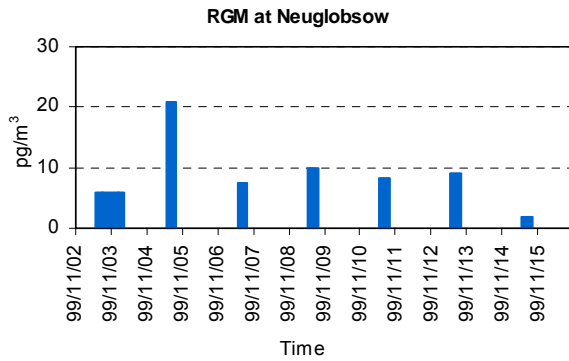


**Figure 2.3.** Measured RGM concentrations at Neuglobsow station

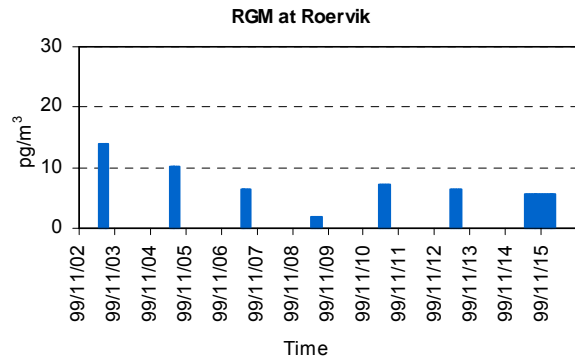


**Figure 2.4.** Measured RGM concentrations at Roervik station

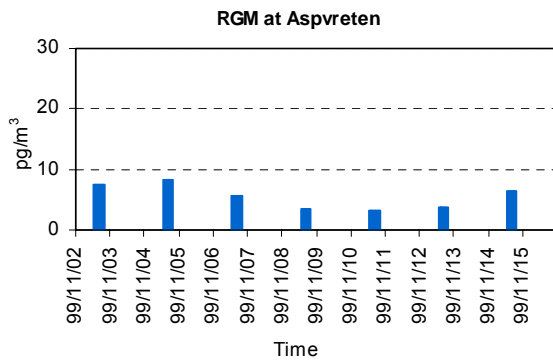


**Figure 2.5.** Measured RGM concentrations at Aspvreten station

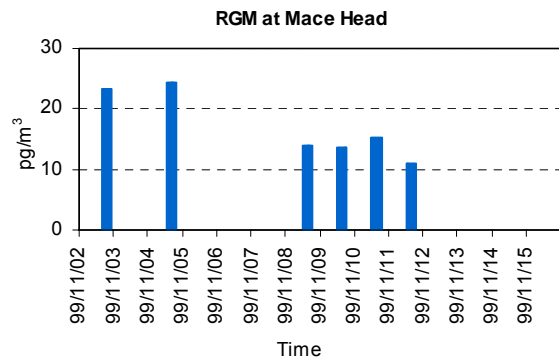


**Figure 2.6.** Measured RGM concentrations at Mace Head station

The results of TPM concentration measurements (Figs. 2.7-2.11) demonstrate a very strong difference between the stations. The highest values are characteristic of Neuglobsow where the TPM concentrations sometimes exceeded 100  $\text{pg}/\text{m}^3$ . Northward the concentration values drop. At Aspvreten they are below 20  $\text{pg}/\text{m}^3$  during the whole period of the experiment. The concentrations at Mace Head station are relatively low and vary between ~0 and 30  $\text{pg}/\text{m}^3$ . Analysing the figures one can notice a practically synchronous peak at Neuglobsow, Zingst and Roervik during November 5-7.

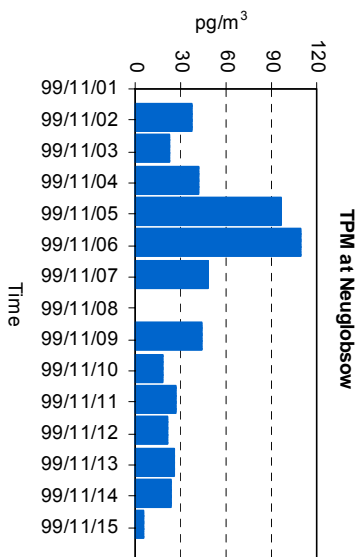


**Figure 2.7.** Measured TPM concentrations at Neuglobsow station

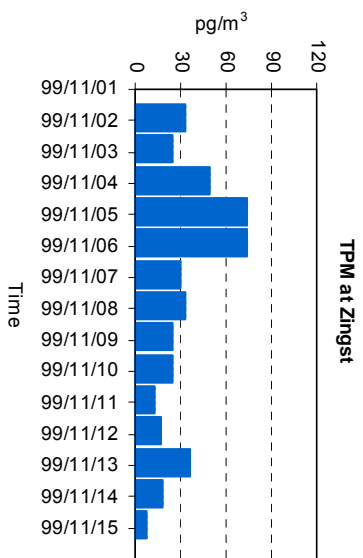


**Figure 2.8.** Measured TPM concentrations at Zingst station

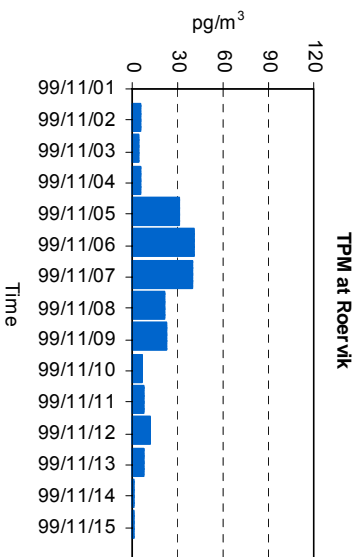


**Figure 2.9.** Measured TPM concentrations at Roervik station

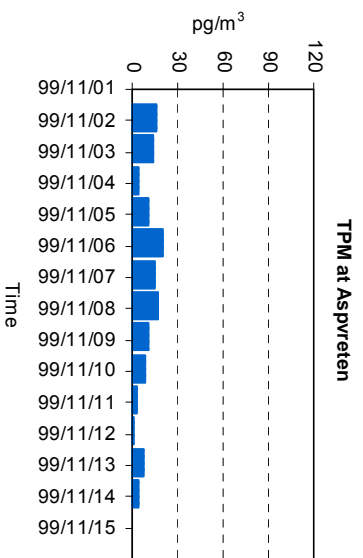


**Figure 2.10.** Measured TPM concentrations at Aspøyeten station

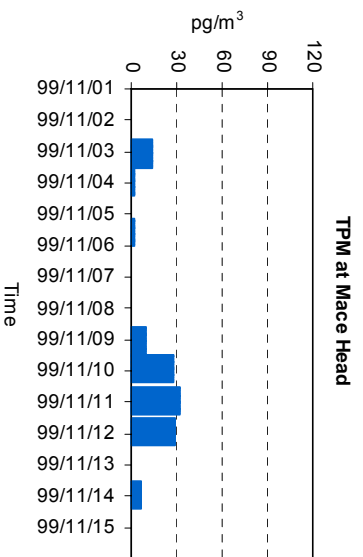


**Figure 2.11.** Measured TPM concentrations at Mace Head station

## Chapter 3

### MERCURY EMISSION DATA

During the last two decades considerable changes both in anthropogenic emission values and in pattern of emission fields took place at both the regional scale in Europe and at the global scale. According to the official anthropogenic emission data, European mercury emissions dropped by at least a factor of 2 between 1990 and 2000 [Vestreng and Klein, 2002]. The largest changes occurred in Germany after the unification when several large emission sources in Eastern Germany were closed. On the global scale the anthropogenic emission dropped in European and North American countries but rose in many developing countries [UNEP, 2002].

Mercury content in air is influenced by all kinds of emissions – direct anthropogenic emission, purely natural emission and secondary anthropogenic re-emission. There are some reasons for ignoring natural emission and re-emission. First, the mercuriferous geochemical belt (Southern Europe) is far from the monitoring stations [Gustin *et al.*, 1999]. Secondly, the possible natural emission the Ocean is not likely to exert strong influence because of its remoteness. Data on re-emission are still very scarce. In Central Europe it is assumed that the main contribution is made by direct anthropogenic emissions. Hence, it was decided to use only direct anthropogenic emissions for 1995 [Pacyna *et al.*, 2001] in the regional models. It was assumed that anthropogenic emissions would dominate. At the same time remote natural emission and re-emission outside the domain are partially taken into account by adopted concentration values on the domain borders (boundary conditions). For the models of global type, all kinds of mercury emissions should be considered within global/hemispheric domain.

For calculations of the two episodes, anthropogenic emission data for 1995 [Pacyna *et al.*, 2001] were used. For the 1999 episode, no corrections were made for changes that might have occurred relative to the estimated 1995 anthropogenic emissions. The data consist of mercury emissions from individual point sources within Europe and national total emission values for area sources in European countries. MSC-E attributed individual point sources to cells of the EMEP grid and distributed the area sources among these cells (50x50 km spatial resolution). All the emission data were divided among three vertical layers. All area sources are within the first layer (0-56 m height). The point sources have their individual heights and can be within the first, the second (56-136 m) and the third (136-251 m) layers. All the area sources have the same mercury speciation ratio: Hg<sup>0</sup> - 80%, RGM - 15%, and TPM - 5%. As to the point sources, each of them has its individual mercury speciation ratio. In this case Hg<sup>0</sup> contribution can vary from 20% (waste disposal) to 80% (cement production). The total anthropogenic emission in Europe estimated by Pacyna *et al.* [2001] was equal in 1995 to 250 t/y. The emission distribution for 1995 over the EMEP region (all mercury forms, all emission levels) is presented in Fig. 3.1.

Preliminary calculations of TGM concentrations by ADOM model on the base of the 1995 emission data showed that the calculated concentrations for locations of measurement sites in Germany were noticeably lower than the observed ones in the cases of peak values. At the same time mean calculated concentrations agreed with mean observed ones. This fact suggests that the local German emission sources (which are mainly responsible for elevated peak concentrations) could be underestimated by the inventory used [Pacyna *et al.*, 2001]. To check this hypothesis it was decided that for two models – ADOM and MSCE – two emission inventories should be used: the commonly accepted 1995 inventory and an inventory for 1990 [Berdowski *et al.*, 1997], which emission values are much higher just for the sources in Germany.

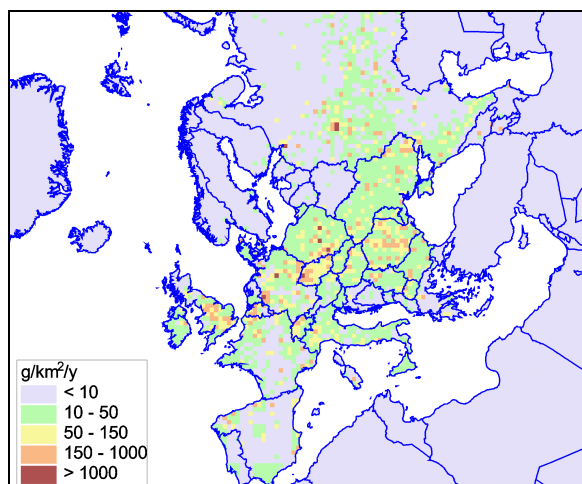


**Figure 3.1.** The mercury emission field in EMEP region for 1995 (50 by 50 km resolution)

The emission field for 1990 was prepared on the base of EMEP official emission data and expert estimates mainly taken from *Berdowski et al.* [1997]. Accordingly to *Berdowski et al.* [1997] the total anthropogenic emission in Europe was 463 t/y in 1990. The ratio of mercury forms in the anthropogenic emission was taken in this case separately for each individual country [*Axenfeld et al.*, 1991]. The emission sources were divided into two categories – low (0-100 m height) and high (>100 m). The ratio of low and high sources was taken as 1:1 [*Ryaboshapko et al.*, 1999]. The field of total anthropogenic mercury emission within EMEP region (50x50 km resolution) for 1990 is shown in Fig. 3.2. The main peculiarity of this field is a “hot spot” in the eastern part of Germany. The comparison of Figs. 3.1 and 3.2 shows that the estimated emissions in the inventories apparently declined during 5 years and that the “hot spot” in Eastern Germany had presumably disappeared by 1995.

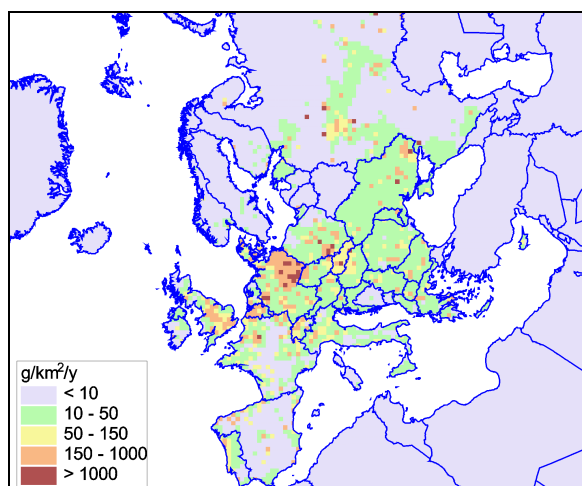


**Figure 3.2.** The mercury emission field in the EMEP region for 1990 (50x50 km resolution)

It was agreed that the global modelling groups (Environment Canada and Danish National Environmental Research Institute) should use their own emission data on the hemispheric/global scale. The anthropogenic mercury emission fields used in the Danish model are given in Fig. 3.3. There are no re-emissions from land and oceans, except for the nested domain where data shown by EMEP/MS-C-E are used.

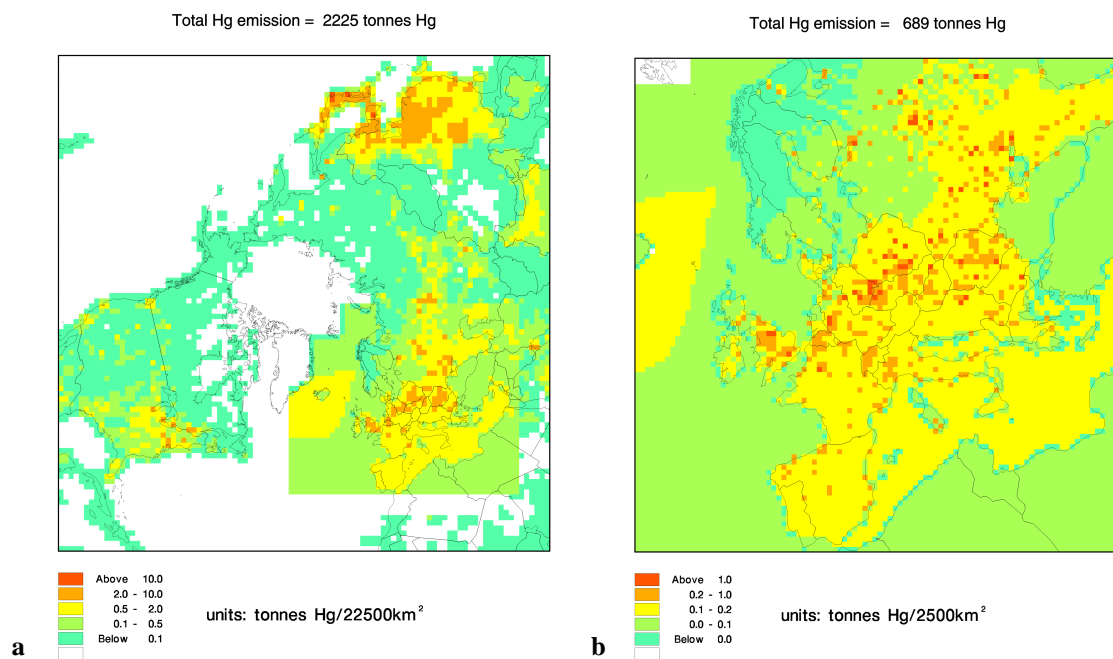


**Figure 3.3.** The mercury emission fields used in DEHM model: *a* – the hemispheric mother domain; *b* – the European nested domain

The Canadian GRAHM model includes a recent global anthropogenic emissions inventory for 1995 at 1x1 degree uniform resolution prepared by *E.Pacyna and J.Pacyna* [2002] who estimated the worldwide anthropogenic emission by value of 1913 t/y. The model also includes natural emissions and re-emissions from previously deposited mercury from land and ocean.

## Chapter 4

### ANALYSIS OF AIR MASS TRANSPORT

Tentative analysis of air mass transport during both episodes has been provided by MSC-E using the back-trajectory feature of the HYSPLIT model developed by US NOAA, available through the Internet ([www.arl.noaa.gov/ready.html](http://www.arl.noaa.gov/ready.html)). Such an analysis helps to distinguish periods when trajectories of air masses were connected with areas of known anthropogenic sources. In these cases one can explain elevated concentration values measured at the monitoring stations. On the regional level airborne transport of polluted air masses takes place mostly within the lower atmosphere. Hence, the back trajectories were plotted for three vertical layers – 100 m, 500 m and 1000 m above ground level.

Such trajectory analysis should help to understand the occurrence of peaks in series of measured concentrations. As it was mentioned above the highest variability of TGM is characteristic of Neuglobsow station located closer to industrial mercury sources. During the first episode at least two cases of obviously elevated TGM concentrations (higher than  $3.5 \text{ ng/m}^3$ ) can be distinguished.

In the first case the maximum was reached at 05:00 29.06.1995. Trajectory analysis displays (Fig. 4.1a) that this period was characterized by very stable air mass transport from the northwest. In this case, it is observed that the air masses do not seem to be connected with any strong anthropogenic sources in the inventory being used. In few hours the concentration dropped to its base-line (lower than  $2 \text{ ng/m}^3$ ). However, wind direction and wind speed remained the same (Fig. 4.1b). It should be mentioned that the concentration peak coincided in time with a cold front passing and heavy rain.

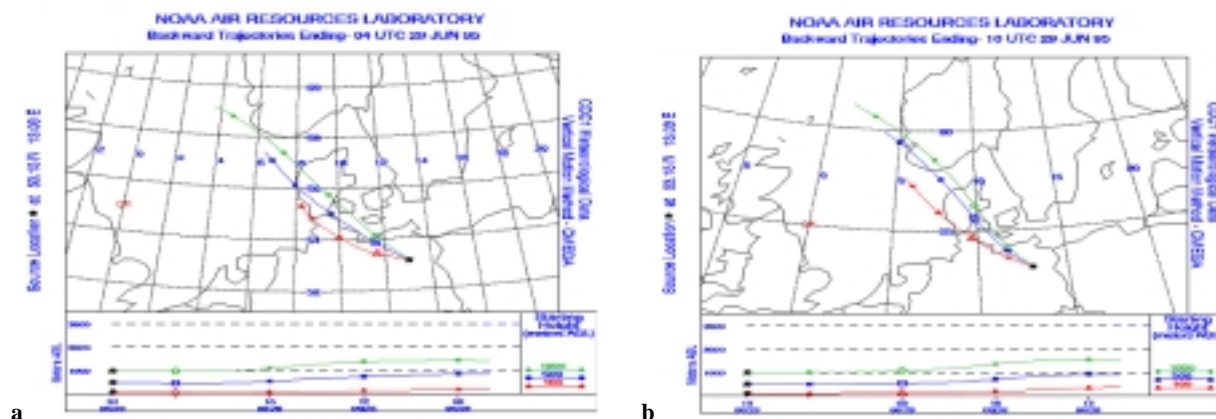


**Figure 4.1.** Air mass back trajectories for Neuglobsow station at 3 vertical levels: a – air masses came to the station at 04:00 June 29, 1995; b – air masses came to the station at 10:00 June 29, 1995

Figs. 4.2 (a and b) present two meteorological situations. During the first one on July 01 (Fig. 4.2a) air masses were transported to Neuglobsow station from the northeastern Atlantic. It could be hardly expected any elevated concentrations of any mercury form. In 24 hours the meteorological situation has changed, and air masses were transported to Neuglobsow from industrialized areas of Germany, Poland and the Czech Republic (Fig. 4.2b). Indeed, the second case is characterized by obvious peak of mercury concentration (see Fig. 2.1).

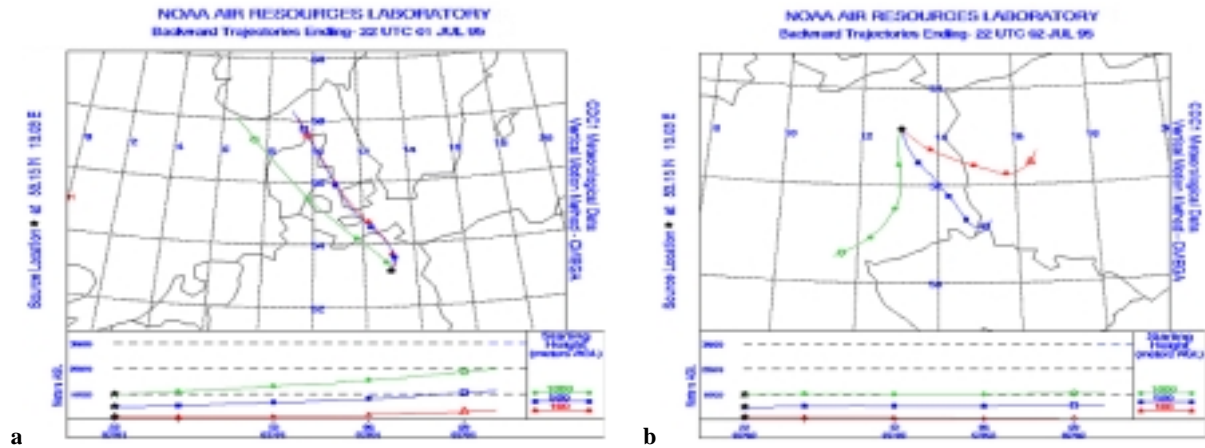


**Figure 4.2.** Air mass back trajectories for Neuglobsow station at 3 vertical levels: a – air masses came to the station at 22:00 July 01, 1995; b – air masses came to the station at 22:00 July 02, 1995

During the 1999 episode relatively elevated TGM concentrations were marked from November 05 to November 08, 1999. This period was characterised by transport (within the lowest atmosphere) of the southeast, south and southwest directions (Fig. 4.3a). In this case it is possible to connect the elevated concentrations with known anthropogenic sources in Poland, the Czech Republic, Leipzig and Berlin areas of Germany. After this period wind direction changed to the northeast, and the TGM concentration dropped to  $2 \text{ ng/m}^3$  and lower (see Fig. 4.3b).

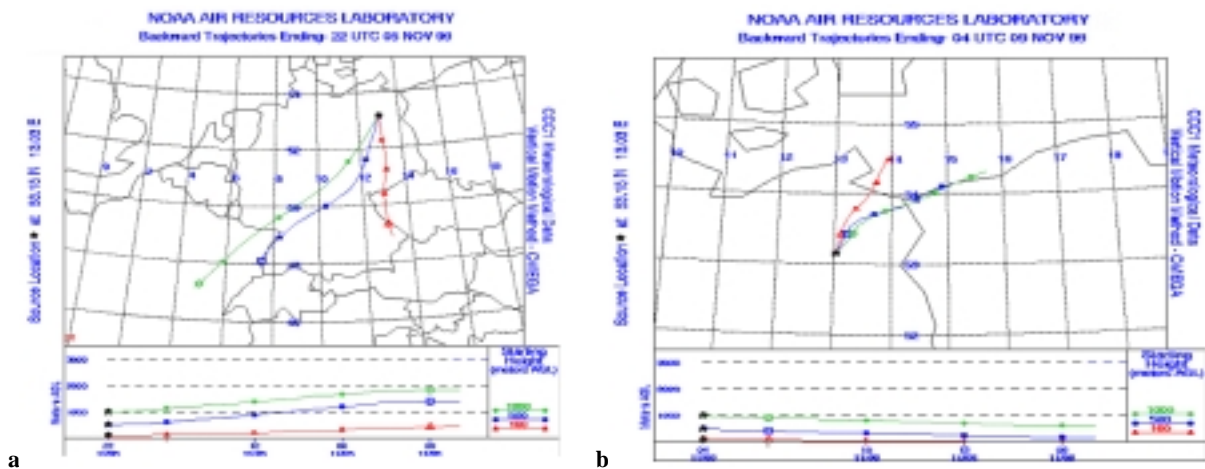


**Figure 4.3.** Air mass back trajectories for Neuglobsow station at 3 vertical levels: a – air masses came to the station at 22:00 November 05, 1999; b – air masses came to the station at 04:00 November 09, 1999

The measurements at background Mace Head station showed that TPM concentrations varied from practically zero level to  $30 \text{ pg/m}^3$  (see Fig. 2.11). The trajectory analysis confirms that such variability is connected most likely with changes of air mass transport direction. During November 05, 1999 stable westward transport was detected (see Fig. 4.4a). This wind direction was connected with very low TPM concentrations. Later the trajectories became loop-shape, and local wind was eastward (see Fig. 4.4b). The influence of mercury sources led to rise of TPM concentrations.

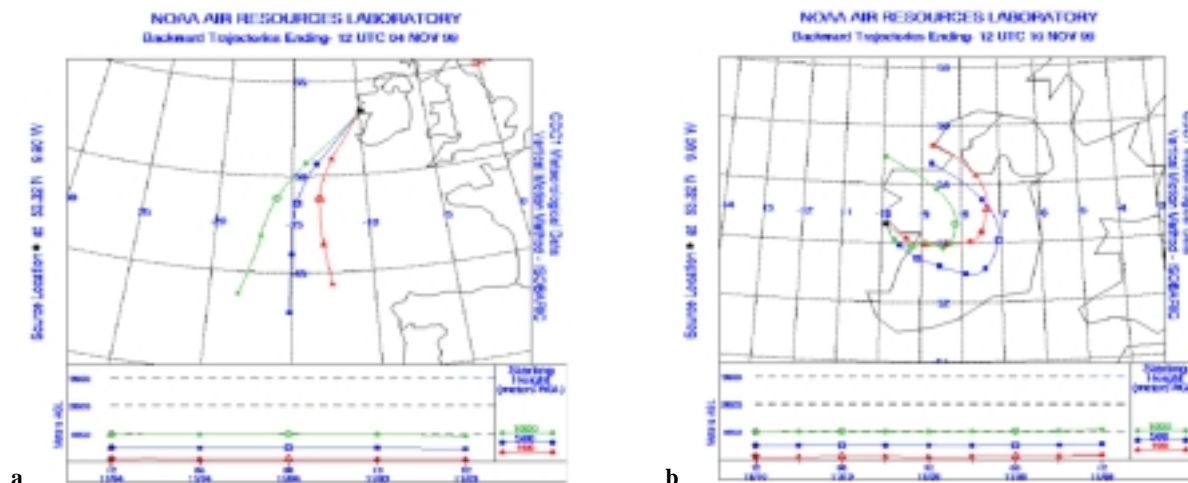


**Figure 4.4.** Air mass back trajectories for Mace Head station at 3 vertical levels: a – air masses came to the station at 12:00 November 04, 1999; b – air masses came to the station at 12:00 November 10, 1999

Analysis of the TGM concentration data obtained at Swedish stations reveals some cases of very low values (down to 1.1 ng/m<sup>3</sup>). Such values are lower than the boundary concentrations or initial concentrations accepted in all models, and, naturally, cannot be reproduced by the models. To understand the origin of air masses with these extremely low concentrations backward trajectory was plotted for Aspveten station (see Fig. 4.5). In this case the measured TGM concentration was extremely low (1.10 ng/m<sup>3</sup>) in the morning of July 02, 1995. The trajectory clearly indicates that this air mass had its origin in the Arctic.

It is very difficult to explain very low TGM concentrations by possible influence of Arctic mercury depletion, because this phenomenon typically comes to the end by the middle of June. Moreover, such extremely low TGM concentrations (TGM = 1.17 ng/m<sup>3</sup> at Zingst) were observed during the second episode on November that is totally untypical for mercury depletion phenomenon. The nature of these low concentrations remains to be uncertain, however, this phenomenon should be taken into account when boundary concentrations for EMEP domain are estimated.

It must be acknowledged that trajectory analysis is a somewhat simplified analysis methodology that does not include all the complexities of mercury's atmospheric fate and transport. However, in many cases it can help to explain reasons for variations of mercury concentrations and to connect elevated values with the influence of known anthropogenic mercury sources.

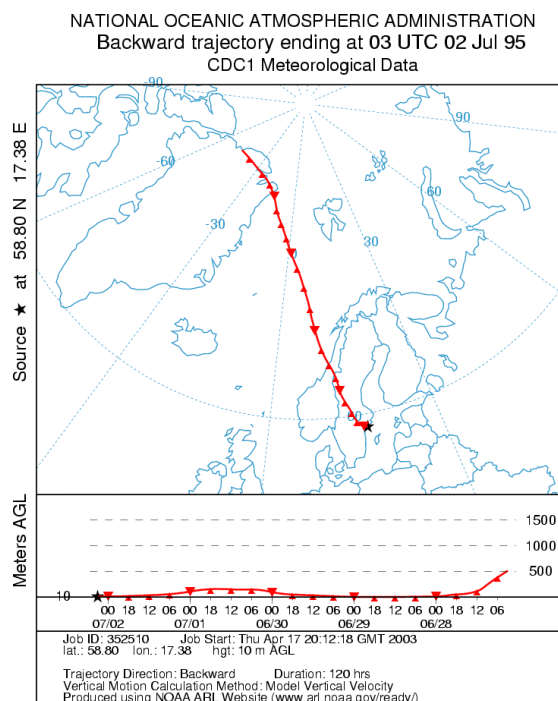


**Figure 4.5.** Back trajectory (at ground level) for air masses came to Aspveten station at 03:00 (Greenwich) July 02, 1995

## Chapter 5

### DESCRIPTIONS OF THE PARTICIPATING MODELS

The modelling efforts described in the subsequent paragraphs have been made to simulate the atmospheric transport and fate of mercury and to derive model predicted time series of mercury concentrations in ambient air to be compared with observations. The participating models comprise a regional Lagrangian formulation and Eulerian approaches on regional, hemispheric and global scales. All the models employ extensive gas- and aqueous phase chemical mechanisms and explicitly tracking numerous species concentrations. In these mechanisms, mercury species are transferred among different phases in the atmosphere (e.g., gas, aqueous, particles in air, and particles in liquid) according to equilibrium and/or mass transfer considerations. The mechanisms are described to simulate the equilibrium chemistry of mercury within the aqueous phase in the atmosphere, including the complexation of mercury species with other compounds. Finally, each model includes a simulation of chemical reactions affecting mercury species in the atmosphere. Some of these reactions oxidize  $\text{Hg}^0$  to  $\text{Hg}^{+2}$  and some reduce  $\text{Hg}^{+2}$  to  $\text{Hg}^0$ . As deposition processes can be dramatically different for  $\text{Hg}^0$  vs.  $\text{Hg}^{+2}$ , an accurate description of these transformation reactions is vitally important to predicting the fate of mercury species in the atmosphere. Some aspects of the equilibrium and chemical reaction schemes are similar from model to model, but there are differences. As with all aspects of the simulations, there are still uncertainties in physics and chemistry of this system. Some of the models additionally simulate photochemistry (e.g., to derive estimates for ozone concentrations) and/or sulfur fate and transport (to derive estimates for  $\text{SO}_2$  concentrations), while some of the models use pre-determined estimates for these species based on other models and/or measurements.

Further progress in understanding the atmospheric cycling of mercury has emphasised the need for direct modelling of the complex physico-chemical transformations of atmospheric mercury species by comprehensive models. Typically, the modern models contain modules designed to calculate explicitly the chemical interactions that move gas-phase species into and among the various aqueous phases within clouds as well as calculate the aqueous-phase chemical transformations that occur within cloud- and precipitation droplets. However, a more detailed numerical formulation of physical and chemical processes occurring within and below precipitating and non-precipitating clouds should be included.

#### 5.1 CMAQ-Hg description

The Community Multiscale Air Quality model (CMAQ) is an Eulerian type model used to simulate the transport, transformation and deposition of air pollutants and their precursors. The pollutants simulated by the standard version of CMAQ include tropospheric ozone, acidic and nutrient substances, and aerosol matter of various composition and particle size. The standard version of CMAQ available at <http://www.epa.gov/asmdnerl/models3/index.html> as of June 1, 2001, was employed as the basis for the mercury version of CMAQ (CMAQ-Hg) used for the model intercomparison. A complete description of all special CMAQ model formulations for the simulation of atmospheric mercury is given in *Bullock and Brehme* [2002]. Basic transport and diffusion simulation in the CMAQ-Hg was kept the same as in the standard CMAQ. All pollutant species normally simulated by the standard CMAQ are also simulated in CMAQ-Hg along with three added mercury species and molecular chlorine.

The CMAQ-Hg modelling domain for the intercomparison covers central and northern Europe with an array of grid cells 36 km by 36 km in size. The vertical dimension is resolved by 21 layers of varying

thickness, with the finest resolution near the surface. All CMAQ-Hg simulations performed for this study used the Carbon Bond-IV (CB-IV) gaseous chemistry mechanism and the SMVGEAR numerical solver. Meteorology was defined using the Fifth-Generation Pennsylvania State University / National Center for Atmospheric Research (NCAR) Mesoscale Model [Grell *et al.*, 1994] employing the surface energy flux and the planetary boundary layer model of Pleim and Xiu [1995]. Descriptions of the standard CMAQ in Byun and Ching [1999] provide a definition of all elements of the CMAQ-Hg except for those described below.

The mercury emissions data used for this study were those provided by the MSC-East. Low-level emissions (below 56 meters) were apportioned entirely to layer 1 of the CMAQ-Hg model. Middle-level (56-136 meters) emissions were apportioned one-third each to layers 2, 3, and 4. High-level (136-251 meters) emissions were apportioned one-fourth to layers 4 and 6, and one-half to layer 5.

The CMAQ-Hg simulates gas-phase mercury as three separate pollutant species; (1) gaseous  $\text{Hg}^0$ , (2) reactive gaseous mercury (RGM), and (3) particulate mercury (TPM). Four gas-phase oxidation reactions for mercury are simulated in the CMAQ-Hg as shown in Table 5.1. The  $\text{Hg}^{2+}$  products of these reactions are modelled in CMAQ-Hg as either RGM or TPM based on the vapour pressure of the compounds produced, and these  $\text{Hg}^{2+}$  species are converted to  $\text{Hg}^0$  only in the cloud chemistry mechanism. While some chemical reduction of  $\text{Hg}^{2+}$  to  $\text{Hg}^0$  may occur in the gas phase, the mechanism and rate for this type of reaction remains poorly understood. In general, gas-phase reactions of mercury appear to be of minor importance to its oxidation state as compared to its aqueous-phase reactions.

Chlorine photolysis is known to occur with rather rapid rate, similar to nitrogen dioxide, another gas-phase species in CMAQ. The  $\text{Cl}_2$  photolysis rate is referenced to the CMAQ photolysis rate for  $\text{NO}_2$  with a proportionality factor of 0.295. This referencing is based on ongoing efforts at the University of Texas to expand the CB-IV mechanism to include  $\text{Cl}_2$  [David Allen, personal communication] and is based on their analysis of updated actinic flux data for  $\text{Cl}_2$  and  $\text{NO}_2$  [Finlayson-Pitts and Pitts, 1999].

The cloud chemistry mechanism for mercury in CMAQ-Hg is illustrated in Fig. 5.1. It simulates gas/liquid partitioning, aqueous chemistry and sorption of  $\text{Hg}^{2+}$  complexes to elemental carbon suspended in cloud water, and was developed based on the approach of Pleijel and Munthe [1995]. This additional aqueous chemistry of  $\text{Hg}^0$ , the  $\text{Hg}^{2+}$  ion, and six  $\text{Hg}^{2+}$  compounds is simulated simultaneously with the pre-existing aqueous chemistry from the original CMAQ. Gas/liquid partitioning of  $\text{Hg}^0$  and RGM is simulated using Henry's law equilibrium assumptions. RGM is assumed to partition based on the Henry's constant for mercuric chloride ( $\text{HgCl}_2$ ). Particulate mercury is assumed to be completely incorporated into cloud water and composed of  $\text{Hg}^{2+}$  sorbed to ECA at the start of the CMAQ operator splitting technique that is employed to simulate cloud chemistry and wet deposition [Byun and Ching, 1999]. All aqueous chemical reactions for mercury and their rate constants are shown in Table 5.1. Chemical equilibria used in the aqueous mechanism are also in Table 5.1, as are the Henry's constants used for gas/liquid partitioning. Sorbed aqueous  $\text{Hg}^{2+}$  complexes are not subject to aqueous chemical reduction to the elemental form and subsequent out gassing from cloud droplets [Seigneur *et al.*, 1998]. Thus, sorption to ECA can affect the amount of mercury in cloud water subject to removal by precipitation.

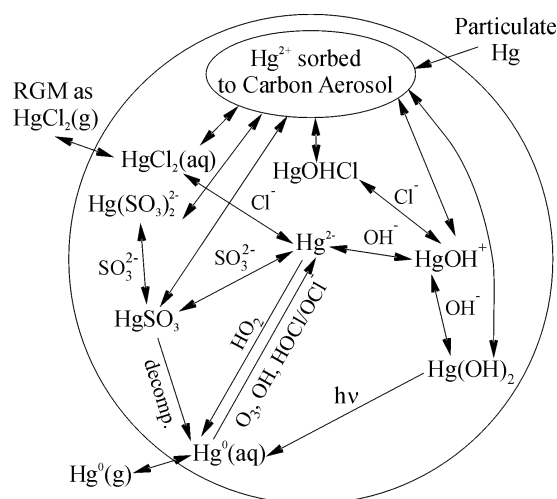


Figure 5.1. Schematic representation of the aqueous mercury chemical mechanism in CMAQ model

Table 5.1. Chemical reactions for mercury and their rate constants used in CMAQ model

No.	Reaction	k or K	References
<i>Gaseous-phase reaction of Hg</i>			
RG1	$\text{Hg}^0_{(g)} + \text{O}_{3(g)} \rightarrow \text{TPM}$	$3.0 \times 10^{-20} \text{ cm}^3 \text{ molecules}^{-1} \text{ s}^{-1}$	Hall [1995]
RG2	$\text{Hg}^0_{(g)} + \text{Cl}_{2(g)} \rightarrow \text{RGM}$	$4.8 \times 10^{-18} \text{ cm}^3 \text{ molecules}^{-1} \text{ s}^{-1}$	Calhoun and Prestbo [2001]
RG3	$\text{Hg}^0_{(g)} + \text{H}_2\text{O}_{2(g)} \rightarrow \text{TPM}$	$8.5 \times 10^{-19} \text{ cm}^3 \text{ molecules}^{-1} \text{ s}^{-1}$	Tokos et al. [1998]
RG4	$\text{Hg}^0_{(g)} + \text{OH}_{(g)} \rightarrow \text{TPM}$	$8.7 \times 10^{-14} \text{ cm}^3 \text{ molecules}^{-1} \text{ s}^{-1}$	Sommar et al. [2001]
<i>Aqueous-phase reactions of Hg</i>			
RA1	$\text{Hg}^0_{(aq)} + \text{O}_{3(aq)} \rightarrow \text{Hg}^{2+}_{(aq)} + \text{products}$	$4.7 \times 10^7 \text{ M}^{-1} \text{ s}^{-1}$	Munthe [1992]
RA2	$\text{HgSO}_{3(aq)} \rightarrow \text{Hg}^0_{(aq)} + \text{products}$	$T \times e^{((31.971 \times T) - 12595)/T} \text{ s}^{-1}$	Van Loon et al. [2000]
RA3	$\text{Hg}(\text{OH})_{2(aq)} + h\nu \rightarrow \text{Hg}^0_{(aq)} + \text{products}$	$6.0 \times 10^{-7} \text{ s}^{-1}$ (maximum) †	adapted from Xiao et al. [1994]
RA4	$\text{Hg}^0_{(aq)} + \text{OH}_{(aq)} \rightarrow \text{Hg}^{2+}_{(aq)} + \text{products}$	$2.0 \times 10^9 \text{ M}^{-1} \text{ s}^{-1}$	Lin and Pehkonen [1997]
RA5	$\text{Hg}^{2+}_{(aq)} + \text{HO}_{2(aq)} \rightarrow \text{Hg}^0_{(aq)} + \text{products}$	$1.1 \times 10^4 \text{ M}^{-1} \text{ s}^{-1}$	Pehkonen and Lin [1997]
RA6	$\text{Hg}^0_{(aq)} + \text{HOCl}_{(aq)} \rightarrow \text{Hg}^{2+}_{(aq)} + \text{products}$	$2.09 \times 10^6 \text{ M}^{-1} \text{ s}^{-1}$	Lin and Pehkonen [1998]
RA7	$\text{Hg}^0_{(aq)} + \text{OCl}_{(aq)} \rightarrow \text{Hg}^{2+}_{(aq)} + \text{products}$	$1.99 \times 10^6 \text{ M}^{-1} \text{ s}^{-1}$	Lin and Pehkonen [1998]
<i>Aqueous-phase chemical equilibria for Hg</i>			
E1	$\text{Hg}^{2+} + \text{SO}_3^{2-} \rightarrow \text{HgSO}_3$	$2.0 \times 10^{-13} \text{ M}$	Smith and Martell [1976]
E2	$\text{HgSO}_3 + \text{SO}_3^{2-} \rightarrow \text{Hg}(\text{SO}_3)_2^{2-}$	$4.0 \times 10^{-12} \text{ M}$	Smith and Martell [1976]
E3	$\text{Hg}^{2+} + 2\text{Cl}^- \rightarrow \text{HgCl}_2$	$1.0 \times 10^{-14} \text{ M}^2$	Lin and Pehkonen [1999]
E4	$\text{Hg}^{2+} + \text{OH}^- \rightarrow \text{HgOH}^+$	$2.51 \times 10^{-11} \text{ M}$	Smith and Martell [1976]
E5	$\text{HgOH}^+ + \text{OH}^- \rightarrow \text{Hg}(\text{OH})_2$	$6.31 \times 10^{-12} \text{ M}$	Smith and Martell [1976]
E6	$\text{HgOH}^+ + \text{Cl}^- \rightarrow \text{HgOHCl}$	$3.72 \times 10^{-8} \text{ M}$	Smith and Martell [1976]
<i>Henry's equilibria for Hg</i>			
H1	$\text{Hg}^0_{(g)} \rightleftharpoons \text{Hg}^0_{(aq)}$	$1.1 \times 10^{-1} \text{ M atm}^{-1}$	Sanemasa [1975]
H2	$\text{HgCl}_{2(g)} \rightleftharpoons \text{HgCl}_{2(aq)}$	$1.4 \times 10^6 \text{ M atm}^{-1}$	Lindqvist and Rodhe [1985]

† Rate constant for RA3 is scaled to the cosine of solar zenith angle

Upon completion of the CMAQ operator splitting function for cloud chemistry and wet deposition, all aqueous chemical species are transferred back to the gas phase for the simulation of transport and dry deposition. This transfer is necessary because the current versions of the CMAQ and CMAQ-Hg

have no explicit simulation of cloud water transport. Cloud water concentration is estimated at the beginning of each aqueous chemistry time loop based on the previous MM5 meteorological model simulation. Given the assumptions of Henry's equilibrium for all gaseous species and complete incorporation of TPM into cloud water at the beginning of the cloud chemistry time loop, the effect on the aqueous chemistry simulation from this transfer to the gas phase is minimal. Methods for explicit simulation of the transport of cloud water and its chemical constituents by the CMAQ modeling system are currently under development. In the mean time, dissolved  $\text{Hg}^0$  is transferred as gaseous  $\text{Hg}^0$ , all dissolved  $\text{Hg}^{2+}$  species are transferred collectively as RGM, and all  $\text{Hg}^{2+}$  species sorbed to ECA are transferred collectively as TPM.

It should be noted that emissions of sea salt aerosol and other sources of chloride ion ( $\text{Cl}^-$ ) in cloud water are not yet defined for the standard version of CMAQ. A constant aqueous  $\text{Cl}^-$  concentration of  $1.0 \times 10^{-3} \text{ g l}^{-1}$  is assumed in the current form of CMAQ-Hg (the other models used  $2.5 \text{ mg l}^{-1}$  – see Chapter 1). The speciation of dissolved  $\text{Hg}^{2+}$  compounds in cloud water is dependent on  $\text{Cl}^-$  concentration. A top priority for future development of CMAQ is the addition of sea salt and crustal aerosol emissions.

The CMAQ-Hg model parameterization for the sorption of aqueous  $\text{Hg}^{2+}$  species to ECA suspended in cloud water is adapted from previous work by *Seigneur et al.* [1998]. A complete description of the CMAQ-Hg treatment of  $\text{Hg}^{2+}$  sorption in the aqueous media is available in *Bullock and Brehme* [2002].

The CMAQ-Hg model simulates the wet deposition of  $\text{Hg}^0$ , RGM, and TPM, in the same manner as for all other aqueous pollutant species previously resolved in the standard CMAQ model. The cloud-water concentration of each pollutant is deposited to the surface based on the simulated rate of precipitation falling from each clouded grid volume during the cloud chemistry time splitting operation. The cloud water concentration of  $\text{Hg}^0$  is relatively low compared to the total dissolved and sorbed  $\text{Hg}^{2+}$ , and the simulated wet deposition of  $\text{Hg}^0$  is minor compared to that of RGM and TPM. The cloud-water concentration of RGM is calculated as the sum of the dissolved-phase concentrations of all seven  $\text{Hg}^{2+}$  species in the aqueous chemistry mechanism. The cloud-water concentration of TPM is calculated as the sum of the concentrations of all sorbed  $\text{Hg}^{2+}$  species.

Dry deposition of  $\text{Hg}^0$  is assumed to be negligible in comparison to RGM and TPM, and is not simulated by the CMAQ-Hg model. On the other hand, RGM dry deposition is assumed to occur very readily, especially to lush vegetation and to water surfaces. The standard CMAQ dry deposition parameterization for gaseous nitric acid is also used for RGM. Dry deposition of TPM is simulated based on pre-existing deposition velocity formulations in the standard CMAQ for sulfuric acid. Mercury aerosols will eventually be incorporated into the CMAQ aerosol dynamics model [*Binkowski, 1999*], which is an extension of the Regional Particulate Model [*Binkowski and Shankar, 1995*]. Dry deposition of TPM will then be dependent on the evolution of its particle morphology. This portion of the CMAQ model code is not adaptable using standard Models-3 CMAQ framework tools. Careful and deliberate modification of these codes will be required.

For this modeling exercise, the initial air concentration and all four lateral boundary values for the three mercury species were;  $2.0 \cdot 10^{-13}$  (mol/mol) for  $\text{Hg}^0$  and  $2.0 \cdot 10^{-15}$  (mol/mol) for RGM and TPM. These values are equivalent to  $1.7 \cdot 10^{-9} \text{ g m}^{-3}$  ( $1.7 \text{ ng m}^{-3}$ ) for  $\text{Hg}^0$  and  $1.7 \cdot 10^{-11} \text{ g Hg m}^{-3}$  ( $17 \text{ pg Hg m}^{-3}$ ) for RGM and TPM under the conditions of 1 atm and 288°K. For molecular chlorine gas, the initial and boundary air concentrations were set to zero.

The model calculates simultaneously nitrogen oxides, carbon oxides, sulfur dioxide, VOCs, chlorine species, black carbon concentrations. Hence, corresponding emission fields were required as input data. The  $\text{NO}_x$  and total VOC emission data used for this study were provided by EMEP/MS-CW for

1995. For the 1999 tests, the VOC emission rates were divided by 1.1, and the NO<sub>x</sub> emission rates were divided by 1.05 in line with emission reductions during the late 90s. The total VOC emissions were assumed to be from anthropogenic sources only. A generic profile for VOC speciation was used to define the emission rate for each VOC species [Vestreng and Klein, 2002].

The carbon monoxide and dioxide as well as sulfur dioxide emissions data for 1990 were obtained from the RIVM EDGAR web site (<http://www.rivm.nl/env/int/coredata/edgar/>). These emission data have a horizontal resolution of 1 degree latitude by 1 degree longitude and were apportioned to the CMAQ horizontal grid space based on a simple area transformation between the grid systems. Emissions from major industrial sources were assumed to have a release height of 100 meters, while all other emissions were assumed to be at the ground level. Information on 1990 to 1995 trends in CO and SO<sub>2</sub> emissions was obtained from the RIVM EDGAR web site and was used to adjust the 1990 data for these pollutants to 1995 levels. No additional adjustments were made for the 1999 test period.

These emission data for black carbon were obtained from GEIA (Global Emission Inventory Activity) (<http://weather.engin.umich.edu/geia/>). Separate data sets were obtained for black carbon emissions from "anthropogenic sources" and "biomass burning". These emissions data also have a horizontal resolution of 1 degree latitude by 1 degree longitude and were apportioned to the CMAQ horizontal grid space based on a simple area transformation between the grid systems. These emissions estimates are for the 1984-1987 time period. Due to lack of supporting information, no adjustments were made for the 1995 and 1999 model application periods. All black carbon emissions from biomass burning were assumed to be released from the ground level, whereas the anthropogenic emissions were distributed evenly with height among the lowest 6 model layers.

Like in the case of black carbon the model used its own chlorine emission field. However, no suitable industrial emission inventory for Cl<sub>2</sub> was available. As an interim approach, the production of Cl<sub>2</sub> from sea-salt aerosol has been modeled as a continuous emission rate per unit area over all salt-water surfaces. The emission rate for CMAQ-Hg simulations was based on an assumed yield of 100 ppt Cl<sub>2</sub> per day within a marine atmospheric layer 100 m deep over the oceanic surface with a typical mid-oceanic saline concentration. Under typical atmospheric conditions (1 atm, 20°C) about  $2.95 \times 10^{-5}$  g Cl<sub>2</sub> m<sup>-2</sup> day<sup>-1</sup> is the emission rate calculated over ocean surfaces. Emissions from the Baltic Sea were modelled to be one-fifth the normal oceanic value to account for its lower average salinity. All Cl<sub>2</sub> emissions were simulated to occur only in the lowest model layer.

It is believed that soot particles can play a significant role in mercury redox processes within cloud drops. To check the sensitivity of the CMAQ model to black carbon concentration in the aqueous phase, two versions of the initial data for this parameter have been used in the model. In the basic version it was assumed that 1% of all primary aerosol emissions are in the form of elemental carbon. In the second case for the European region this value was multiplied by a factor of 5.

## 5.2. The ADOM model description

A comprehensive mercury modelling system using the Eulerian reference frame of the Acid Deposition and Oxidant Model (ADOM) has been developed under the Canada-Germany Science & Technology Co-operation Agreement and applied within various projects funded by the European Commission to study the regional transport and deposition fluxes of atmospheric mercury species (Petersen et al., 2001). The cloud mixing, scavenging, chemistry and wet deposition modules of the ADOM, originally designed for regional-scale acid precipitation and photochemical oxidants studies have been restructured to accommodate recent developments in atmospheric mercury chemistry. A stand-alone version of these modules referred to as the Tropospheric Chemistry Module (TCM) was designed to simulate the meteorology and chemistry of the entire depth of the troposphere to study cloud mixing, scavenging and chemical reactions associated with precipitation systems that generate wet deposition fluxes [Petersen et al., 1998]. The TCM chemistry scheme was developed by systematic simplification of the detailed Chemistry of Atmospheric Mercury (CAM) process model, which is based on current knowledge of physico-chemical forms and transformation reactions of atmospheric mercury species [Pleijel and Munthe, 1995].

After comprehensive testing under different environmental conditions the TCM has been implemented into the full ADOM model. Within the constraints of the available computer resources and input data, these models incorporate an up-to-date understanding of the detailed physical and chemical processes in the atmosphere. The vertical grid consists of 12 unequally spaced levels between the surface and the top of the model domain at 10 km. The model is run for a grid cell size 55 by 55 km (High Resolution Limited Area Model (HIRLAM) grid) over a 76 by 76 domain.

The transport and diffusion module uses a sophisticated cell-centered flux formulation solver for the 3-dimensional advection-diffusion equation. Dry deposition is modelled in terms of a deposition velocity for gaseous and particle associated mercury species, which is calculated as the inverse of the sum of the aerodynamic, deposition layer and surface canopy resistance. The mass transfer, chemistry and adsorption component of the model incorporates 14 mercury species and 21 reactions including mass transfer, aqueous phase and gas phase chemical reactions and adsorption processes on particles. The reaction rates are derived from published data and from assumption of the rates of complex formation. The cloud physics module simulates the vertical distribution of mercury species in clouds. Two different modules are incorporated: one describes stratus (layer) clouds and the other simulates cumulus (convective) type clouds. One or the other or a combination (cumulus deck embedded in a stratus cloud) is used in the calculation depending on the characteristics of the precipitation observed.

The meteorological input data needed by ADOM are three-dimensional fields of wind speed, wind direction, pressure, temperature, relative humidity, vertical velocity and vertical diffusivity, and two-dimensional fields of surface winds, surface pressure, surface air temperature, friction velocity, Monin-Obukhov length, mixing height, cloud base and top height, amount of cloud cover and the amount of precipitation at every one hour model time step. These data sets are derived diagnostically using the weather prediction model HIRLAM.

The geophysical data include files for 8 land use categories (i. e. deciduous forest, coniferous forest, grassland, cropland, urban, desert, water and swamp) and 12 soil categories. The database also includes information on terrain height and the growing season. This geophysical data affects meteorology, dry deposition processes and air-surface exchange of gaseous mercury species.

Initial and boundary conditions are needed for all advected species in the model. This includes the emitted compounds and mercuric oxide (HgO) formed by gas phase oxidation of Hg<sup>0</sup>. A typical

European background mixing ratio of 0.18 ppt corresponding to a mass per unit volume concentration of about  $1.5 \text{ ng m}^{-3}$  is used for  $\text{Hg}^0$  in the atmospheric boundary layer (layers 1-4 in the vertical model grid) with a slight vertical mixing ratio decrease of approximately 80% of the boundary layer value at the top of the modelling domain. Observations for mercury species other than  $\text{Hg}^0$  are still scarce in Europe and vertical profiles are not available at all. Therefore, initial and boundary concentrations of  $2 \text{ pg m}^{-3}$ , and  $20 \text{ pg m}^{-3}$  estimated to be average values from a limited number of observations in Europe are used for  $\text{HgCl}_2$  and  $\text{Hg}(\text{part.})$  in the boundary layer. Due to their relative short atmospheric residence time and due to anthropogenic emissions occurring near the ground concentrations of  $\text{HgCl}_2$  and  $\text{Hg}(\text{part.})$  are allowed to decrease with height to a value of about 10 % of the boundary value at the model top. In addition to  $\text{HgCl}_2$ , boundary concentrations for  $\text{HgO}$  are also given.  $\text{HgO}$  is believed to be the initial product from the gas phase reaction with  $\text{Hg}^0$  and  $\text{O}_3$  and is included in the chemistry scheme employed in the model. No information on ambient air concentrations of  $\text{HgO}$  or its physical/chemical properties such as Henry's law constant are available. For this reason,  $\text{HgO}$  is treated using the same parameterisation as for  $\text{HgCl}_2$ , believed to be the main gaseous divalent species in the atmosphere. In the absence of reliable measurement data, a very low initial value of  $0.7 \cdot 10^{-6} \text{ pg m}^{-3}$  constant with height is used for  $\text{HgO}$ . The more realistic initial value for  $\text{HgCl}_2$  ( $2 \text{ pg m}^{-3}$ ) is thus assumed to represent all divalent mercury compounds in the boundary air masses.

The mercury chemistry in ADOM, described in [Petersen *et al.* 1998], requires the specification of  $\text{O}_3$ ,  $\text{SO}_2$ , and soot carbon concentrations in ambient air as well as  $\text{Cl}^-$  concentrations in cloud water and cloud water pH. For the results with the European version of ADOM, the concentrations of  $\text{O}_3$ ,  $\text{SO}_2$ , and soot carbon were fixed at 35 ppb, 1 ppb and 1 microgram per  $\text{m}^3$ . The cloud water concentration of  $\text{Cl}^-$  and the cloud-water pH were specified as  $2 \cdot 10^{-6} \text{ mol l}^{-1}$  and 4.5, respectively.

### 5.3. The MSCE-Hg model description

The EMEP/MSCE-Hg model has been developed to evaluate mercury pollution levels in the EMEP region. A detail description of the model is done in [Ryaboshapko *et al.*, 1999; Ryaboshapko *et al.*, 2001; Ilyin *et al.*, 2002]. The model considers basic processes governing transport and deposition of mercury - advection, diffusion, dry/wet removal and chemical reactions.

The model consists of five non-uniform layers along the vertical. Top of the model is at height of about 4 km. Therefore, the model domain covers the entire atmospheric boundary layer and a part of the middle troposphere. Heights of the layers are 100, 300, 700, 1000 and 1800 m (from bottom to top).

The advection scheme is conservative, stable and positively defined. The horizontal diffusion is described according to the approach assuming that the pollutant dispersion is proportional to the travel distance. The model description of vertical turbulent diffusion is based on a classical law: a substance flux is proportional to the concentration gradient. The proportionality factor (the coefficient of turbulent diffusion) is calculated by the boundary layer parameterisation.

Scavenging of mercury encompasses wet removal by precipitation and dry uptake by the underlying surface. Wet removal of TPM and RGM is described using a washout ratio approach. Within clouds  $\text{Hg}^{2+}$  and  $\text{Hg}^0$  are rained out via dissolution in cloud drops. It is assumed that half the mercury is contained in the composition of insoluble particles within cloud and rainwater droplets. After drop evaporation an aerosol particle is formed containing in its composition all earlier dissolved and insoluble mercury compounds. Dry uptake of TPM (mean aerodynamic diameter -  $0.61 \text{ }\mu\text{m}$ ) is differentiated with regard to land-use category of the underlying surface and depends basically on

properties of the underlying surface and atmospheric stability. Dry uptake of  $\text{Hg}^0$  is calculated depending on the vegetation type. Dry deposition velocity of  $\text{Hg}^0$  is assumed to exhibit the diurnal cycle. Dry deposition velocity of RGM is prescribed basing on data available in the literature [Ryaboshapko *et al.*, 1999; Ilyin *et al.*, 2002].

Parameterization of chemical processes includes both aqueous-phase and gaseous-phase reactions and equilibria [Ryaboshapko *et al.*, 2001]. In spite of a wide variety of reactions involving mercury species, only several key reactions were introduced into the modelling scheme. They are oxidation of elemental mercury by  $\text{O}_3$ , dissolution of  $\text{Hg}^0$  and RGM in cloud droplets, oxidation of mercury within drops by  $\text{O}_3$  with further sorption on insoluble particles within drops and partial reduction by dissolved  $\text{HO}_2$ -radical and because of decomposition of mercury-sulfite complex. All products of gaseous-phase oxidation are treated as aerosol particles.

Temperature in the atmosphere can vary in a wide range and the liquid phase can occur in clouds down to  $-40^\circ\text{C}$ . Hence, the temperature can significantly change reaction rates and equilibrium states. A very important peculiarity of the MSCE-Hg model, which distinguishes it from the others, is taking into account temperature dependencies of different process rates and equilibrium ratios. For Henry's law constants (dimensionless) the following equations were used:

$$H_{\text{Hg}^0}(T) = 0.00984 \cdot T \cdot \exp [2800 \cdot (1/T - 1/298)] \quad [\text{Ryaboshapko and Korolev, 1997}];$$

$$H_{\text{O}_3}(T) = 0.000951 \cdot T \cdot \exp [2325 \cdot (1/T - 1/298)] \quad [\text{Sander, 1997}];$$

$$H_{\text{HgCl}_2}(T) = 105369 \cdot T \cdot \exp [5590 \cdot (1/T - 1/298)] \quad [\text{Ryaboshapko et al., 2001}].$$

Most likely, a very important reaction of mercury oxidation by ozone in the gas phase is temperature dependent. The following equation for reaction rate constant was used in the MSCE-Hg model to consider this dependence (derived from [Hall, 1995]):

$$k(\text{Hg}^0 + \text{O}_3) = 2.1\text{E-}18 \cdot \exp (-1246/T) \quad (\text{cm}^3 \text{ molec}^{-1} \text{ s}^{-1}).$$

On the base of the analysis of available literature data [Ilyin *et al.*, 2002] the following concentration values are taken at the boundaries of the EMEP domain:  $\text{Hg}^0$  concentration is  $1.7 \text{ ng/m}^3$  at the eastern, southern, western borders and  $1.6 \text{ ng/m}^3$  at the northern border. RGM concentration is equal to zero at all the borders. TPM concentration is  $0.02 \text{ ng/m}^3$  at the northern and western borders and  $0.03 \text{ ng/m}^3$  – and the eastern and southern ones. Mixing ratio of  $\text{Hg}^0$  decreases linearly with height up to 90-% of its surface value on the level of the tropopause. TPM mixing ratio is constant with height up to the top of the domain.

## 5.4. The GRAHM model description

Global/Regional Atmospheric Heavy Metals (GRAHM) model is MSC's (Meteorological Service of Canada) Eulerian multi-scale, comprehensive, on-line, high resolution (horizontally and vertically) mercury model. GRAHM was developed starting from the Canadian Meteorological Centre's operational weather forecasting model which was designed to meet the needs of operational weather forecasting and research and to provide a dynamical framework for air quality modelling on scales from global to urban by making use of a variable-resolution grid. One of the important features of GRAHM, where it significantly departs from the other models, is that this is an on-line model, which means that the model integrates dynamic equations for all meteorological processes and physio-chemical processes for atmospheric mercury species in a common manner. This has the advantage of retaining the high temporal resolution of the meteorological fields such as winds and clouds required for the transport, transformation and deposition of mercury. The model uses 3-D finite element spatial discretisation. The transport scheme for the tracers is a mass conserving 3-D quasi-monotonic semi-Lagrangian scheme.

GRAHM utilises state-of-the-science meteorological process parameterizations to drive the mercury physical and chemical processes. For example, Sundqvist stratiform and Kain-Fritsch cumulus condensation schemes are used to derive detailed cloud fields for aqueous-phase processes of mercury species. The scheme carries cloud water field explicitly (an important cloud field for chemistry) and parameterizes cloud micro-physical processes. Vertical turbulent diffusion of mercury in the planetary boundary layer is based on the assumption of the existence of an eddy diffusivity coefficient specified by a time-dependent equation for turbulent kinetic energy and a mixing length governed by a relaxation process. A detailed resistance based dry deposition for gas and particle phase mercury is utilized in the model. The parameterization depends on the land surface characteristics, vegetation and boundary layer stability.

Four mercury species ( $\text{Hg}^0$ ,  $\text{HgCl}_2$ ,  $\text{HgO}$ ,  $\text{HgP}$ ) are included in the model. The model uses TCM (see section 5.2) gas and aqueous phase mercury chemistry parameterizations as described by *Petersen et al.* [1998]. It incorporates 14 mercury species and 21 reactions including mass transfer reactions, aqueous-phase and gas-phase chemical reactions and equilibrium reaction for adsorption on particles.

GRAHM is an on-line global model therefore at each time-step, all the meteorological fields and the mercury fields are integrated. Mercury species fields are set at zero at the start of the integration. The model was integrated for three years at horizontal resolution 5x5 degree latitude-longitude, 28 vertical levels with top at 10 mb, sufficiently high resolution in the surface planetary boundary and 30 minutes time-step until the beginning of November 1999. Subsequently, the model was integrated at 1x1 degree resolution for comparison with the observations. In order to represent the observed atmosphere accurately during the integration, observed meteorological data from Canadian Meteorological Centre were introduced into the model every 24 hours. This choice is based on the fact that the model shows good forecast skills for 24 hours integration when compared with the observations.

## 5.5. The DEHM model description

The original version of Danish Euclarian Hemispheric Model (DEHM) have been used to study the transport of SO<sub>2</sub>, SO<sub>4</sub><sup>2-</sup> and Pb into the Arctic [Christensen, 1997; 1999]. Currently a 3-d mercury model based on DEHM is in the progress of development within the Danish AMAP program. The simplified sulphur model system has been used in the first phase of the AMAP program [Kämäri *et al.*, 1998] while the results with the Pb version were presented at the AMAP workshop on Techniques and Associated Uncertainties in Quantifying the Origin and Long-Range Transport of Toxic Chemicals to the Arctic, Bergen, Norway 14-16 June 1999 [Christensen, 1999].

The system consists of two parts: a meteorological part based on the PSU/NCAR Mesoscale Model version 5 (MM5) modelling subsystem [Grell *et al.*, 1995] and an air pollution model part, the DEHM model (see Fig. 5.2). The MM5 model produces the final meteorological input for the DEHM model. Global meteorological data, used as input to the MM5 mesoscale modelling system, are obtained from the European Centre for Medium-range Weather Forecasts (ECMWF) on a 2.5°x2.5° grid with a time resolution of 12 hours.

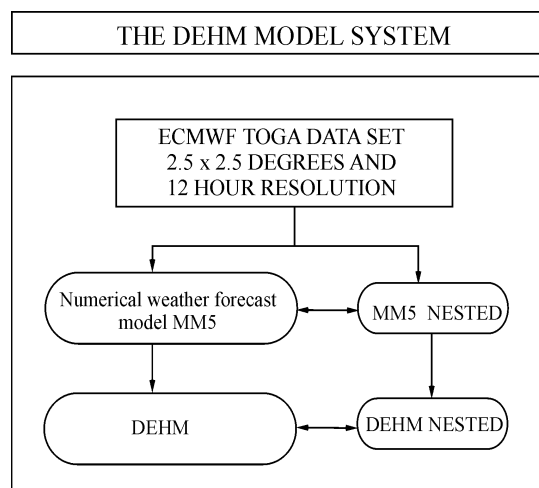


Figure 5.2. Overview of the DEHM model system

The whole system includes 2-way nesting capabilities, so it is possible to do finer (150 km → 50 km → 16.67 km, etc) model calculations over e.g. the Arctic Ocean or Greenland. 23 years of meteorological data from 1979 to 2001 are available, but the MM5 model system for the mother domain has only been run for a period of 11 years from 1990 to 2001, while the model system with 1 nest have been run for the period 1995-2001 for Europe (50 km) and 1 month for Greenland (50 km) as demonstration. In the used version the model has been run for the mother domain and with 1 nest for Europe.

The DEHM model is based on set of coupled full three-dimensional advection-diffusion equations. In the present version there are 13 mercury species, 3 in the gas-phase (Hg<sup>0</sup>, HgO and HgCl<sub>2</sub>), 9 species in the aqueous-phase and 1 in the particulate phase.

The horizontal mother domain of the model is defined on a regular 96x96 grid that covers most of the Northern Hemisphere with a grid resolution of 150 km × 150 km at 60°N. The nested domain for Europe is also defined on a regular 96x96 grid with a grid resolution of 50 km × 50 km at 60°N, and is

a sub-grid of the EMEP grid. The vertical discretization is defined on an irregular grid with 20 layers up to  $\approx 15$ km.

The vertical diffusion is parameterised by using a  $K_z$  profile for the surface layer based on the Monin-Obukhov similarity theory. The  $K_z$  profile for the surface layer is extended to the whole boundary layer by using a simple extrapolation [Christensen, 1997].

The chemistry is based on the scheme developed by G.Petersen *et al.* [1998] (see section 5.2). During the polar sunrise in the Arctic an additional fast oxidation rate of  $\text{Hg}^0$  to  $\text{HgO}$  is assumed: inside the boundary layer over sea ice during sunny conditions it is assumed that there is an additional oxidation rate of  $\frac{1}{4} \text{ hour}^{-1}$ . The fast oxidation stops, when surface temperature exceeds  $-4^\circ\text{C}$ . The removals of  $\text{Hg}^0$  are due to the chemistry and the uptake by cloud water.

The dry deposition velocities of the reactive gaseous mercury species are based on the resistance method, where the surface resistance similar to  $\text{HNO}_3$  is used. The dry deposition velocity for particulate mercury is similar to  $\text{SO}_4^{2-}$ , and over land it is given in Walcek *et al.* [1986], while the dry deposition over open water is based on the work by Slinn and Slinn [1980]. The wet deposition of reactive and particulate mercury is parameterised by using a simple scavenging coefficients formulation with different in-cloud and below-cloud scavenging coefficients [Christensen, 1997].

## 5.6. The HYSPLIT model description

The HYbrid Single Particle Lagrangian Integrated Trajectory model, Version 4 (*HYSPLIT\_4*) is a Lagrangian model, in which puffs of pollutant are emitted from user-specified locations, and are then advected, dispersed, and subjected to destruction and deposition phenomena throughout the model domain. It was developed at the U.S. National Oceanic and Atmospheric Administration (NOAA) to model releases of radioactive materials and is widely used for emergency response [e.g., Draxler *et al.*, 1997]. The development, validation, and operation of HYSPLIT are summarized elsewhere [Draxler and Hess, 1997, 1998; Draxler, 1999]. It has been used to simulate many different atmospheric processes, including regional ozone formation [Draxler, 2000; Stein *et al.*, 2000], sulfur transport and deposition [Rolph *et al.*, 1992, 1993], and dispersion of pollutants from oil fires [McQueen and Draxler, 1994; Draxler *et al.*, 1994]. The methodology used in the mercury modeling presented here is an extension of earlier HYSPLIT-based modeling analyses of atrazine [Cohen *et al.*, 1997a] and dioxin [Cohen *et al.*, 1995, 1997b, 2002; Commoner *et al.*, 1998, 2000].

HYSPLIT uses gridded meteorological data computed by an external model. For the simulations presented here, hourly MM5 data for the periods of interest were generously provided by Russ Bullock of NOAA/USEPA (personal communication, 2002). These MM5 data were computed on a  $82 \times 88$   $36\text{km}$  grid and a  $60 \times 62$   $108\text{km}$  grid (both centered at Latitude =  $50\text{N}$ , Longitude =  $10\text{E}$ ). The data were converted from MM5 output format to "ARL packed format", suitable for use with the HYSPLIT model. We note that the precipitation in the MM5 data used is model estimated, and hence subject to some uncertainty. Emissions data supplied by MSC-East (on the base of Pacyna *et al.* [2001]) were utilized according to the project specifications. We note that this analysis assumed that emissions were constant and continuous for all sources. This assumption may not be valid, of course, and this can lead to large simulation errors for estimating concentrations at a given location, especially for short periods of time.

At each model time step (approximately 15 minutes) for a given mercury-containing puff, a determination was first made as to whether the atmospheric particles were wetted or dry; droplets were assumed if the relative humidity was above 80%, while the particles were assumed to be dry for lower relative humidities. Table 5.2 shows the chemistry scheme used in this modeling, based primarily on the syntheses of *Bullock* [2001] and *Seigneur* [EPRI, 2000]. In the droplet situation, the set of eight gas-liquid equations plus eleven aqueous phase equilibrium equations were solved (equations 1-19 in Table 5.2), and then the gas-phase (20-23) and aqueous phase (24-29) reactions were allowed to proceed. If the particles were dry, then a simple vapor/particle partitioning calculation was done for Hg(0) and Hg(II) [Junge, 1997; Bidleman, 1998], and only the gas-phase reactions were considered (20-23). Hg(p) was obviously assumed to reside only on particles in the dry-particle case.

**Table 5.2.** Physical-chemical parameters used in the HYSPLIT model

#	Equilibrium / Reaction	Equation	Equilibrium or Rate Constant
1	gas-liquid eqbrm	$\text{Hg}(0)(\text{aq}) = K1 \cdot \text{Hg}(0)(\text{gas})$	$K1 = 0.11$ molar/atm
2	gas-liquid eqbrm	$\text{HgCl}_2(\text{aq}) = K2 \cdot \text{HgCl}_2(\text{gas})$	$K2 = 1.4\text{E}+006$ molar/atm
3	gas-liquid eqbrm	$\text{Hg}(\text{OH})_2(\text{aq}) = K3 \cdot \text{Hg}(\text{OH})_2(\text{gas})$	$K3 = 1.2\text{E}+004$ molar/atm
4	gas-liquid eqbrm	$\text{O}_3(\text{aq}) = K4 \cdot \text{O}_3(\text{gas})$	$K4 = 0.0113$ molar/atm
5	gas-liquid eqbrm	$\text{SO}_2(\text{aq}) = K5 \cdot \text{SO}_2(\text{gas})$	$K5 = 1.23$ molar/atm
6	gas-liquid eqbrm	$\text{HCl}(\text{aq}) = K6 \cdot \text{HCl}(\text{gas})$	$K6 = 1.1$ molar/atm
7	gas-liquid eqbrm	$\text{Cl}_2(\text{aq}) = K7 \cdot \text{Cl}_2(\text{gas})$	$K7 = 0.076$ molar/atm
8	gas-liquid eqbrm	$\text{H}_2\text{O}_2(\text{aq}) = K8 \cdot \text{H}_2\text{O}_2(\text{gas})$	$K8 = 7.4\text{E}+004$ molar/atm
9	aq phase eqbrm	$\text{HgCl}_2(\text{aq}) \leftrightarrow \text{Hg}^{2+} + 2 \text{Cl}^{-1}$	$K9 = 1.00\text{E}-014$ molar <sup>2</sup>
10	aq phase eqbrm	$\text{Hg}(\text{OH})_2(\text{aq}) \leftrightarrow \text{Hg}^{2+} + 2 \text{OH}^{-1}$	$K10 = 1.00\text{E}-022$ molar <sup>2</sup>
11	aq phase eqbrm	$\text{HCl}(\text{aq}) \leftrightarrow \text{H}^{+} + \text{Cl}^{-1}$	$K11 = 1.7\text{E}+006$ molar
12	aq phase eqbrm	$\text{Cl}_2(\text{aq}) \leftrightarrow \text{HOCl} + \text{Cl}^{-1} + \text{H}^{+}$	$K12 = 5.00\text{E}-004$ molar <sup>2</sup>
13	aq phase eqbrm	$\text{HOCl} \leftrightarrow \text{OCl}^{-1} + \text{H}^{+}$	$K13 = 3.2\text{E}-008$ molar
14	aq phase eqbrm	$\text{SO}_2(\text{aq}) + \text{H}_2\text{O}_2(\text{aq}) \leftrightarrow \text{SO}_4^{-2} + 2 \text{H}^{+}$	$K14 = \text{instantaneous titration}$
15	aq phase eqbrm	$\text{SO}_2(\text{aq}) + \text{H}_2\text{O} \leftrightarrow \text{HSO}_3^{-1} + \text{H}^{+}$	$K15 = 1.23\text{E}-002$ molar
16	aq phase eqbrm	$\text{HSO}_3^{-1} \leftrightarrow \text{SO}_3^{-2} + \text{H}^{+}$	$K16 = 6.6\text{E}-008$ molar
17	aq phase eqbrm	$\text{Hg}^{+2} + \text{SO}_3^{-2} \leftrightarrow \text{HgSO}_3$	$K17 = 5.00\text{E}+012$ molar <sup>-1</sup>
18	aq phase eqbrm	$\text{HgSO}_3 + \text{SO}_3^{-2} \leftrightarrow \text{Hg}(\text{SO}_3)_2^{-2}$	$K18 = 2.5\text{E}+011$ molar <sup>-1</sup>
19	aq phase eqbrm	$\text{Hg}(\text{II})(\text{aq}) \leftrightarrow \text{Hg}(\text{II})(\text{p})$	$K19 = 34$ liters/gram
20	gas phase rxn	$\text{Hg}(0)(\text{g}) + \text{O}_3(\text{g}) \rightarrow \text{Hg}(\text{II})(\text{g})$	$R20 = 3.00\text{E}-020$ cm <sup>3</sup> /molec-sec
21	gas phase rxn	$\text{Hg}(0)(\text{g}) + \text{HCl}(\text{g}) \rightarrow \text{HgCl}_2(\text{g})$	$R21 = 1.00\text{E}-019$ cm <sup>3</sup> /molec-sec
22	gas phase rxn	$\text{Hg}(0)(\text{g}) + \text{H}_2\text{O}_2(\text{g}) \rightarrow \text{Hg}(\text{OH})_2(\text{g})$	$R22 = 8.5\text{E}-019$ cm <sup>3</sup> /molec-sec
23	gas phase rxn	$\text{Hg}(0)(\text{g}) + \text{Cl}_2(\text{g}) \rightarrow \text{HgCl}_2(\text{g})$	$R23 = 4.00\text{E}-018$ cm <sup>3</sup> /molec-sec
24	aq phase rxn	$\text{Hg}(0)(\text{aq}) + \text{O}_3(\text{aq}) \rightarrow \text{Hg}^{+2}$	$R24 = 4.7\text{E}+007$ (molar-sec) <sup>-1</sup>
25	aq phase rxn	$\text{Hg}(0)(\text{aq}) + \text{OH}^{-1}(\text{aq}) \rightarrow \text{Hg}^{+2}$	$R25 = 2.00\text{E}+009$ (molar-sec) <sup>-1</sup>
26	aq phase rxn	$\text{HgSO}_3(\text{aq}) \rightarrow \text{Hg}(0)(\text{aq})$	$R26 = 0.0106$ sec <sup>-1</sup>
27	aq phase rxn	$\text{Hg}(\text{II})(\text{aq}) + \text{HO}_2(\text{aq}) \rightarrow \text{Hg}(0)(\text{aq})$	$R27 = 1.7\text{E}+004$ (molar-sec) <sup>-1</sup>
28	aq phase rxn	$\text{Hg}(0)(\text{aq}) + \text{HOCl}(\text{aq}) \rightarrow \text{Hg}^{+2}$	$R28 = 2.09\text{E}+006$ (molar-sec) <sup>-1</sup>
29	aq phase rxn	$\text{Hg}(0)(\text{aq}) + \text{OCl}^{-1} \rightarrow \text{Hg}^{+2}$	$R29 = 1.99\text{E}+006$ (molar-sec) <sup>-1</sup>

Sulfur dioxide, ozone, and soot concentrations over the model domain were supplied by MSC-East for this study (the data were routinely calculated by MSC-West). As it was agreed by the study participants a constant pH value of 4.5 and chloride ion cloud-water concentration of 2.5 mg/liter were used, per the study specifications. A constant, total concentration of H<sub>2</sub>O<sub>2</sub> equivalent to 1 ppb was

used. For gas-phase reactions in the dry particle situation, a  $\text{Cl}_2$  (gas) concentration of 0.005 ppb was used, and it was assumed that the HCl (gas) concentration in that case was 0.001 times that  $\text{Cl}_2$ (gas) concentration. The gas-phase hydroxyl radical concentration at any point and time in the modeling domain was estimated using an interpolation procedure based on the results of *Lu and Khalil* [1991], who presented modeled concentrations of OH as a function of hour, season, elevation, and latitude. For the dry-particle situation, we assumed that the aerosol was the same everywhere, with a surface area of  $3.5 \times 10^{-6} \text{ cm}^2$  per  $\text{cm}^3$  of air and a typical size distribution [*Bidleman*, 1988], divided into 14 segments, corresponding to a typical distribution [*Whitby*, 1975].

A resistance-based dry deposition algorithm [*Hicks et al.*, 1987; *Wesely*, 1989; *Chang*, 1989; *Draxler and Hess*, 1997] was used for both terrestrial and water surfaces. In formulating the canopy resistance in this methodology, the value of the surface reactivity parameter was assumed to be 1 for gaseous Hg(II). The net dry deposition of Hg(0) was assumed to be zero. For dry deposition of particles and gases to water surfaces, the approach of *Slinn and Slinn* [1980] was used. In this methodology, the deposition resistance in the quasi-laminar sublayer over water is relatively significant, consistent with recent experimental results [*Larsen et al.*, 1995]. In the use of this method, we have used the near-surface particle- growth estimation approach [*Williams*, 1982], assuming 99% humidity in the surface layer. Wet deposition is simulated as three different phenomena: (a) in-cloud particle washout; (b) below-cloud particle scavenging; and (c) vapor-phase wet deposition.

The modeling system used here was originally developed to enable detailed source-receptor information to be obtained. While this feature is not required for this phase of the intercomparison study, the same methodology was used. In this technique, explicit HYSPLIT modeling of emissions from a given location was only performed for a limited number of source locations. These *standard source locations* were chosen to (a) provide satisfactory geographical resolution in areas of strong source emissions; (b) provide satisfactory resolution in the areas close to each receptor of interest; and (c) provide satisfactory resolution for the entire modeling domain. In cases where emissions from a given source were not explicitly simulated, a spatial interpolation method was used to estimate the source's impact on any given receptor based on a weighted average of the nearest explicitly modeled locations. The weighting was done by distance and angular orientation. To deal with the varying proportions of different Hg species being emitted from different sources, separate unit-emissions simulations of Hg(II), Hg(0), and Hg(p) emissions were made at each standard source location. The impact of each actual emissions inventory source – emitting a mixture of Hg(0), Hg(II), and Hg(p) – was estimated based on a linear combination of these “pure-component” unit emissions simulations. In sum, both a spatial and chemical interpolation procedure was used to estimate the impact of each source in the inventory on each receptor of interest.

This methodology assumes that atmospheric fate and transport of mercury from any given source is not influenced by the emissions from any other source, based on the following arguments. First, in the model used here, each of the fate processes affecting mercury species in the atmosphere is algorithmically described by a first-order rate expression (i.e.,  $\text{rate} = \mathbf{k} \cdot \mathbf{c}$ , where  $\mathbf{k}$  is a rate constant and  $\mathbf{c}$  is the concentration of the mercury species). Second, because of its trace concentration in the atmosphere, mercury species are highly unlikely to have any significant effect on concentrations of fate-relevant compounds (e.g.,  $\text{SO}_2$ ,  $\text{O}_3$ ) or processes (e.g., precipitation). Thus, in the case of atmospheric mercury, we believe it is valid to consider mercury sources to be linearly independent of one another. This assumed linear independence is likely to be valid for many other trace pollutants in the atmosphere, but is certainly not valid, for example, for emissions of VOC's and  $\text{NO}_x$ .

## 5.7. The EMAP model description

EMAP (Eulerian Model for Air Pollution) is a simulation model that allows one to describe the dispersion of multiple pollutants [BC-EMEP, 1994-1998; Syrakov, 1995]. Such processes as horizontal and vertical advection, horizontal and vertical diffusion, dry deposition, wet removal, gravitational settling and specific chemical transformations are accounted for in this model. Within EMAP, the semi-empirical diffusion-advection equations for scalar quantities are treated. The numerical solution is based on discretization applied on Arakawa C-type staggered grids. Conservative properties are fully preserved within the discrete model equations. The horizontal resolution depends on the task solved. Vertically, the governing equations are solved in terrain-following coordinates. Non-equidistant grid spacing (log-linear gridding) is settled in that direction. Time splitting is applied as solution technique that transforms the complex problem to a number of simple tasks. For one time step, one-dimensional schemes are applied sequentially for every dimension for advection and diffusion and for all other processes included in the model. As to decrease the splitting error their order is reversed at the next time step. The temporal resolution depends on the Courant stability condition. All related parameters can be defined by the user.

The EMAP model is applied for studying annual acid loads in the region of Southeastern Europe. It is also applied to calculating the Bulgarian impact of lead, cadmium, mercury and benzo(a)pyrene in the same region for different years [BC-EMEP, 1994-1998]. The model passed validation and evaluation in some international exercises: participation in the ETEX study, its results ranged 9th among 34 models [Syrakov and Prodanova, 1997]; EMEP/MSC-E inter-calibrations of lead and cadmium models [Syrakov and Galperin, 1997a; Gussev et al., 2000].

Advective terms are treated with the TRAP scheme [Syrakov, 1996; Syrakov and Galperin, 1997b], which is a Bott type (i.e. flux-type) one. The version applied in the model is 1st order explicit in time and 3rd order Bessel polynomial is used for fitting the concentration distribution in the space around any grid point. While displaying the same simulation properties as the Bott scheme (explicitness, conservativeness, positive definiteness, transport ability, limited numerical dispersion), the TRAP-scheme occurs to be several times faster. The advective boundary conditions are fixed at income flows and 'open boundary' type – at outcome ones. Special version of the scheme able to perform on non-equidistant grid is applied to vertical direction.

Turbulent diffusion equations are digitized by means of the simplest implicit (vertical) and explicit (horizontal) schemes. The accuracy of both schemes is 1st order in time and 2nd order in space. The horizontal diffusion coefficients are constants (defined by the user), the vertical diffusion coefficient can vary in space and time. The lateral boundary conditions for diffusion are of the 'open boundary' type. The bottom boundary condition for the vertical diffusion equation is flux-type; the top boundary condition is optionally of an 'open boundary' and 'hard-lid' type.

The dry deposition is accounted for as bottom boundary condition in the vertical diffusion equation. The dry deposition flux is determined as roughness level concentration multiplied by the dry deposition velocity. The last parameter depends on many factors. In EMAP, it is assumed to be dependent only on the type of the pollutant and on the character of land coverage and must be specified in advance. As surface level concentration is necessary for calculating the dry deposition flux, in the surface layer (SL), a parameterization is applied permitting one to have the first computational level at the top of the SL. This parameterization provides a good estimate for the roughness level concentration and accounts also for the action of continuous sources on the earth surface [Syrakov and Yordanov, 1998]. The gravitational settling and the wet removal of pollutants carried by aerosols are described on the base of Galperin's parameterization [Syrakov and Galperin, 1997a].

The simplest “first-order mechanism” approach is applied to describe the wet removal process. Corresponding coefficient depends on pollutant properties and on rain intensity.

The mercury scheme developed in MSC-East [Ryaboshapko *et al.*, 2001] is incorporated in the model describing the transformation of 8 Hg species in air and cloud droplets. Elemental mercury, gaseous oxidised mercury (treated as HgCl<sub>2</sub>) and particulate mercury (treated as HgCl<sub>2</sub>) are emitted to the atmosphere by anthropogenic sources. Particulate mercury (TPM) is divided to two equal parts – soluble and insoluble ones that further evolve separately. The first form is entirely adopted by cloud water, if any. The second one does not take part in wet reactions. It is believed that in air only oxidation by ozone takes place, and the products are treated as HgCl<sub>2</sub>. Different transformations between species occur in the cloud liquid phase. Some of them depend on the sun height, which is calculated for every grid point and a day of the year.

## **5.8. Similarities and distinctions**

As it follows from the model descriptions above the models are different in their horizontal scales, in their vertical extent, in treatment of removal mechanisms, and in treatment of atmospheric transport and dispersion (Eulerian and Lagrangian) approaches. At the same time there are similarities in the models. All the models use more or less similar chemical schemes. The modellers consider ozone both in gas and in liquid phase as the main oxidant of elemental mercury. In the liquid phase of cloud droplets both oxidation and reduction processes are taken into account. Application of the sulfite mechanism of mercury reduction is common for all models. In addition to this mechanism reduction by HO<sub>2</sub> radical is included into three models.

A very important characteristic when short-term variability of mercury concentration is simulated is the spatial resolution of the model. It may be critical if any local emission sources are situated in the vicinity of the calculating point (location monitoring station). In the case of coarse resolution an emission source can be located within the same grid cell as the calculating point. This can lead to distortion of the modelling results.

All mentioned differences and similarities should be taken into account when the modelling data are compared with the observations or with other modelling data. The main properties of the participating models are presented in Table 5.3.

**Table 5.3.** Main properties of the participating models

Model	Type	Scale/domain	Model top height, m	Resolution	Boundary concentrations			Oxidation agents		Reduction agents
					Hg(0) <sub>3</sub> , ng/m <sup>3</sup>	RGM <sub>3</sub> , pg/m <sup>3</sup>	TPM <sub>3</sub> , pg/m <sup>3</sup>	Gas phase	Liquid phase	Liquid phase
CMAQ-Hg	Eulerian	Regional/Central–Northern Europe	about 15000	36 x 36 km	1.7 <sup>(a)</sup>	17 <sup>(a)</sup>	17 <sup>(a)</sup>	O <sub>3</sub> , H <sub>2</sub> O <sub>2</sub> , Cl <sub>2</sub> , OH <sup>•</sup>	O <sub>3</sub> , OH <sup>•</sup> , HOCl, OCl <sup>•</sup>	SO <sub>3</sub> <sup>•-</sup> , hv, HO <sub>2</sub>
ADOM	Eulerian	Regional, Central Europe	10000	55 x 55 km	1.5	2	20	O <sub>3</sub>	O <sub>3</sub>	SO <sub>3</sub> <sup>•-</sup>
HYSPLIT	Lagrangian	Regional	15000	36 x 36 km, 108 x 108 km <sup>(b)</sup>	(c)	(c)	(c)	O <sub>3</sub> , H <sub>2</sub> O <sub>2</sub> , Cl <sub>2</sub> , HCl	O <sub>3</sub> , OH <sup>•</sup> , HOCl, OCl <sup>•</sup>	SO <sub>3</sub> <sup>•-</sup> , HO <sub>2</sub>
EMAP	Eulerian	Regional/EMEP	5000, 8 layers	50 x 50 km	1.5	10	10	O <sub>3</sub> , OH <sup>•</sup>	O <sub>3</sub>	SO <sub>3</sub> <sup>•-</sup>
GRAHM	Eulerian	Global	about 30000	1 x 1 degree	No	No	No	O <sub>3</sub>	O <sub>3</sub>	SO <sub>3</sub> <sup>•-</sup>
DEHM	Eulerian	Hemispheric	15000	50 x 50 km 150 x 150 km <sup>(d)</sup>	1.5	0	0	O <sub>3</sub>	O <sub>3</sub>	SO <sub>3</sub> <sup>•-</sup>
MSCE-Hg	Eulerian	Regional/EMEP	3900	50 x 50 km	1.6-1.7 <sup>(e)</sup>	0	20	O <sub>3</sub> <sup>(f)</sup>	O <sub>3</sub>	SO <sub>3</sub> <sup>•-</sup> , HO <sub>2</sub>

<sup>(a)</sup> – at 288°K, 1 atm;

<sup>(b)</sup> – for primary domain and outside the domain, respectively;

<sup>(c)</sup> – cannot be specified for Lagrangian model in an explicit form;

<sup>(d)</sup> – for EMEP domain and outside the domain, correspondingly;

<sup>(e)</sup> – depending on a boundary;

<sup>(f)</sup> – temperature dependent.

## Chapter 6

# COMPARISON OF INDIVIDUAL MODEL RESULTS AGAINST OBSERVATIONS

The comparison of the results of the calculations by each participating model and the observations are presented below in graphical and tabular forms. The graphs and tables demonstrate to what extent this or that model can follow the observational variations, including the peaks of elevated concentrations.

Basic statistical parameters for modelled against observed values are the following:

- **Relative Bias ( $R_{bias}$ )** between the observations and modelling for the whole episode as a measure of closeness of arithmetic mean values of the modelled and observed results;  $R_{bias}$  is determined as

$$R_{bias} = ABS\left[\frac{(Observational\ Arithmetic\ Mean) - (Calculated\ Arithmetic\ Mean)}{Observational\ Arithmetic\ Mean}\right] * 100\% .$$

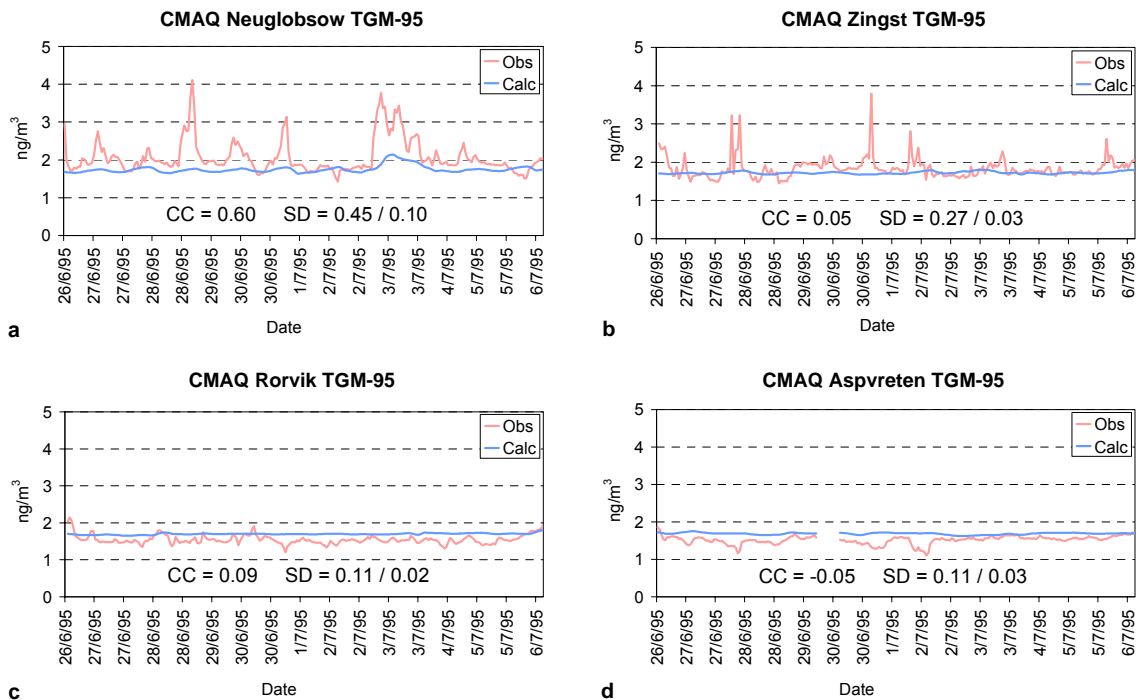
- **Standard Deviation (SD)** as a measure of variability both observational and modelling results; it can reflect influence of strong emission sources in the vicinity of a station.
- **Correlation Coefficient (CC)** as a measure of synchronism of variations of both observational values and modelling values.
- **Factor Two Coverage ( $F_2$ )** as a measure of closeness of the comparison results to the theoretical regression line; it is determined as a number of results (in per-cent), which are within the factor of 2.
- **Mean Deviation Factor ( $F_{mean}$ )** as a measure of scattering of the comparison results; it is obtained as a geometric mean value of all ratios of the greater to the smaller concentration values in each compared pair.

To provide strict comparability of measured and calculated data the result series were reduced to the same size. For example, for the first episode all time series were reduced to the period from 12:00 26.06.1995 to 00:00 06.07.1995 (the shortest series was produced by the ADOM model). In some cases the observed data had gaps in the time series. These gaps were filled using a linear interpolation method.

Results of statistical treatment (correlation coefficients, for example) depend on periods of averaging. In the case of TGM two versions of averaging is used: hourly and daily means. In the first case one can see the ability of the models to reproduce very short-term variations of the observed values. In the second case more smooth curves give general concepts of agreements between the observations and the modeling results.

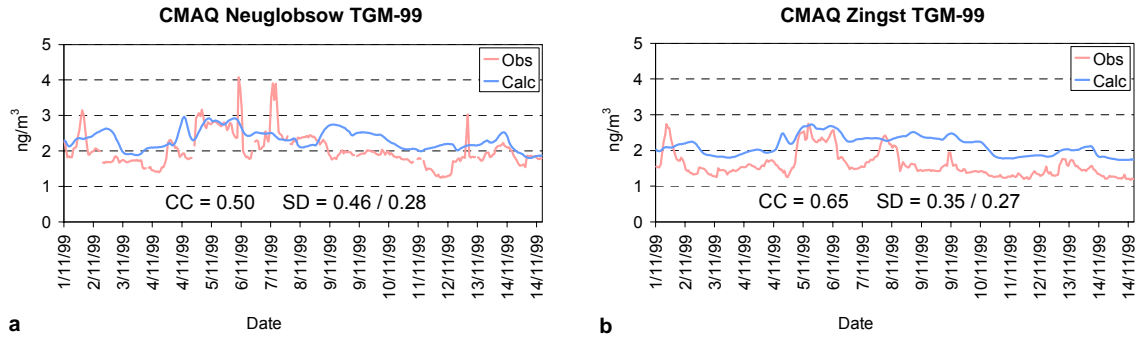
## 6.1. The CMAQ model

Fig. 6.1 shows the results of observations of TGM during the first episode and corresponding modelling curves with 1-hour time resolution. Correlation coefficients between the observations and calculations as well as standard deviation values (observations/calculations) are also presented in this figure (these parameters will be presented in all similar figures below). For Neuglobsow station (Fig. 6.1a) the model reproduces practically all observational peaks, that is confirmed by significant correlation coefficient (0.60). However, these peaks are much less pronounced in calculation results. It is naturally, that SD value of the observations is higher than the calculations (0.45 against 0.10). In general, the base-lines of the observations and the modelled data coincide ( $1.8\text{-}1.9\text{ ng/m}^3$ ). The same coincidence is characteristic of Zingst station (Fig. 6.1b). At this station the observational peaks are rather high but very narrow and sharp. The model cannot reproduce such peaks. Observational variability at Roervik and Aspvreten stations (Figs. 6.1c – 6.1d) is not very high and rather chaotic. Both for the observations and for calculations SD value is low. From time to time observed concentrations drop down to about  $1.1\text{ ng/m}^3$ . In contrast, the modelled curves are rather smooth. One can note that the base-line for the modelling data are about  $0.2\text{ ng/m}^3$  higher than for the observations. Most likely, it is connected with overestimation in the model of the boundary TGM concentration in the Arctic sector of the domain.



**Figure 6.1.** Modelled TGM concentrations by CMAQ against observed ones during the 1995 episode:  
a - Neuglobsow; b - Zingst; c - Roervik; d - Aspvreten stations

During the second episode (1999) the Swedish stations did not measure TGM concentrations. The comparisons of values modelled by CMAQ with observations at German stations are demonstrated in Fig. 6.2. One can see that in general the model can reproduce the shapes of the observational curves. In both cases the correlation coefficients are significant (0.50 for Neuglobsow and 0.65 for Zingst). It is important to note that as a whole the model overestimates the observations – 1.2 times at Neuglobsow and 1.3 times at Zingst. Most likely, it is connected with the fact that the emission for 1995 was used in the calculations while real anthropogenic emission has been reduced by 1999. The calculated curves are smoother than the observational ones. It is confirmed by lower SD values.



**Figure 6.2.** Modelled TGM concentrations by CMAQ against observed ones during the 1999 episode  
a - Neuglobsow; b - Zingst stations

The daily mean values have, naturally, no sharp peaks both for observations and modeling results. The comparison of daily mean data for both episodes is shown in Fig. 6.3 (a-d). One can see that for 1995 the model reproduces both absolute values of the concentrations and the day-to-day variations. For 1999 the model overestimates the observations but all day-to-day variations are captured. As a whole, the correlation coefficients of daily mean values are higher than of hourly mean ones.

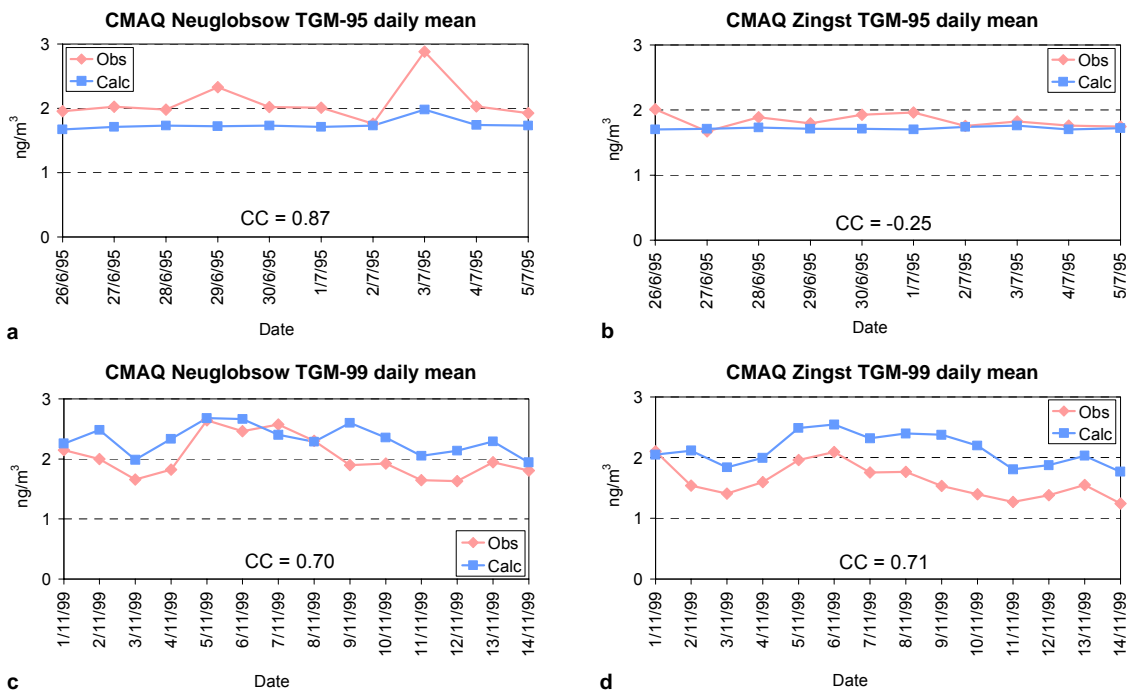


**Figure 6.3.** Comparison of daily mean values of CMAQ modeled and observed concentrations for:  
a - Neuglobsow in 1995; b - Zingst in 1995; c - Neuglobsow in 1999; d - Zingst in 1999

The second episode pays more attention to the comparison of RGM and TPM concentrations. Fig. 6.4 represents the observed and simulated RGM concentration values at German and Swedish stations (RGM was not sampled at Zingst). For Neuglobsow (Fig. 6.4a) it is possible to note significant (more than 3 times) overestimation of the concentrations. For Swedish stations the agreement is much better (Fig. 6.4b and c). The number of RGM measurements at each station (as well as TPM measurements) is low for any statistical treatment. Hence, the data from all stations were combined into one statistical sample. The plot for all compared pairs is showed in Fig. 6.4d. The regression line (CAL=2.30\*OBS) indicates obvious overestimation by the model and scattering of the results.

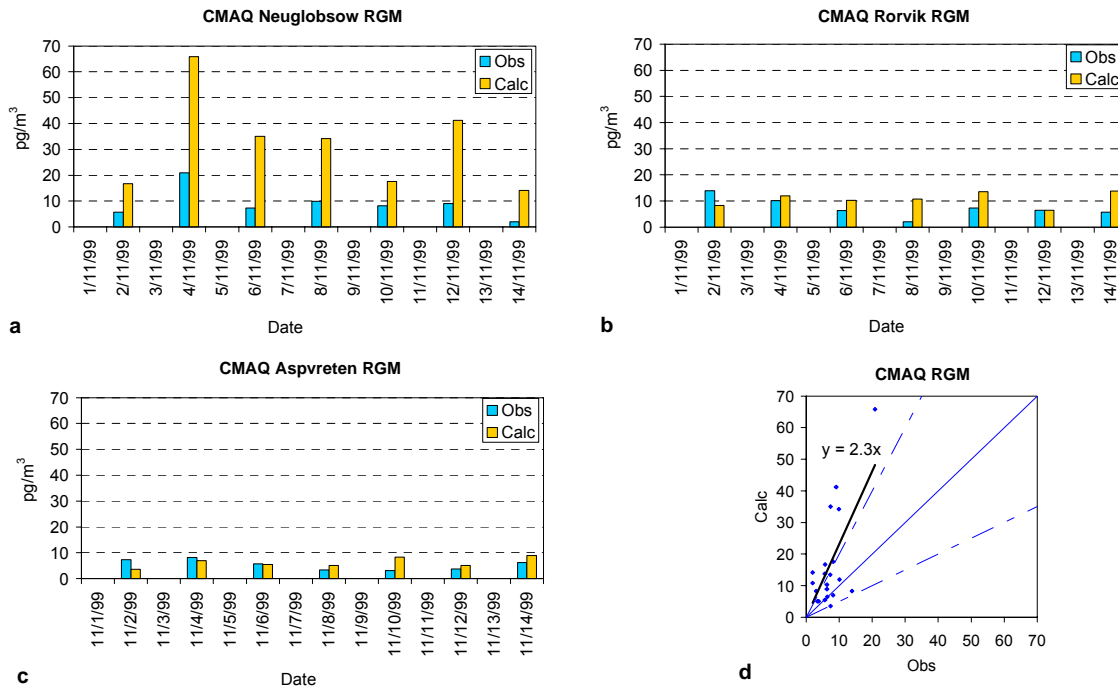


**Figure 6.4.** Modelled RGM concentrations by CMAQ against observed ones during the 1999 episode: a - Neuglobsow; b - Roervik; c - Aspveten station; d - regression for all compared pairs

The comparison of the data for TPM is presented in Fig. 6.5 for four stations. The model obviously overestimates the TPM concentrations especially for Swedish stations. For the most polluted Neuglobsow station the difference between observations and calculations is on the level of the factor of 2. The comparison of all pairs is showed in Fig. 6.5e. The regression line (CAL=1.82\*OBS) lies much higher than the theoretical “one-by-one” line. Practically all dots are outside the area of the factor of 2.

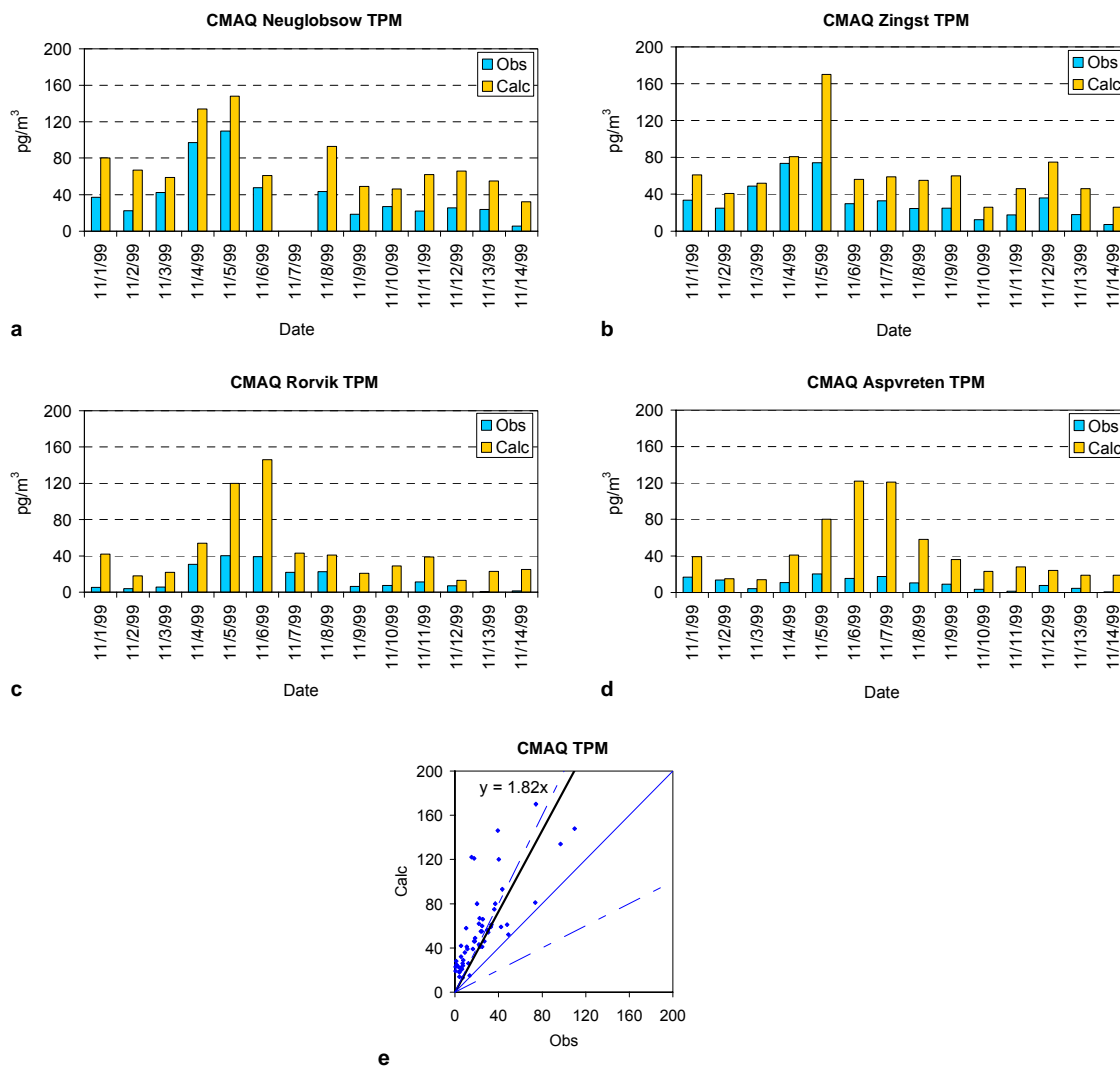
The statistical parameters characterizing the CMAQ results for RGM and TPM are summarized in Table 6.1.

**Table 6.1.** Statistical parameters for the RGM and TPM results obtained by CMAQ model

Parameter	RGM	TPM
CC	0.68	0.77
R <sub>bias</sub> , %	125	133
F <sub>2</sub> , %	48	29
F <sub>mean</sub>	2.2	3.1

Analyzing the data in the table one should note rather high correlation coefficients both for RGM and TPM. At the same time the difference between observations and calculations is noticeable. Less than half the ratios in both cases are within the factor of 2. The model systematically overpredicts the concentration values.

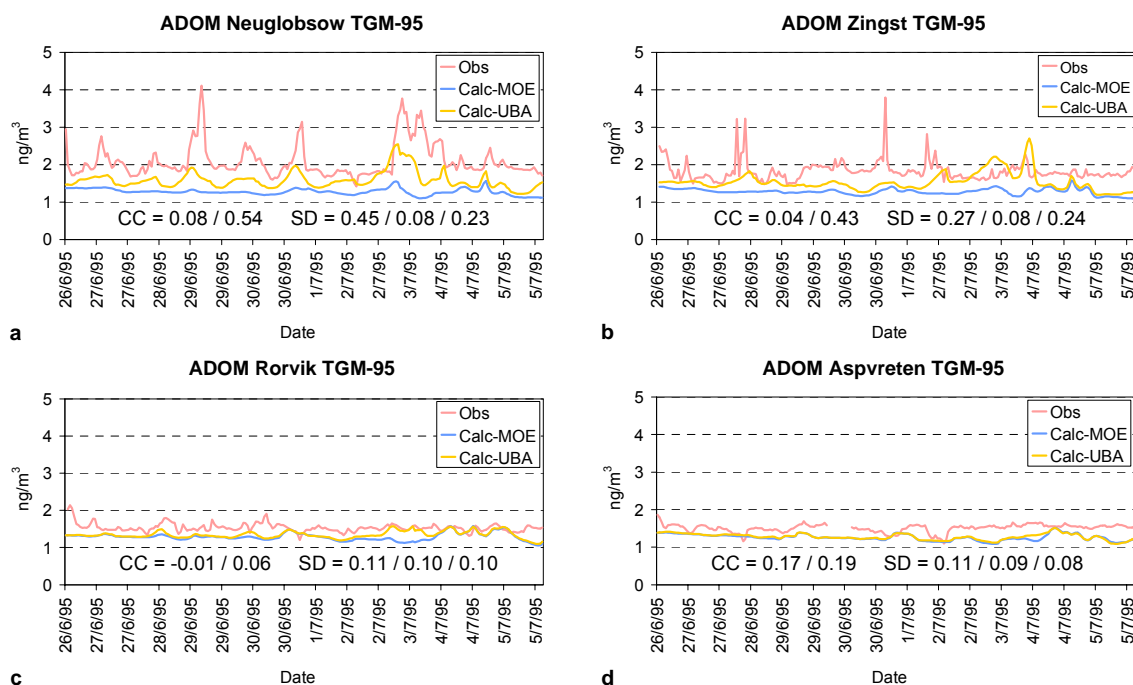
In addition to the "standard" program of the comparison, sensitivity of the CMAQ model to soot concentration in air was checked. It was revealed that a five-fold increase of soot concentration lead to a very small increase in TPM concentration (5% on average) and to a very small decrease in RGM concentration (3% on average). Also, the variations in soot concentration did not significantly affect the elemental mercury concentrations estimated by this model.



**Figure 6.5.** Modelled TPM concentrations by CMAQ against observed ones during the 1999 episode: a – Neuglobsow; b – Zingst; c – Rorvik; d - Aspvreten stations; e – regression for all compared pairs

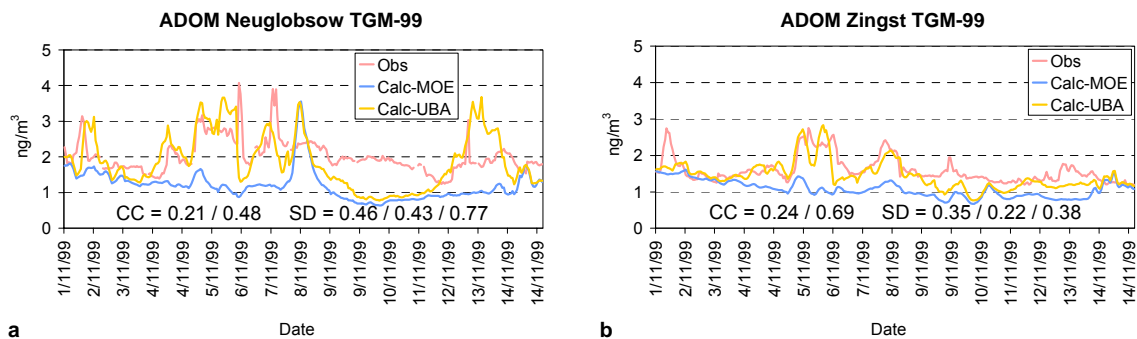
## 6.2. The ADOM model

Two calculation runs were done by ADOM using two emission scenarios – the scenario for 1995 (mentioned as MOE-scenario) and for 1990 (mentioned as UBA-scenario). In chapter 3 it was explained that the anthropogenic emission according to the UBA-scenario was considerably higher and included some strong point sources in southeast Germany. The results for the first episode are showed in Fig. 6.6 (CC for MOE/UBA; SD for OBS/MOE/UBA). At Neuglobsow the MOE scenario gives a very smooth curve for TGM (Fig. 6.6a) and SD is very low (0.08). In this case the calculated base-line is obviously lower than the observed one. The correlation coefficient is insignificant (0.08). The situation becomes much better when UBA-scenario is used. The calculation curve repeats all observed peaks, however it is still lower than the observed one. Correlation coefficient becomes significant (0.54). The SD value increases to 0.23. For the other stations (Fig. 6.6 b,c,d) the UBA scenario gives slightly higher TGM concentrations, closer to the observations. However, the correlations for these stations are insignificant.



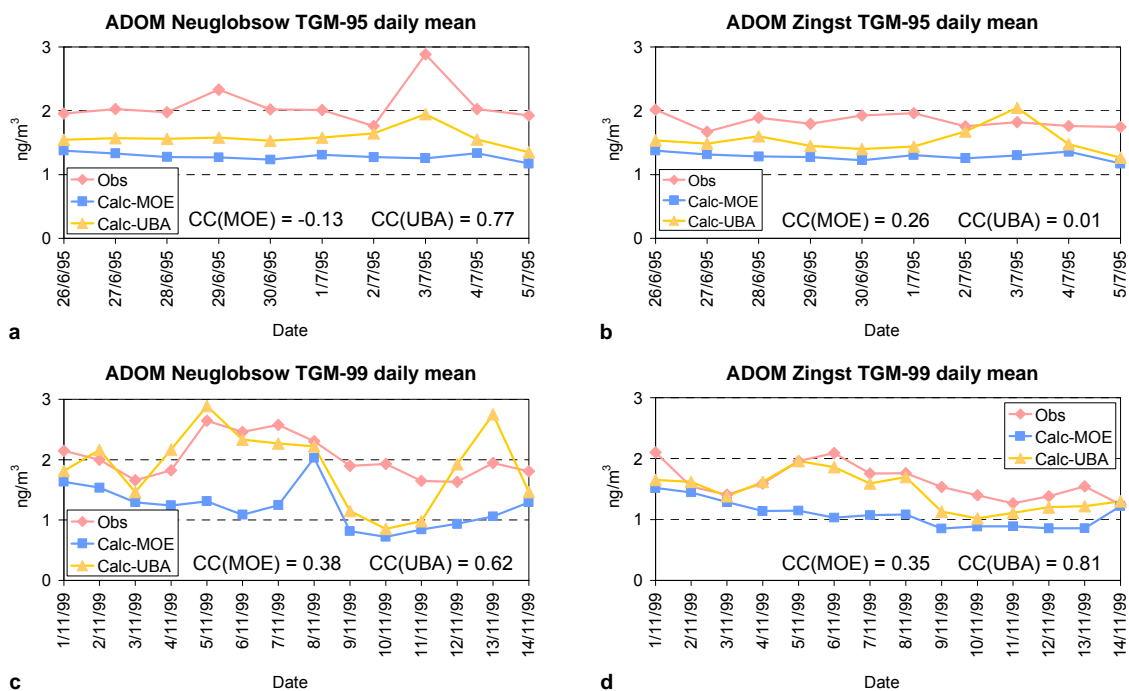
**Figure 6.6.** Modelled TGM concentrations by ADOM against observed ones during the 1995 episode: a - Neuglobsow; b - Zingst; c - Rorvik; d - Aspvreten stations

The 2<sup>nd</sup> episode comparisons of modelled values by ADOM with TGM observations are demonstrated in Fig. 6.7 (a and b). Again the two emission scenarios were used. In general, the second scenario gives much better agreement than the first one. The model reproduces well the shapes of the observational curves and the amplitudes of some peaks in this case. The better agreement is confirmed by higher significant correlation coefficients. The SD values for calculated curves are closer to the observational SD.



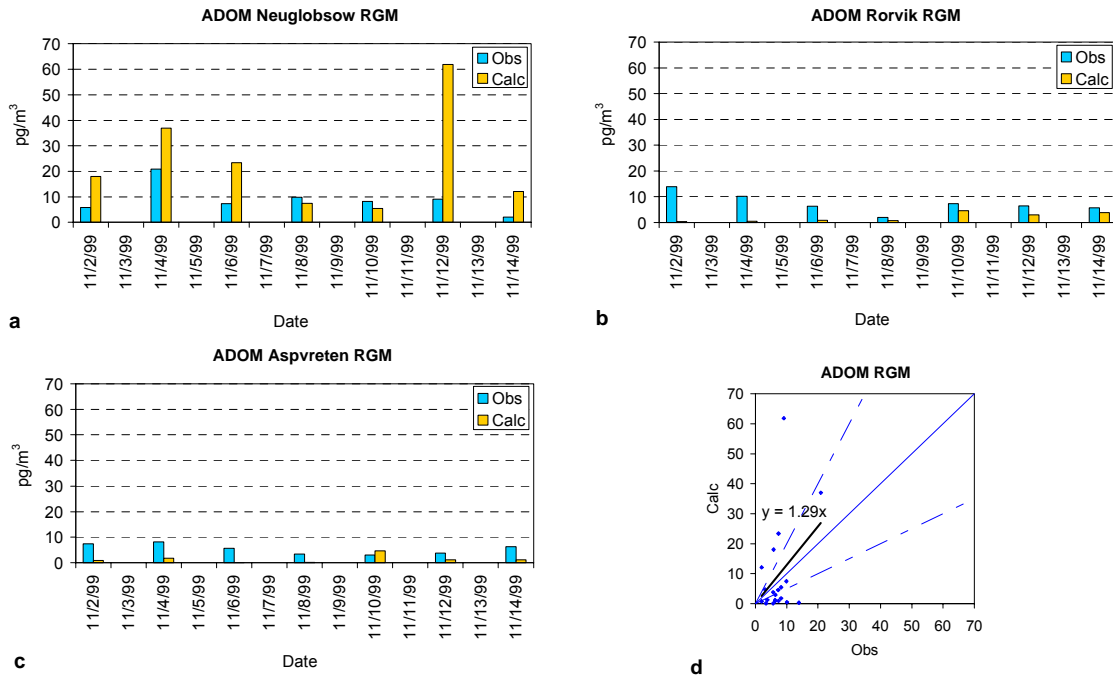
**Figure 6.7.** Modelled TGM concentrations by ADOM against observed ones during the 1999 episode  
 a - Neuglobsow; b - Zingst stations

The comparison of daily mean data for both episodes is shown in Fig. 6.8 (a-d). For 1995 the model underpredicts the daily mean concentrations when both emission scenarios are used. However, for Neuglobsow the UBA scenario gives very good correlation between the modeled and observed values. Role of emission scenarios becomes obvious in the case of the second episode: correlation coefficients for the UBA scenario are significantly higher than for the MOE scenario. Moreover, the UBA scenario provides good agreement between the compared concentration values.



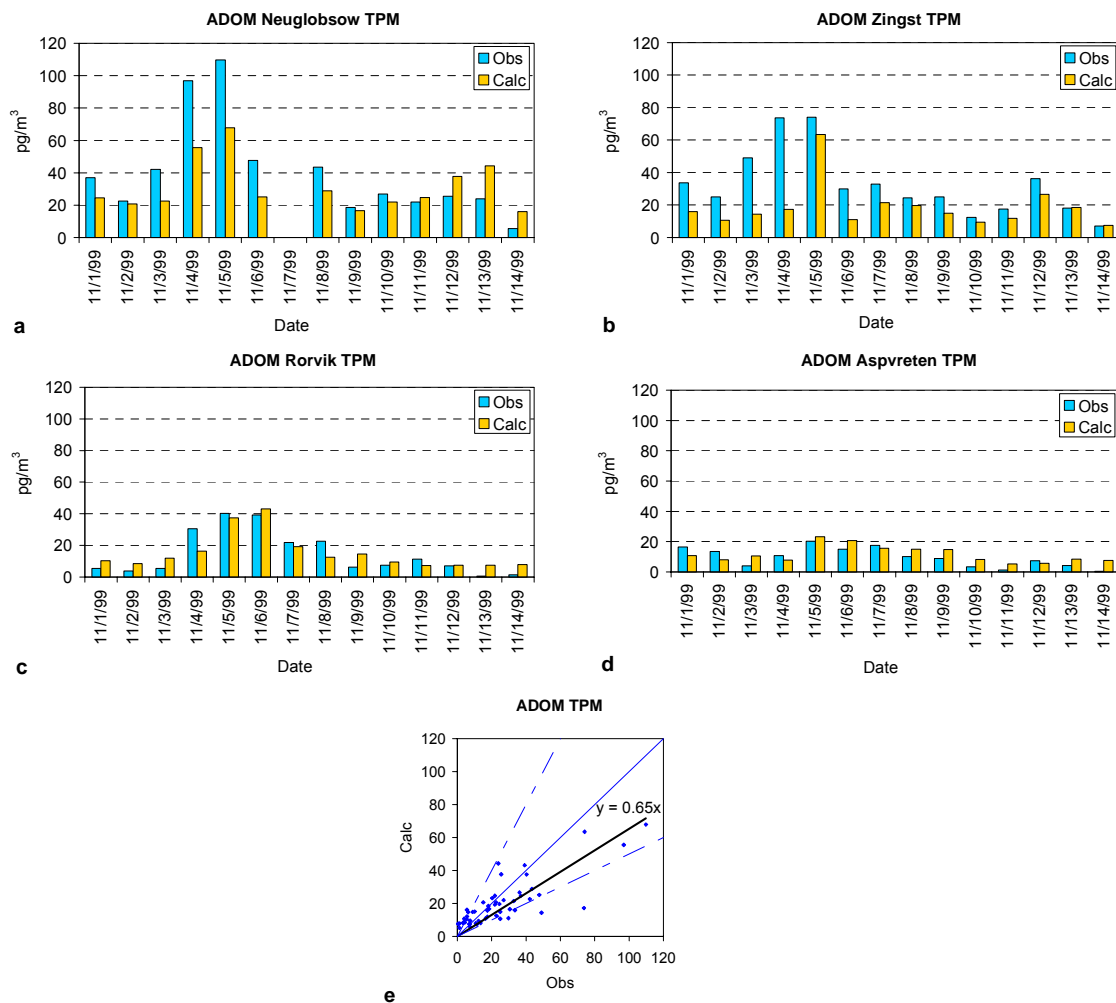
**Figure 6.8.** Comparison of daily mean values of ADOM modeled and observed concentrations for:  
 a - Neuglobsow in 1995; b - Zingst in 1995; c - Neuglobsow in 1999; d - Zingst in 1999

Fig. 6.9 demonstrates the observed and simulated (MOE-1995 emission) by ADOM concentrations of RGM at German and Swedish stations. For Neuglobsow (Fig. 6.9a) it is possible to note that the model generally overestimates the observations. For Swedish stations the pictures are opposite – the model as usual underestimates the observations (Fig. 6.9b and c). As in the case of the CMAQ model (and below – for all other models) the data from all stations were combined into one statistical sample. The plot for all compared pairs of RGM concentrations is showed in Fig. 6.9d. The figure demonstrates a wide scattering of the results. However, the regression line ( $CAL=1.29*OBS$ ) is not so far from the theoretical line.



**Figure 6.9.** Modelled RGM concentrations by ADOM against observed ones during the 1999 episode: a – Neuglobsow; b – Roervik; c – Aspvreten station; d – regression for all compared pairs

The comparison of the data for TPM is presented in Fig. 6.10 for four stations. One can mention a good agreement between the observations and the calculations (MOE-1995 emission), especially for Swedish stations (Fig. 6.10c and d). The comparison of all pairs is showed in Fig. 6.10e. The regression line ( $CAL=0.65*OBS$ ) lies somewhat lower than the theoretical “one-by-one” line. Most of the dots are within the lines of the factor of 2.



**Figure 6.10.** Modelled TPM concentrations by ADOM against observed ones during the 1999 episode: a - Neuglobsow; b - Zingst; c - Roervik; d - Aspvreten stations; e - regression for all compared pairs

The statistical parameters, which characterize the ADOM results, are given in Table 6.2.

**Table 6.2.** Statistical parameters for the RGM and TPM results obtained by ADOM model (MOE-1995 emission)

Parameter	RGM	TPM
CC	0.40	0.81
R <sub>bias</sub> , %	19	21
F <sub>2</sub> , %	29	71
F <sub>mean</sub>	4.9	1.8

The data in the table show that the model can satisfactorily reproduce the TPM concentrations. The correlation coefficient is very high. Mean deviation factor is close to 2. The average calculated TPM concentration for all samples is only 21% lower than corresponding observational value. The RGM data show that the model gives very high scattering of the results. The correlation is insignificant and mean deviation factor is higher than 10. At the same time mean values for all observations and calculations are very close to each other.

### 6.3. The MSCE-Hg model

Two calculation runs were also done by MSCE-Hg model using two emission scenarios – the MOE-scenario and the UBA-scenario. The results for the first episode are presented in Fig. 6.11 (CC for MOE/UBA; SD for OBS/MOE/UBA). At Neuglobsow the MOE scenario gives a very smooth curve for TGM (Fig. 6.11a). The SD for the calculated curve is only 0.12 against 0.45 for observations. The calculated base-line is about  $0.5 \text{ ng/m}^3$  lower than the observed one. When UBA-scenario is used, the calculation curve follows all observed peaks. The amplitudes of the large peak of July 3 practically coincide. Correlation coefficient becomes higher – 0.55. The SD value increases to 0.55. For Zingst station (Fig. 6.11b) the UBA scenario gives slightly higher TGM concentrations. Some peaks are captured, however, the correlation coefficients for Zingst are insignificant. For Roervik and Aspvreten one can mention the coincidence of the base-lines of the TGM concentrations. The calculation curves in these cases are very smooth (SD is 0.03 for both stations).

The comparisons of values modelled by MSCE-Hg (MOE-1995 emission) with TGM observations for the 2<sup>nd</sup> episode are demonstrated in Fig. 6.12 (a, b and c). For Neuglobsow the calculating curve coincides generally with the observational one, while for Zingst it is obviously higher. In both cases the correlation coefficients are poor. Fig. 6.12c shows the results for Mace Head station. Because the model is of a regional character the calculated values should reflect mainly the prescribed boundary concentration of the TGM. Both curves are smooth. At the beginning of the calculating period the model underpredicts the concentration (about  $0.3 \text{ ng/m}^3$ ) and by the end of the period the calculations practically coincide with the observations. In this case there is no sense to evaluate the correlation coefficients.

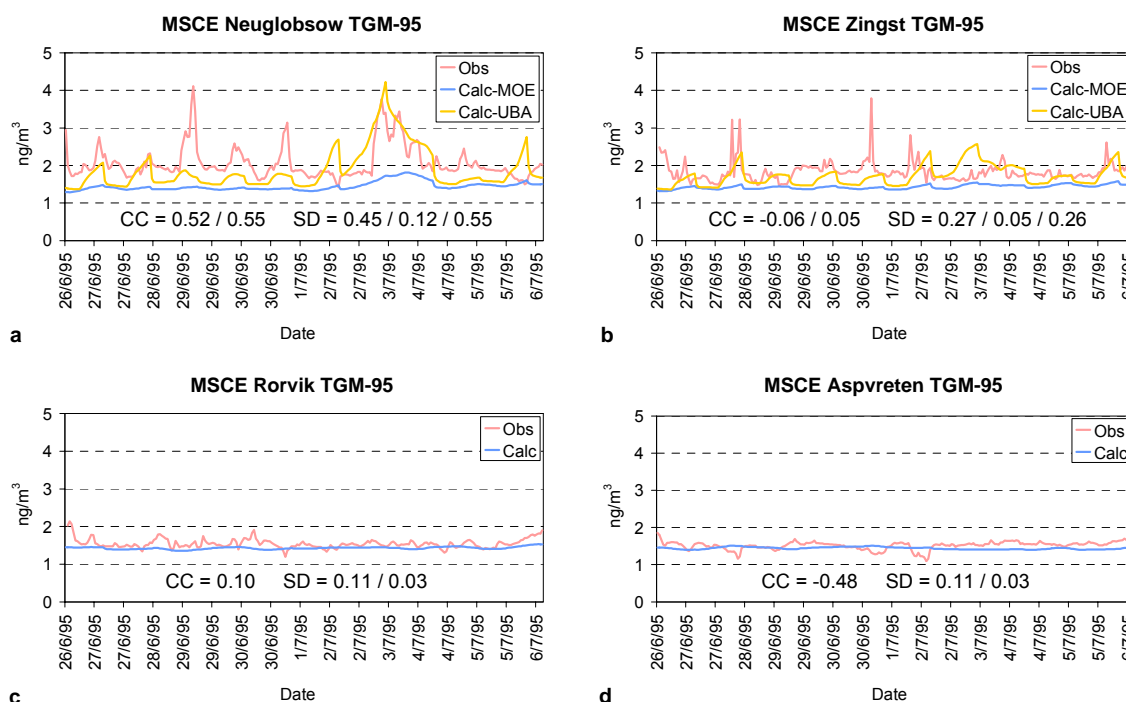


**Figure 6.11.** Modelled TGM concentrations by MSCE-Hg against observed ones during the 1995 episode:  
a - Neuglobsow; b - Zingst; c - Roervik; d - Aspvreten stations

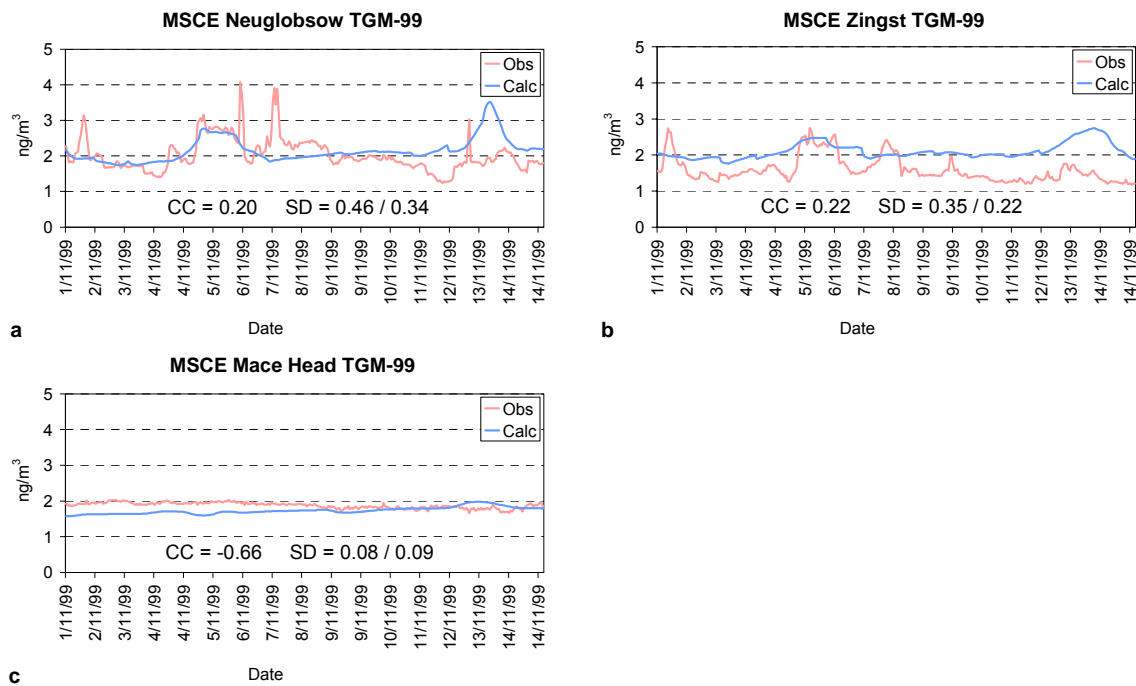


**Figure 6.12.** Modelled TGM concentrations by MSCE-Hg model against observed ones during the 1999 episode  
 a - Neuglobsow; b - Zingst; c - Mace Head stations

The comparison of daily mean TGM data obtained by MSCE-Hg model for both episodes is shown in Fig. 6.13 (a-d). For 1995 the model underpredicts the daily mean concentrations when both emission scenarios are used, however, the UBA results are obviously closer to the observations. As in the case of ADOM model the MSCE-Hg model reproduce well the shapes of the observational curves for the second episode at both stations.

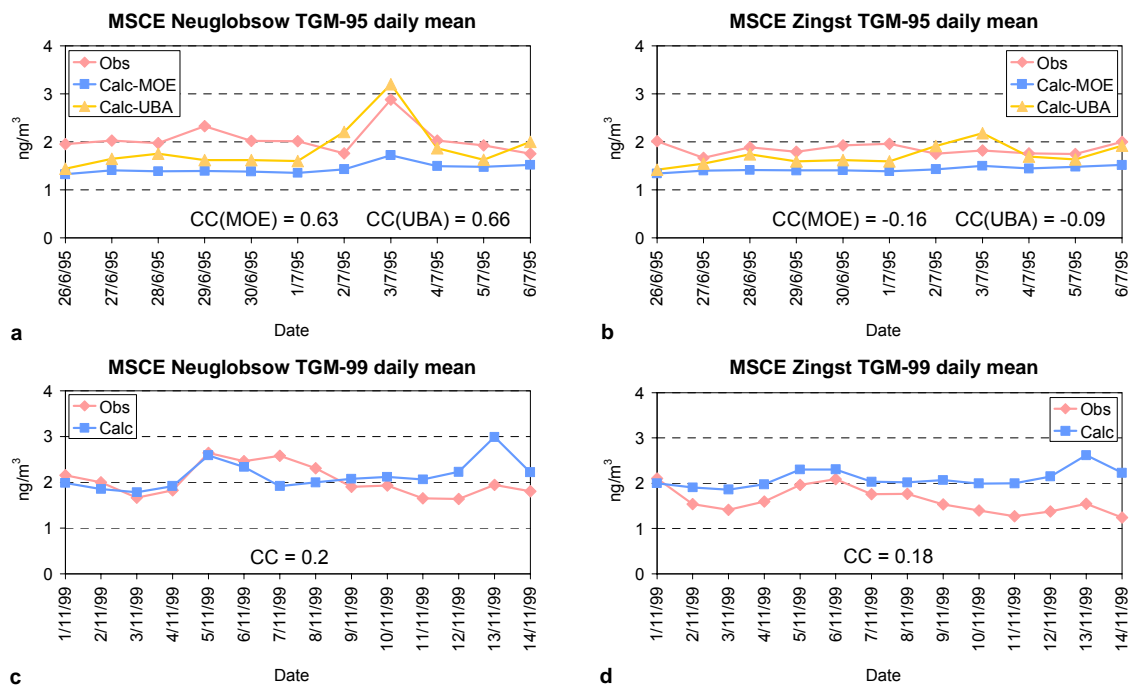


**Figure 6.13.** Comparison of daily mean values of MSCE-Hg modeled and observed concentrations for:  
 a - Neuglobsow in 1995; b - Zingst in 1995; c - Neuglobsow in 1999; d - Zingst in 1999

Fig. 6.14 demonstrates the observed and simulated by MSCE-Hg concentrations of RGM. One can mention a very poor correspondence between calculated and measured concentrations. For Neuglobsow (Fig. 6.14a) the model generally overestimates the observations. For Swedish stations the pictures are uncertain and the data are scattering widely (Fig. 6.14b and c). At Mace Head in the beginning of the episode a very stable western transport of air masses was observed (Chapter 4). In accordance with the model parameterization the RGM concentrations in this case should be close to zero. Surprisingly, the measured concentrations during this period were relatively high (Fig. 6.14d). Starting with November 8 the station was influenced by polluted continental air masses. In this case the model predict noticeable RGM concentrations, however, they are lower than the observed ones.

The plot for all compared pairs of RGM concentrations calculated by MSCE-Hg (MOE-1995 emission) is presented in Fig. 6.14e. It demonstrates a wide scattering of the results. Only a few dots are within the lines of the factor of 2. Nevertheless, the regression line ( $CAL=0.74*OBS$ ) is close to the theoretical one.

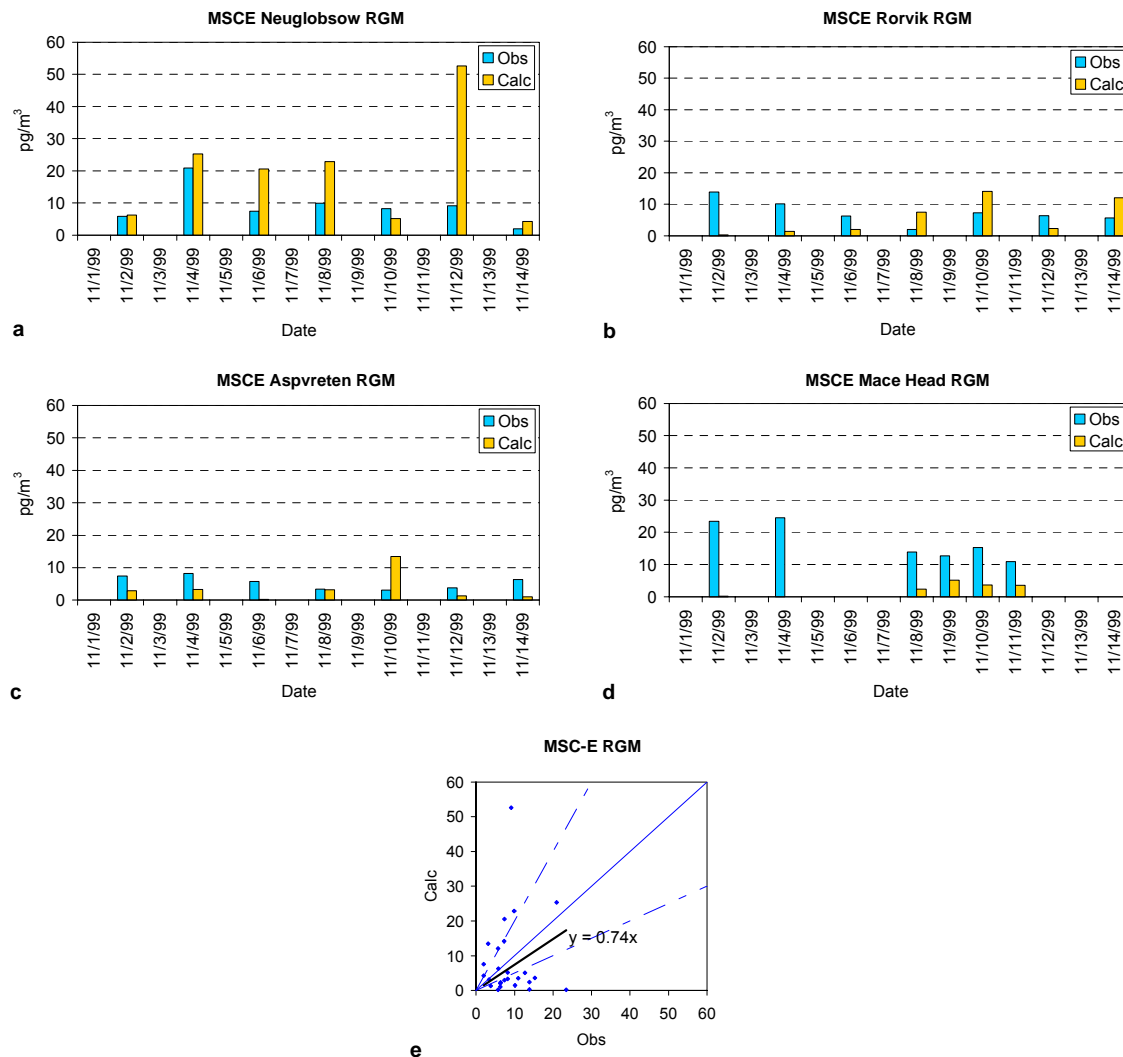


**Figure 6.14.** Modelled RGM concentrations by MSCE-Hg against observed ones during the 1999 episode: a - Neuglobsow; b - Roerвик; c - Aspvreten; d - Mace Head stations; e - regression for all compared pairs

The comparison of the data for TPM is presented in Fig. 6.15 for all five stations. It is possible to mention a good agreement between the calculations and the observations at German stations (Fig. 6.15a and b). The results for the Swedish stations are characterized by higher scattering. It is interesting to mention that the results for Mace Head correspond to changes in synoptical situation. Air mass transport from the continent is described well both by the observations and by the calculations (Fig. 6.15e). The comparison of all pairs is showed in Fig. 6.15f. The regression line ( $CAL=0.76*OBS$ ) is close to the theoretical “one-by-one” line. Most of the dots are within the lines of the factor of 2. The statistical parameters, which characterize the MSCE-Hg results, are given in Table 6.3.

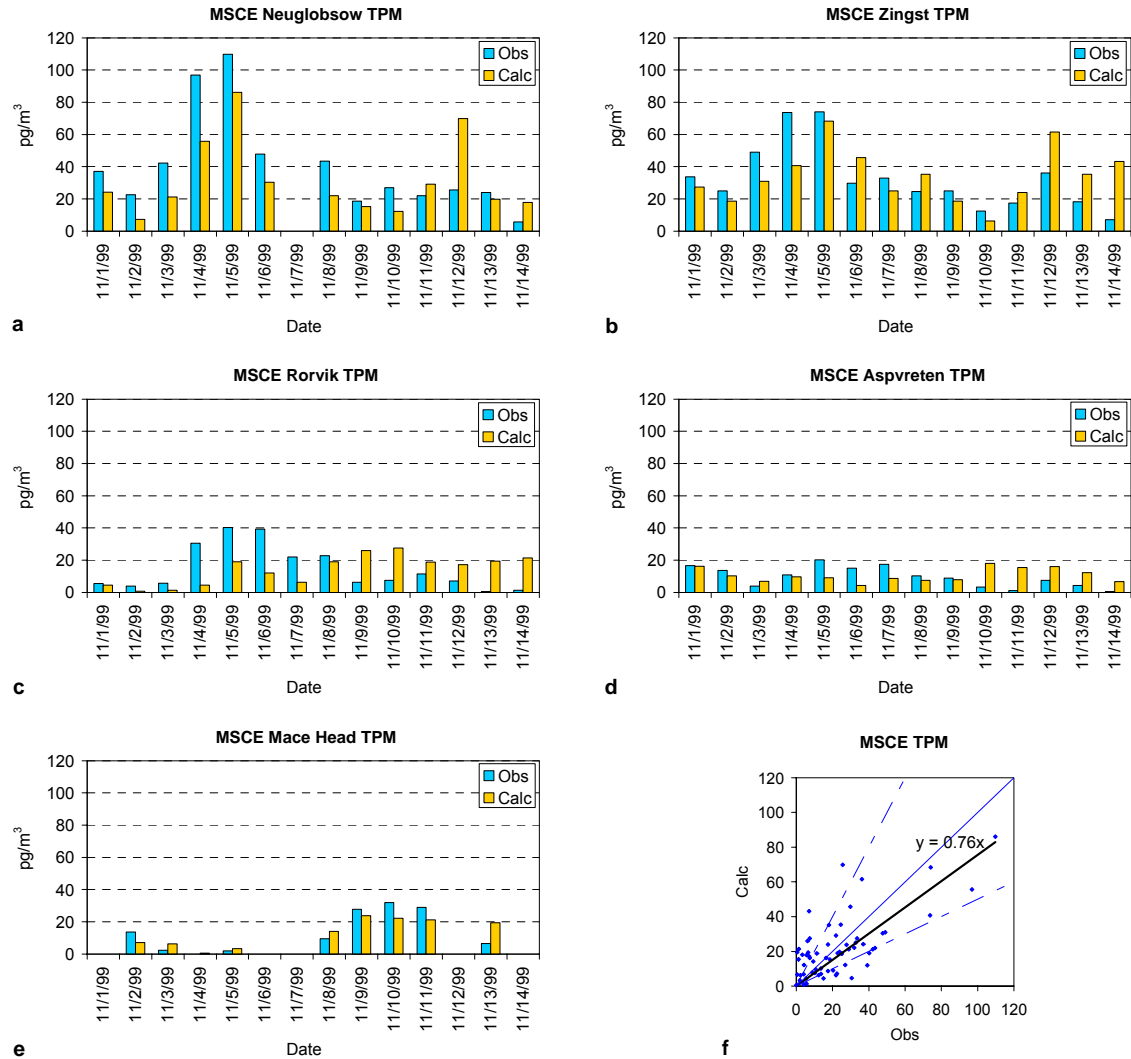


**Figure 6.15.** Modeled TPM concentrations by MSCE-Hg against observed ones during the 1999 episode: a - Neuglobsow; b - Zingst; c - Roervik; d - Aspvreten; e - Mace Head stations; f - regression for all compared pairs

**Table 6.3.** Statistical parameters for the RGM and TPM results obtained by MSCE-Hg model

Parameter	RGM	TPM
CC	-0.01	0.70
R <sub>bias</sub> , %	15	6
F <sub>2</sub> , %	19	58
F <sub>mean</sub>	5.1	2.3

It is possible to mention that the model can satisfactory reproduce TPM concentrations. The correlation coefficient is high. Mean deviation factor is close to 3. The average calculated TPM concentration for all samples is only 6% lower than corresponding observational value. On the contrary, the RGM data show that the model cannot predict concentration values for individual samples. The scattering of the results is high and the correlation is absent. At the same time mean values for all observations and all calculations differ only by 15%.

## 6.4. The GRAHM model

The results for the first episode are presented in Fig. 6.16. In spite of its global character and coarse spatial resolution the model reproduces the base-line very well in the case of German stations (Fig. 6.16a and b). The SD values for modelling are lower than those for observations. For Swedish stations the model slightly overestimates the base-line. The model captures practically all peaks measured at Neuglobsow, however, underpredicts them. The correlation coefficient for Newglobsow is rather high (0.62) while for the other stations it is much lower.

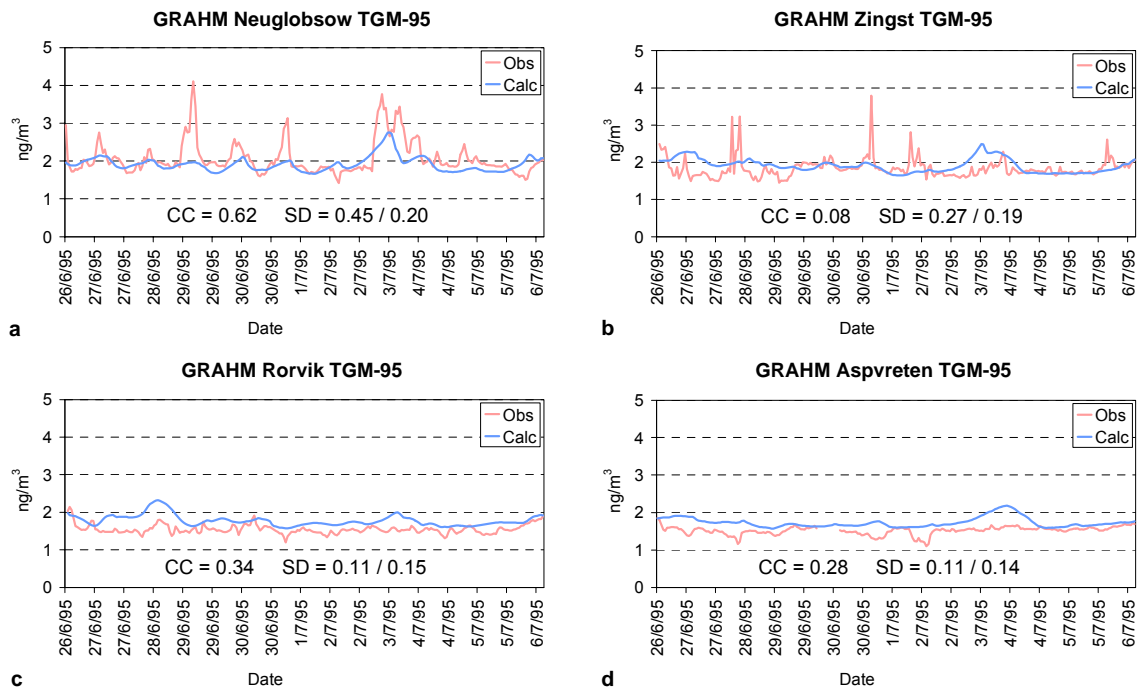


**Figure 6.16.** Modelled TGM concentrations by GRAHM against observed ones during the 1995 episode:  
a - Neuglobsow; b - Zingst; c - Roervik; d - Aspvreten stations

The comparisons of modelled and observed TGM values during the second episode are demonstrated in Fig. 6.17 (a, b and c). For Neuglobsow the calculated curve repeats generally the observed one. It is possible to mention that the model catches most peaks. The mean concentration values for the whole episode are very close to each other. For Zingst the model also catches the main peaks. That is confirmed by significant correlation coefficient (0.54). However, the modeled curve is obviously higher than the observed one. Fig. 6.17c shows the results for Mace Head station. Both observational and modelled curves do not have any obvious peaks. It is interesting to note that the character of the curves obtained by global GRAHM model and regional MSCE-Hg model is practically the same (compare Figs. 6.12c and 6.17c).

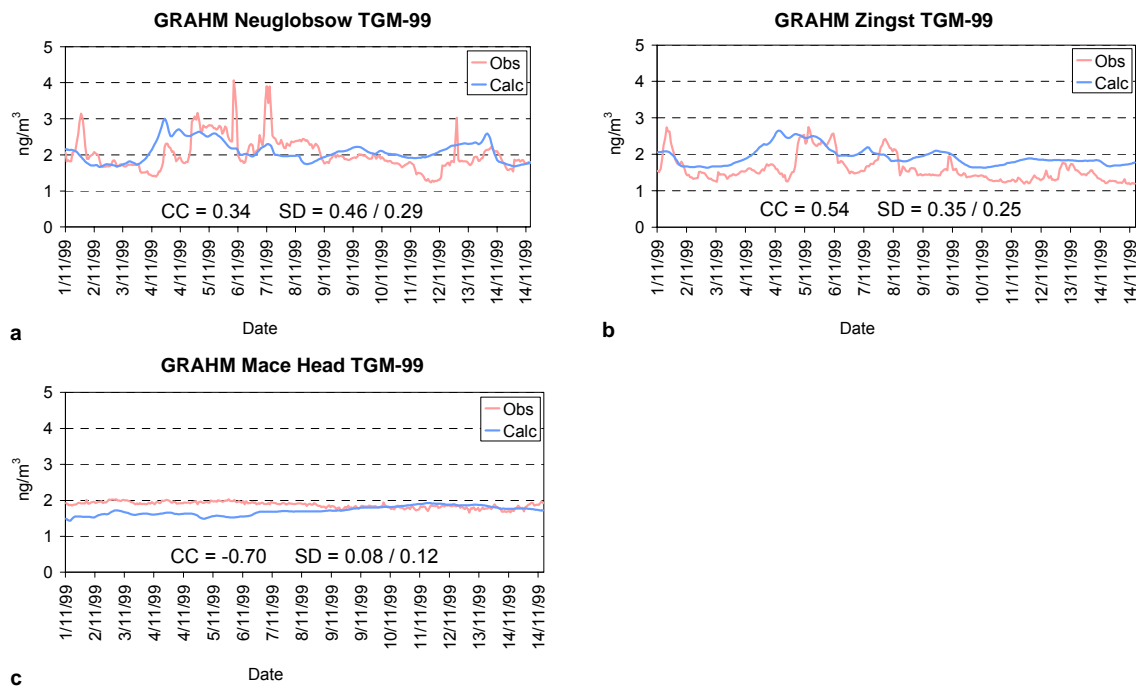


**Figure 6.17.** Modelled TGM concentrations by GRAHM model against observed ones during the 1999 episode  
*a - Neuglobsow; b - Zingst; c - Mace Head stations*

Fig. 6.18 (a, b, c and d) presents variations of daily mean values for both episodes for Neuglobsow and Zingst. One can see that the model reproduces well day-to-day variations of the observed TGM concentrations. Generally, the correlation between modeled and observed data in this case higher than for the hourly mean data. One can mention good correspondence of the absolute concentration values. Only for Zingst in 1999 the model overpredicts the observations, however, the correlation in this case is high.

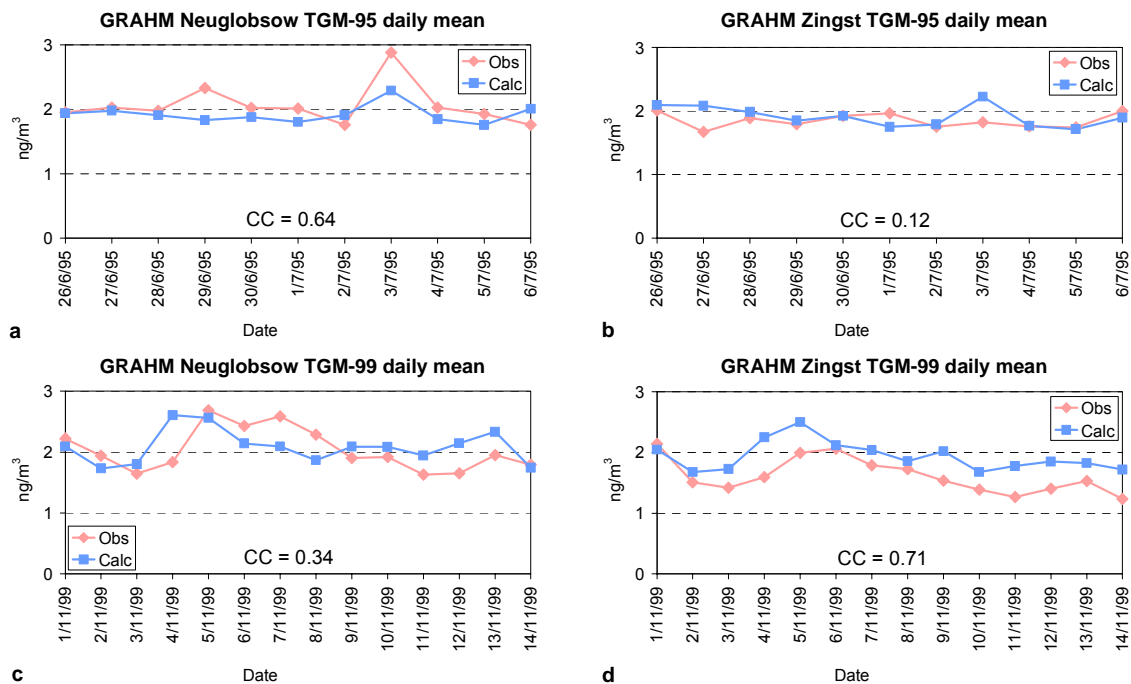


**Figure 6.18.** Comparison of daily mean values of GRAHM modeled and observed concentrations for:  
*a - Neuglobsow in 1995; b - Zingst in 1995; c - Neuglobsow in 1999; d - Zingst in 1999*

Fig. 6.19 demonstrates the comparison of RGM concentrations. It is possible to note rather high scattering of the results. One can mention very poor correspondence between calculated and measured concentrations. For Swedish stations the agreement is generally within the factor of 2 (Fig. 6.19b and c), while for Neuglobsow (Fig. 6.19a) the difference can reach several times. The model totally underpredicts the RGM concentrations measured at Mace Head (Fig. 6.19d). Most likely it is connected with the chemical scheme of the model.

The plot for all compared pairs of RGM concentrations calculated by GRAHM is shown in Fig. 6.19e. It demonstrates a rather wide scattering of the results. Less than half dots are within the lines of the factor of 2. However, the regression line ( $CAL=1.18 \cdot OBS$ ) is very close to the theoretical one.

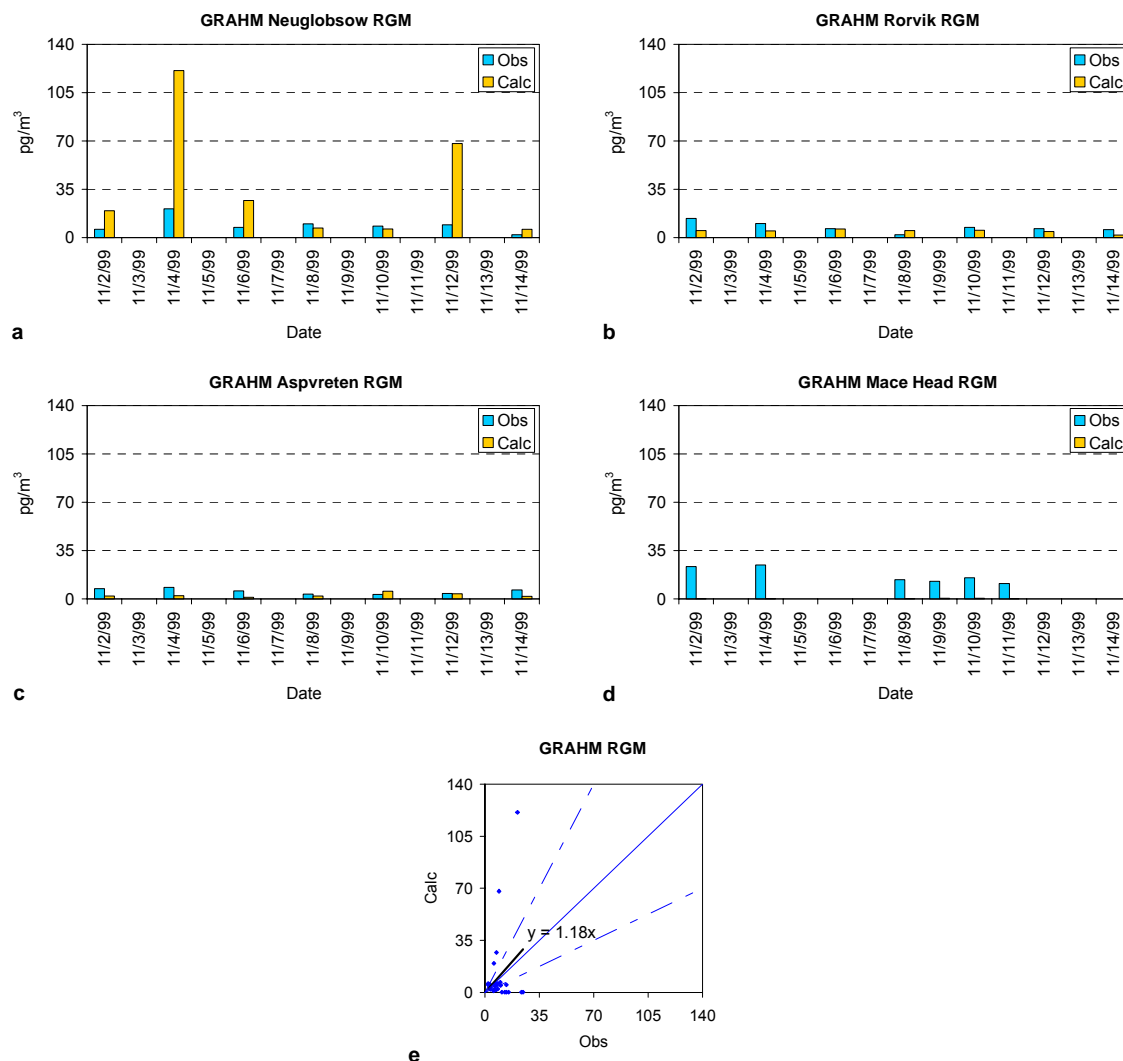


**Figure 6.19.** Modelled RGM concentrations by GRAHM against observed ones during the 1999 episode: a - Neuglobsow; b - Roervik; c - Aspveten; d - Mace Head stations; e - regression for all compared pairs

The comparison of the data for TPM is presented in Fig. 6.20 for all five stations. For German stations (Fig. 6.20a and b) one can mention rather good agreement between the calculations and the observations. For the Swedish stations the model predicts from time to time very high values of TPM concentrations. Most likely it is an effect of the coarse spatial resolution of the model. In these cases the model generally overestimates the observations. It is important to mention that the data for Mace

Head are in a very good correspondence with the changes in synoptical situation (Fig. 6.20e). This fact can confirm that air mass transport scheme of the model can adequately describe the wind field. The comparison of all “observation-calculation” pairs is showed in Fig. 6.20f. The regression line (CAL=1.51\*OBS) is somewhat higher than the theoretical “one-to-one” line. Hence, the model overestimates the observations. However, most of the dots are within the lines of the factor of 2.

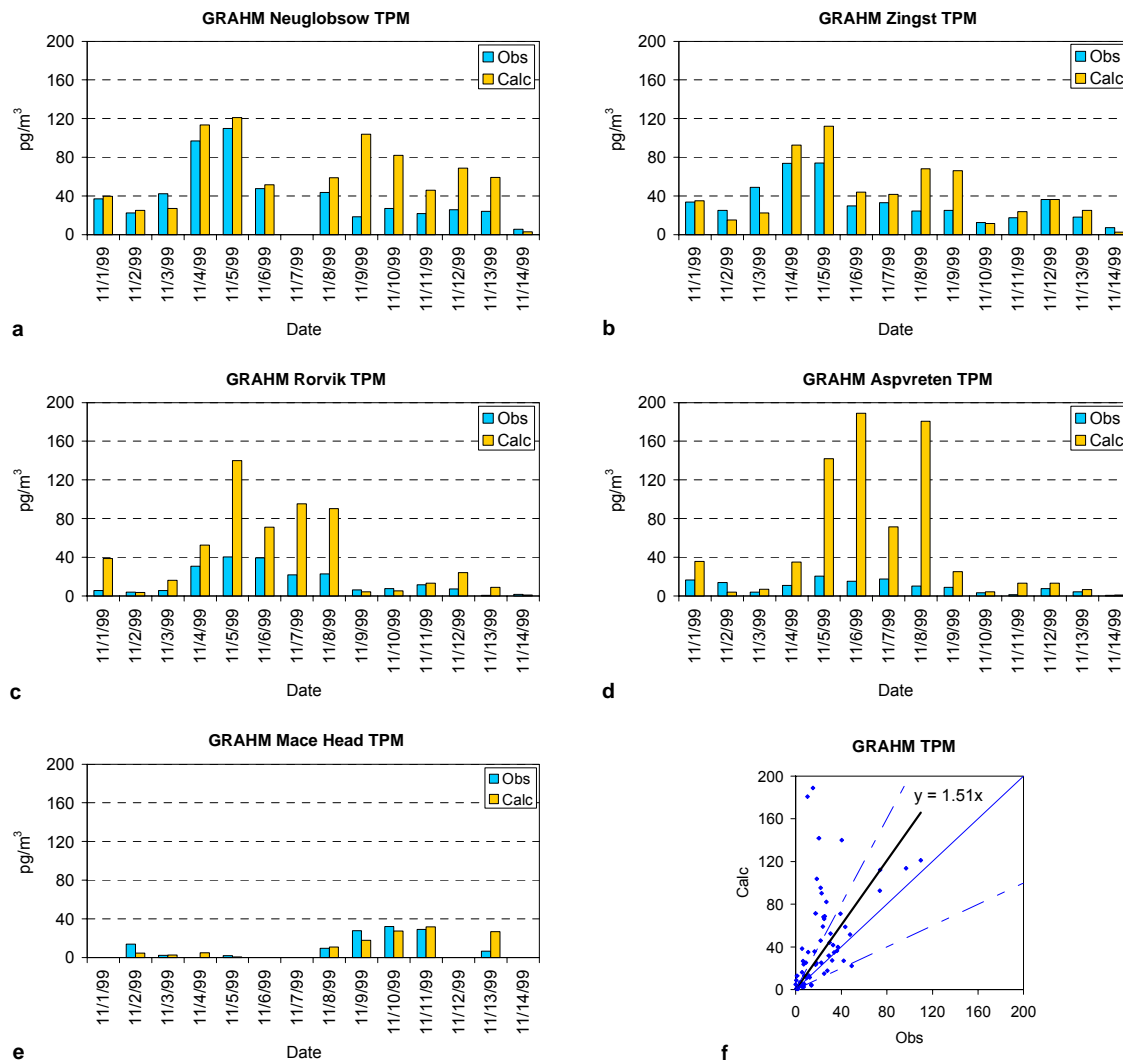


**Figure 6.20.** Modelled TPM concentrations by GRAHM against observed ones during the 1999 episode: a - Neuglobsow; b - Zingst; c - Rorvik; d - Aspvreten; e - Mace Head stations; f - regression for all compared pairs

The statistical parameters, which characterize the GRAHM results, are given in Table 6.4.

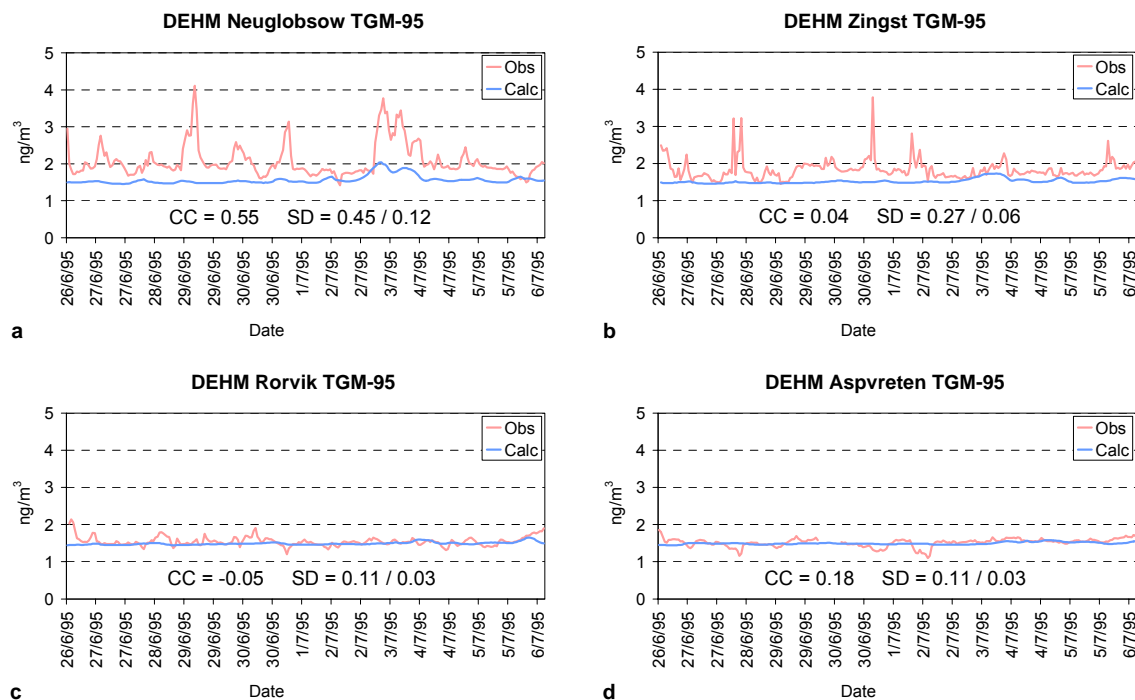
**Table 6.4.** Statistical parameters for the RGM and TPM results obtained by GRAHM model

Parameter	RGM	TPM
CC	0.26	0.51
R <sub>bias</sub> , %	20	96
F <sub>2</sub> , %	30	55
F <sub>mean</sub>	5.6	2.2

It is possible to mention that the model satisfactory reproduces the TPM concentrations. The correlation coefficient is significant (0.51). Mean deviation factor is close to 3. However, the model practically 2 times overestimates the TPM concentrations. As for the RGM data, it is obvious that the model cannot predict concentration values for individual samples. The scattering of the results is very high. The correlation is insignificant and mean deviation factor reaches 30.

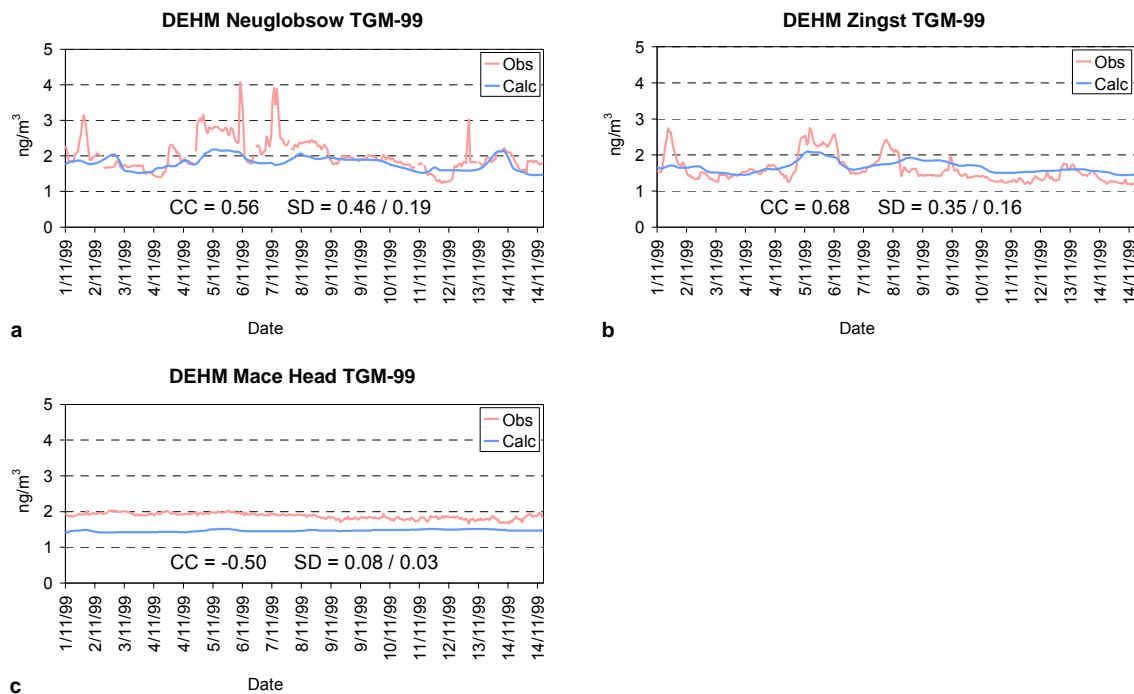
## 6.5. The DEHM model

The results of hemispheric model DEHM for the first episode are presented in Fig. 6.21. The model only slightly reproduces the observational peaks at German stations (Fig. 6.21a and b). The correlation coefficient for Neuglobsow is significant (0.55), and insignificant for Zingst. The base-line for German stations is a little bit underestimated by the model. At the same time the agreement of base-lines for Swedish stations (Fig. 6.21c and d) is excellent. For all stations the SD values for calculations are very low in comparison with the observational data.



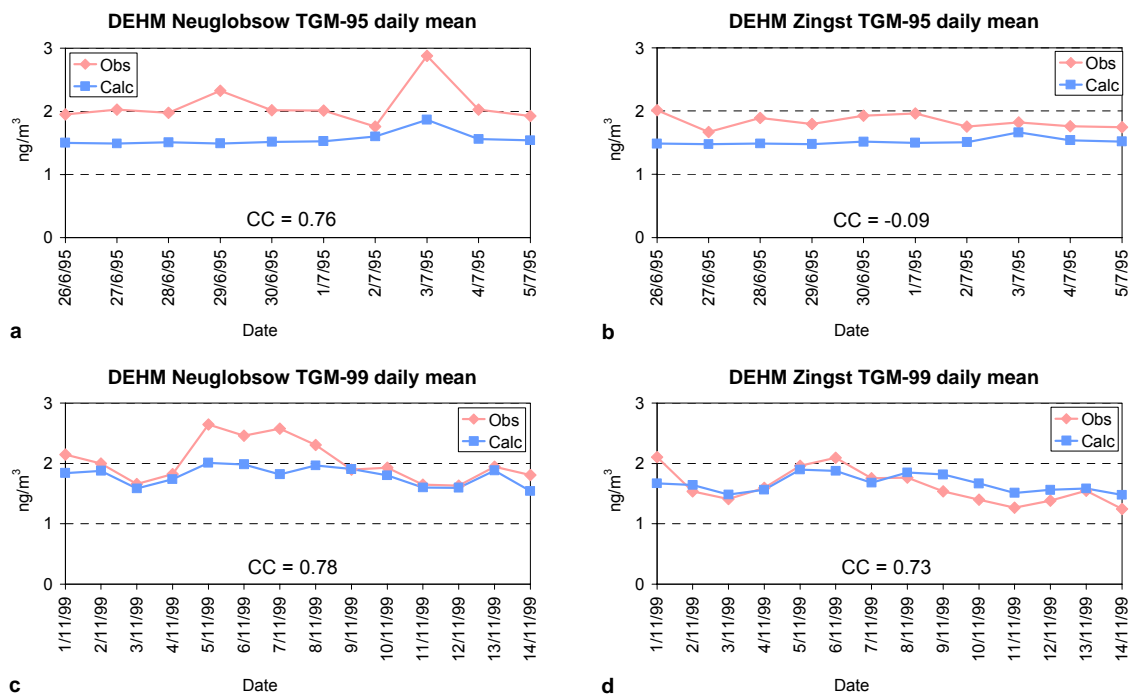
**Figure 6.21.** Modelled TGM concentrations by DEHM against observed ones during the 1995 episode:  
*a - Neuglobsow; b - Zingst; c - Roerвик; d - Aspvreten stations*

For the second episode the comparisons of modelled and observed TGM values are demonstrated in Fig. 6.22 (a, b and c). Both for Newglobsow and Zingst the model can reproduce large peaks. The correlation coefficients are 0.56 and 0.68 correspondingly. The SD values are higher than for the first episode. The base-lines are captured well in both cases. Fig. 6.22c shows the results for Mace Head station. Both observational and modelled curves do not have any obvious peaks. The model underpredicts the observations especially at the beginning of the episode.



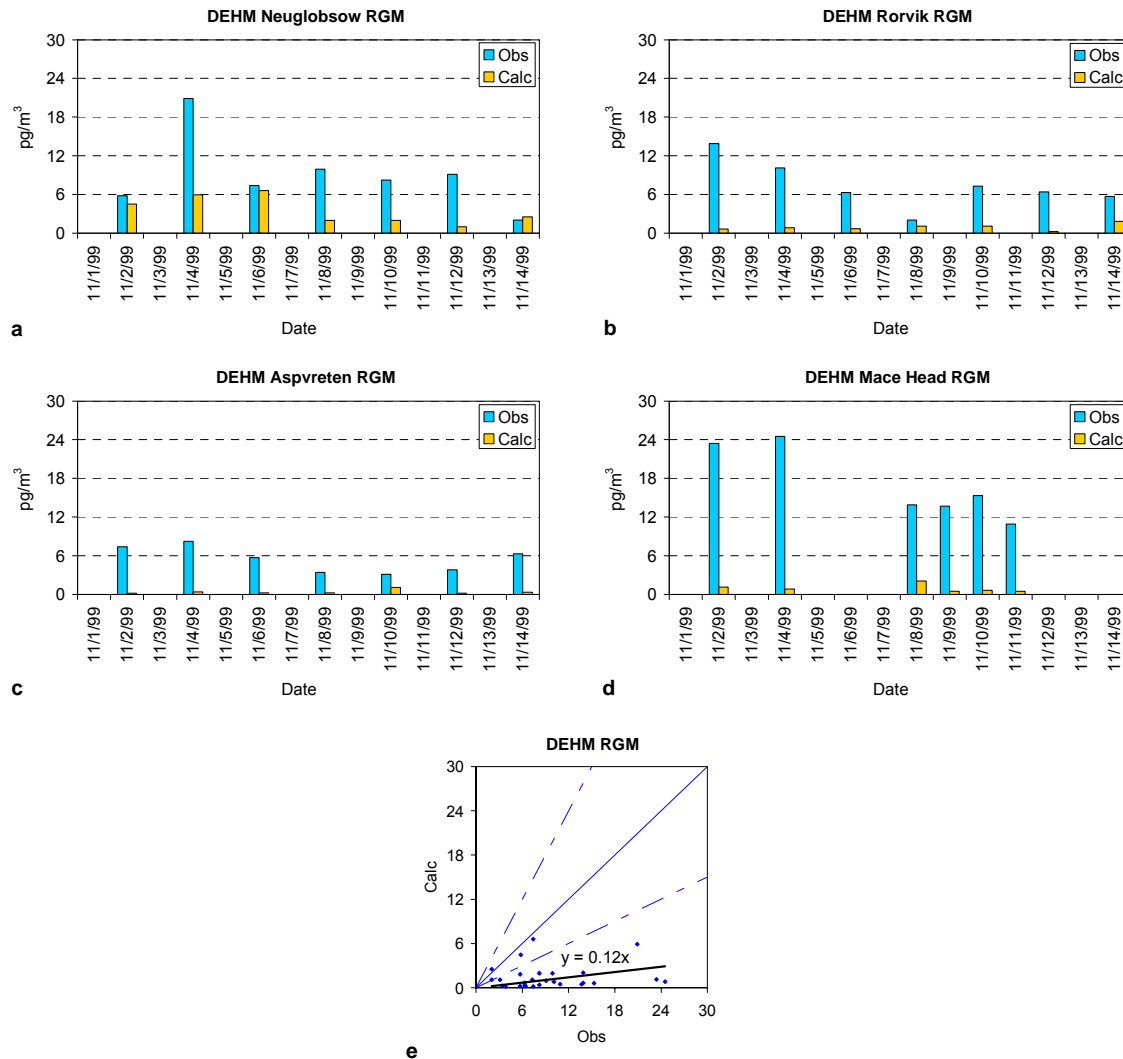
**Figure 6.22.** Modelled TGM concentrations by DEHM model against observed ones during the 1999 episode: a - Neuglobsow; b - Zingst; c - Mace Head stations

Fig. 6.23 (a, b, c and d) presents variations of daily mean values for both episodes for Neuglobsow and Zingst. The model reproduces day-to-day variations of the observed TGM concentrations. For the second episode the correlation coefficients are very high. The correlation coefficients between modeled and observed daily mean data in all case higher that for the hourly mean data. One can mention very good correspondence of the absolute concentration values for Zingst in 1999.



**Figure 6.23.** Comparison of daily mean values of DEHM modeled and observed concentrations for: a - Neuglobsow in 1995; b - Zingst in 1995; c - Neuglobsow in 1999; d - Zingst in 1999

Figs. 6.24 (a - d) demonstrate the comparison of RGM concentrations for all stations. It is possible to note that the model consistently underpredicts the observations at all stations. For individual samples the ratio can exceed an order of magnitude. Most likely it is connected with parameterization of the chemical scheme of the model. The plot for all compared pairs of RGM concentrations calculated by DEHM is showed in Fig. 6.24e. The regression line (CAL=0.12\*OBS) is much lower than the theoretical one. Only few dots are within the lines of the factor of 2.



**Figure 6.24.** Modelled RGM concentrations by DEHM against observed ones during the 1999 episode: a - Neuglobsow; b - Roervik; c - Aspvreten; d - Mace Head stations; e - regression for all compared pairs

The comparison of the data for TPM is presented in Fig. 6.25 for all five stations. First of all, one can mention a very good agreement between observations and calculations for German stations (Fig. 6.25a and b). For the Swedish stations the model sometimes overpredicts the TPM concentrations, however, the agreement in general is also high. The data for Mace Head are in a very good correspondence with the wind pattern changes (Fig. 6.25e). It confirms that the transport scheme of the model can adequately describe the wind field. The comparison of all “observation-calculation” pairs is showed in Fig. 6.25f. The regression line (CAL=1.005\*OBS) practically coincides with the theoretical “one-by-one” line. The correlation coefficient is high (0.78). Most of the dots are within the lines of the factor of 2.

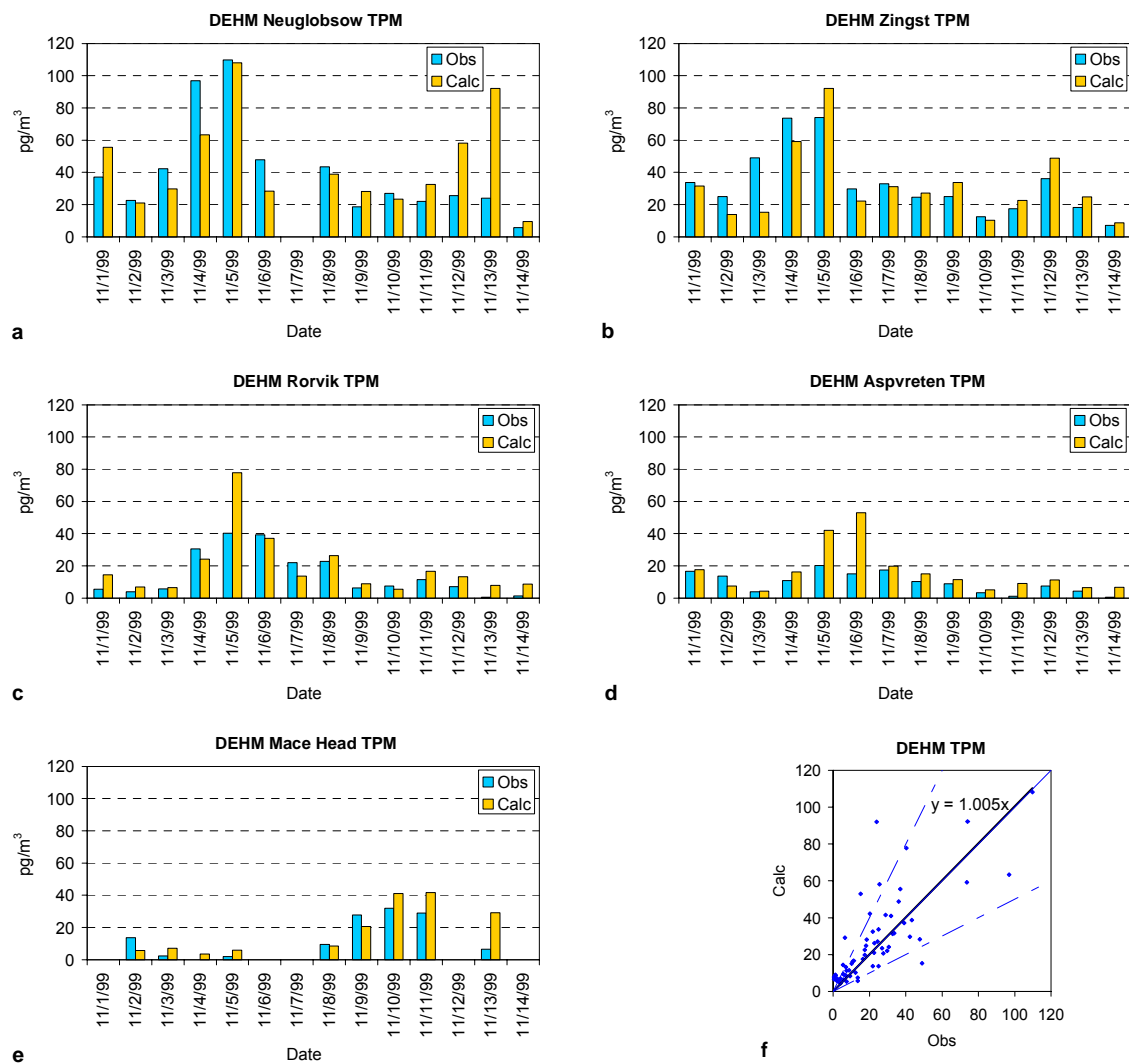


**Figure 6.25.** Modelled TPM concentrations by DEHM against observed ones during the 1999 episode: a - Neuglobsow; b - Zingst; c - Rorvik; d - Aspvreten; e - Mace Head stations; f - regression for all compared pairs

The statistical parameters, which characterize the DEHM results, are given in Table 6.5.

**Table 6.5.** Statistical parameters for the RGM and TPM results obtained by DEHM model

Parameter	RGM	TPM
CC	0.12	0.78
R <sub>bias</sub> , %	85	17
F <sub>2</sub> , %	15	75
F <sub>mean</sub>	9.1	1.7

It is possible to mention that the model can reproduce the TPM concentrations very well. Mean deviation factor is only a little bit higher than 2. The average calculated TPM concentration differs from the observational value only by 17%. As for the RGM data, it is obvious that the model cannot predict concentration values. For all samples (but one) the calculated values are much lower than the observational ones. The correlation is insignificant and mean deviation factor reaches 14.

## 6.6. The HYSPLIT model

The results of HYSPLIT model for the first episode are presented in Fig. 6.26. One can see in Fig. 6.26a that the model reproduces the large TGM peak on July 03. The amplitudes of observational and modelled peaks practically coincide. The model captured also other peaks (June 27, June 29, July 1), but in these cases the amplitudes of the peaks were underestimated. Nevertheless, this model demonstrates high correlation coefficient for Neuglobsow (0.60). At Zingst, the model was able to approximately capture some of the peaks, but the observations exhibited several additional sharp peaks, which could not be reproduced by the model. In Figs. 6.26 c and d one can mention a very good correspondence between the calculated and measured base-lines for Swedish stations.

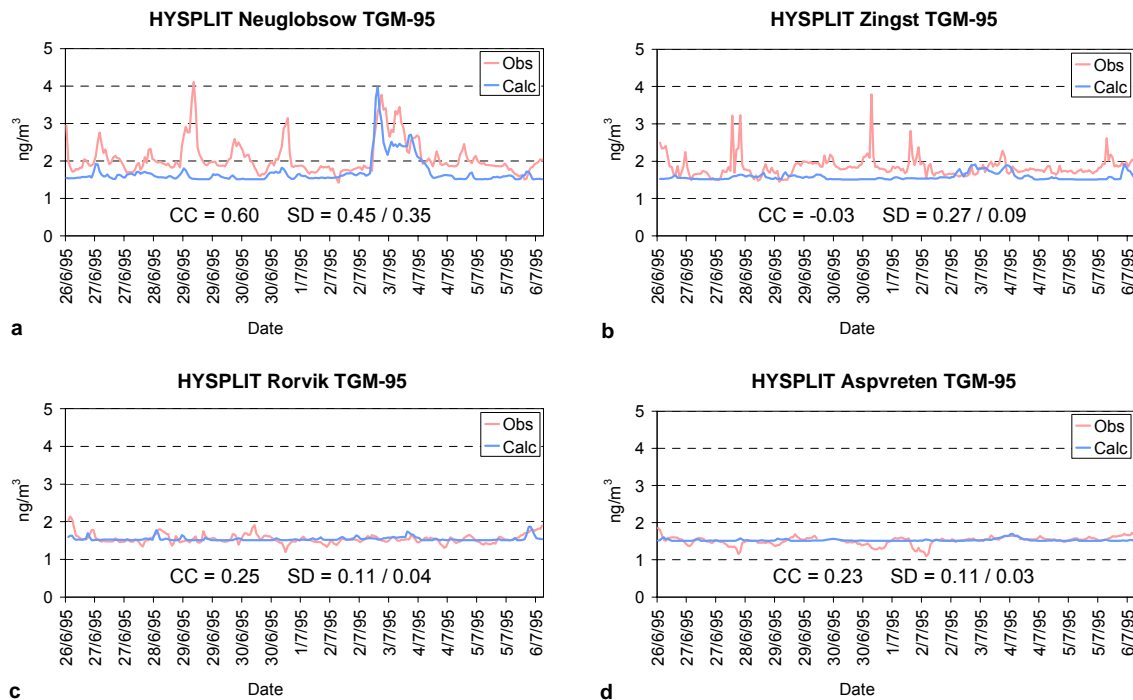


**Figure 6.26.** Modelled TGM concentrations by HYSPLIT against observed ones during the 1995 episode: a - Neuglobsow; b - Zingst; c - Roerвик; d - Aspveten stations

For the second episode the comparisons of modelled and observed TGM values are demonstrated in Fig. 6.27 (a, b and c). For Neuglobsow and Zingst, the model appears to capture many of the observational peaks. However, the correlation coefficients are somewhat low: 0.42 and 0.44, correspondingly. The SD values are close to those of observations. Fig. 6.27c shows the results for Mace Head station. At this station, the measured and calculated values are both very close to the baseline.

The comparison of daily mean data for both episodes is shown in Fig. 6.28 (a-d). One can see that the model reproduces both absolute values of the concentrations and the day-to-day variations rather well. For 1995 the model somewhat underestimates the observations, while for 1999 it is possible to mention good correspondence of modeled and observed results.

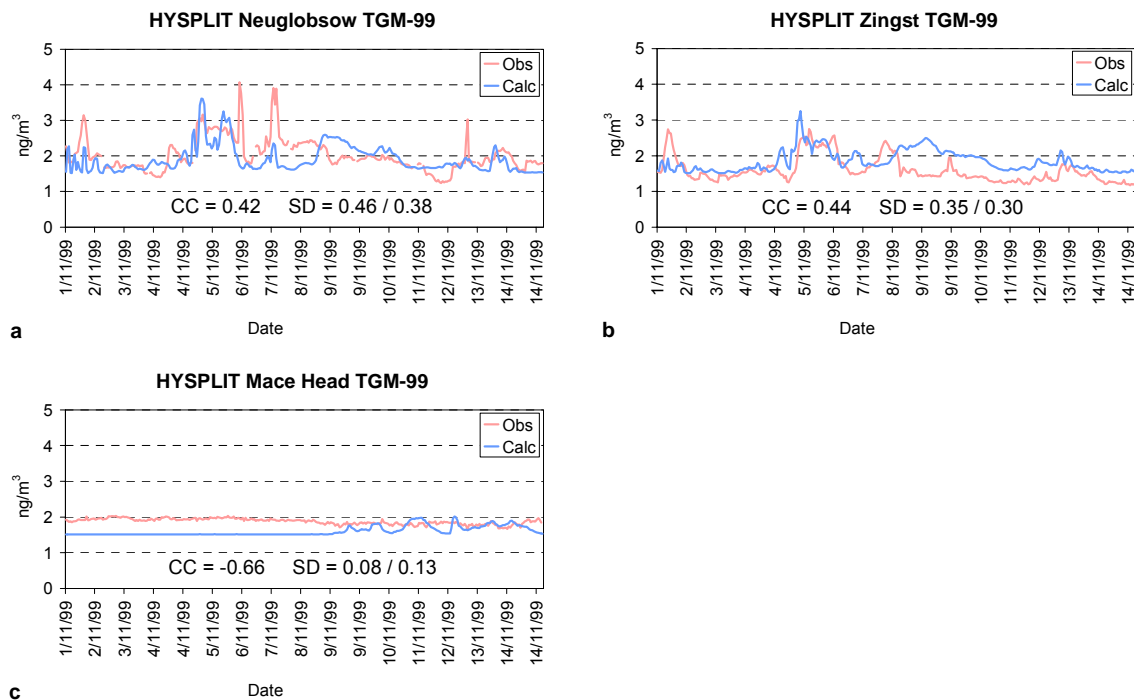


**Figure 6.27.** Modelled TGM concentrations by HYSPPLIT model against observed ones during the 1999 episode  
 a - Neuglobsow; b - Zingst; c - Mace Head stations

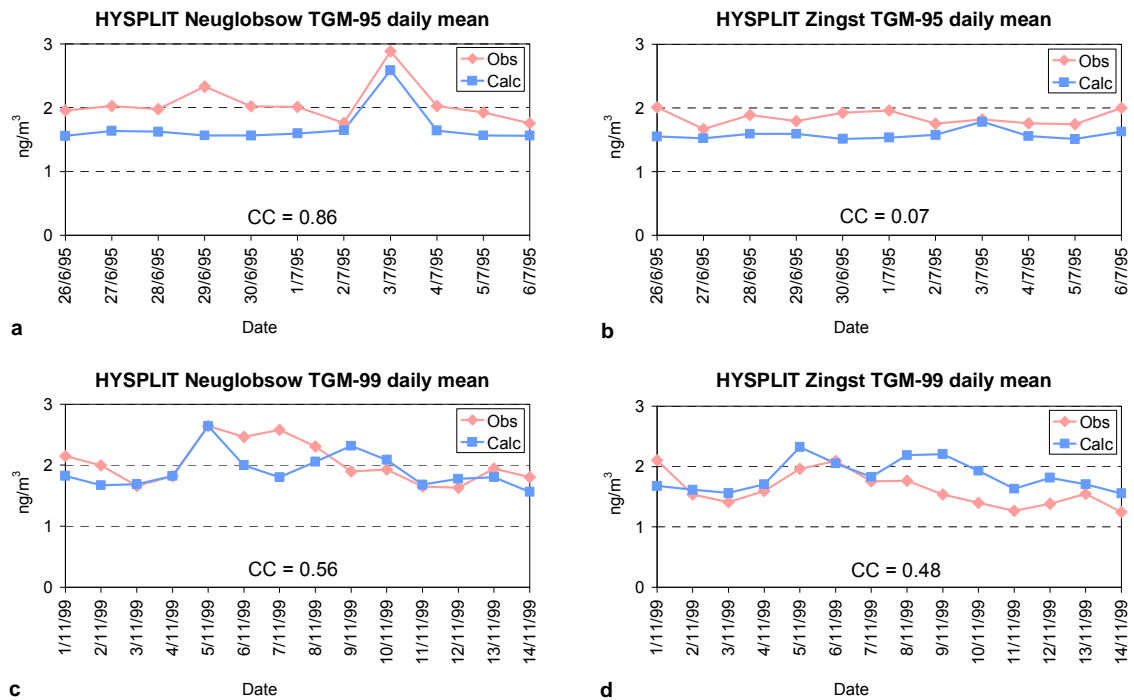


**Figure 6.28.** Comparison of daily mean values of HYSPPLIT modeled and observed concentrations for:  
 a - Neuglobsow in 1995; b - Zingst in 1995; c - Neuglobsow in 1999; d - Zingst in 1999

Figs. 6.29 (a - d) demonstrate the comparison of RGM concentrations for all stations. Due to the Lagrangian nature of the HYSPPLIT model, the “background” was accounted for by adding a constant “background” value to the local model predictions. In the other regional models (all Eulerian), this

background problem was addressed by specifying certain background concentrations at the borders of the model domain. In all cases, these procedures are somewhat uncertain and were adopted to account for the fact that mercury sources outside the model domain will exert some influence over the concentrations observed within the domain. In general, one can note a good agreement between the observations and calculations for all considered monitoring stations. As usual, the modeled results are within the factor of 2. Unlike the other models the difference between measured and observed values during the first part of the episode at Mace Head is not so dramatic (the model gives just the prescribed background value). The plot for all compared pairs of RGM concentrations calculated by HYSPLIT is showed in Fig. 6.29e. The regression line ( $CAL=0.82*OBS$ ) is very close to the theoretical one, however, the scattering is rather high.

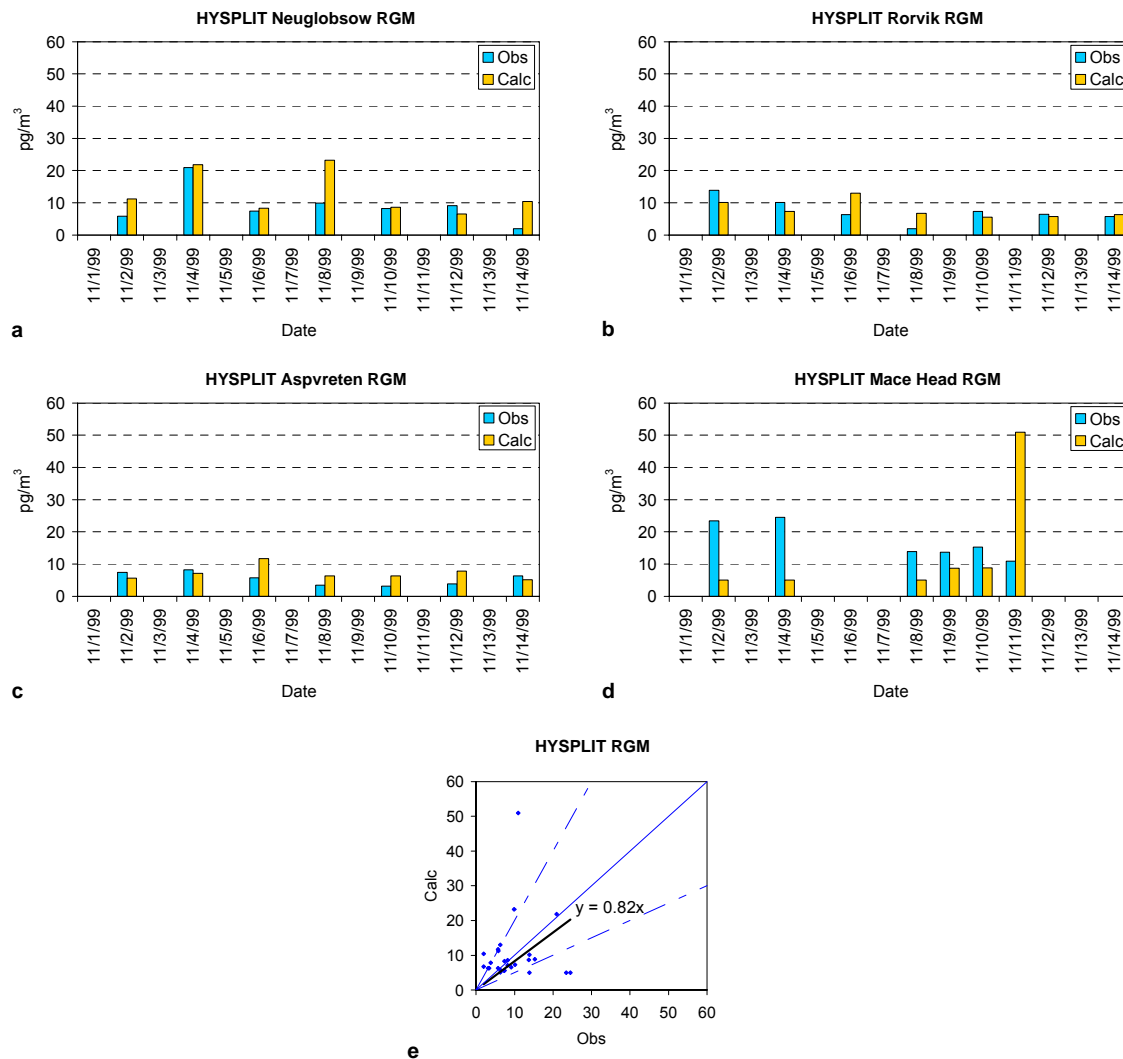


**Figure 6.29.** Modelled RGM concentrations by HYSPLIT against observed ones during the 1999 episode: a - Neuglobsow; b - Roervik; c - Aspveten; d - Mace Head stations; e - regression for all compared pairs

The comparison of the data for TPM is presented in Fig. 6.30 for all five stations. The general picture is optimistic – in many cases the modeled values are close to the observed ones. At the Swedish stations and Mace Head, where very low concentrations were observed (i.e., observations were at or close to the “background”), it appears that the model’s assumed background concentration may be slightly too high. The data for Mace Head are in a good correspondence with the wind pattern changes

(Fig. 6.30e). The comparison of all “observation-calculation” pairs is shown in Fig. 6.30f. The regression line (CAL = 1.15 \* OBS) is very close to the theoretical “one-by-one” line. The correlation coefficient is very high (0.83). Most of the data are within a factor of 2.

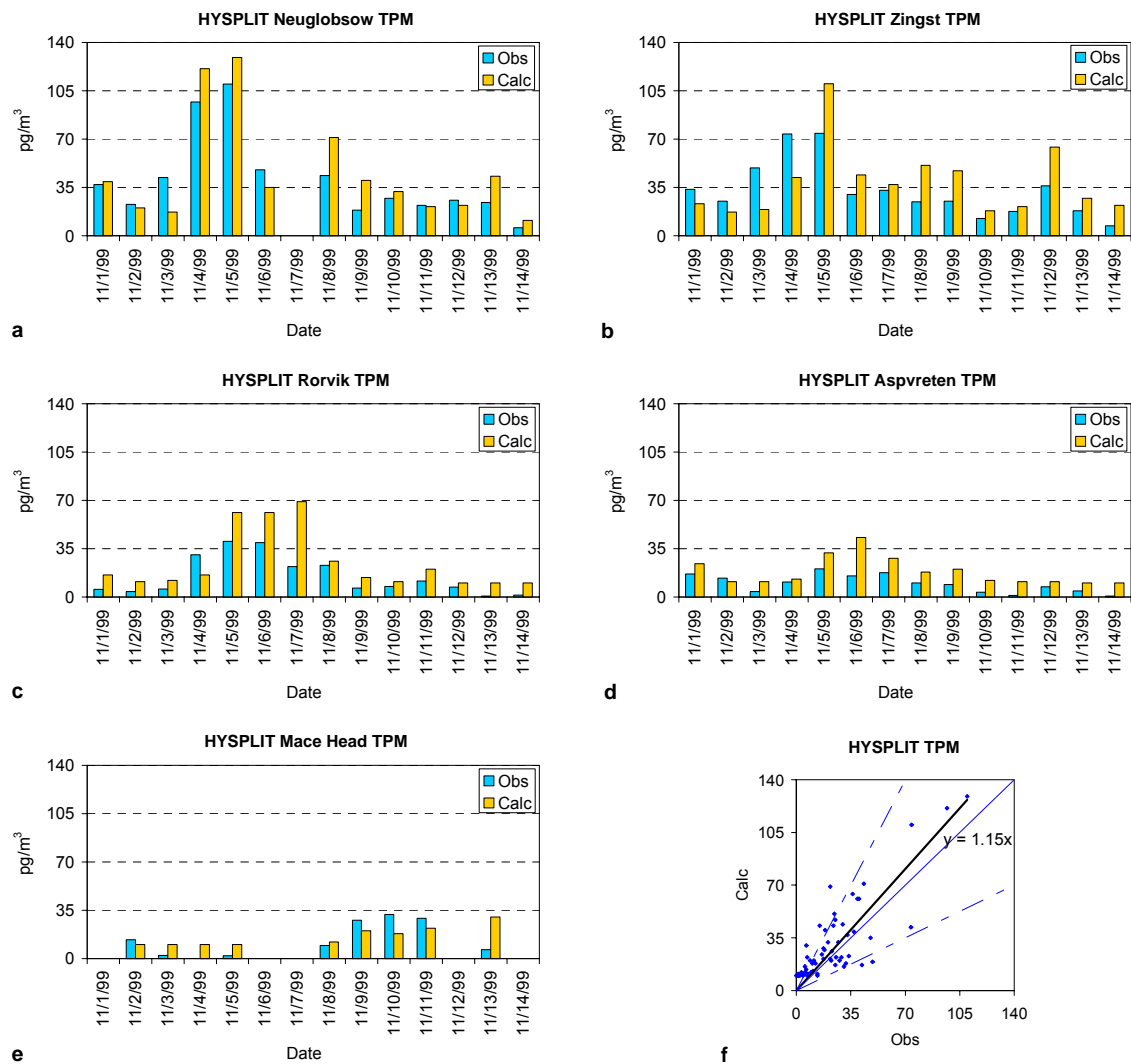


**Figure 6.30.** Modelled TPM concentrations by HYSPLIT against observed ones during the 1999 episode: a - Neuglobsow; b - Zingst; c - Rorvik; d - Aspvreten; e - Mace Head stations; f - regression for all compared pairs

The statistical parameters, which characterize the HYSPLIT results, are given in Table 6.6.

**Table 6.6.** Statistical parameters for the RGM and TPM results obtained by HYSPLIT model

Parameter	RGM	TPM
CC	0.10	0.83
R <sub>bias</sub> , %	10	31
F <sub>2</sub> , %	59	64
F <sub>mean</sub>	1.9	2.0

It appears that the model can reproduce both RGM and TPM concentrations. Mean-deviation factor is lower than 3.0 in both cases. The relative bias in both cases is also low.

## 6.7. The EMAP model

The results of the model EMAP for the first episode are presented in Fig. 6.31 (a-d). For Neuglobsow station the model describes the main peak of July 03 very well. At the same time the modelling base-lines for all four stations are obviously lower than the observed ones. Sometimes the calculated TGM concentration drops below  $1 \text{ ng/m}^3$ . For Neuglobsow the correlation between observations and calculations is significant, while for the other stations – insignificant. EMAP is the only model when the SD values for calculations are obviously higher than for the observational data obtained at German stations.

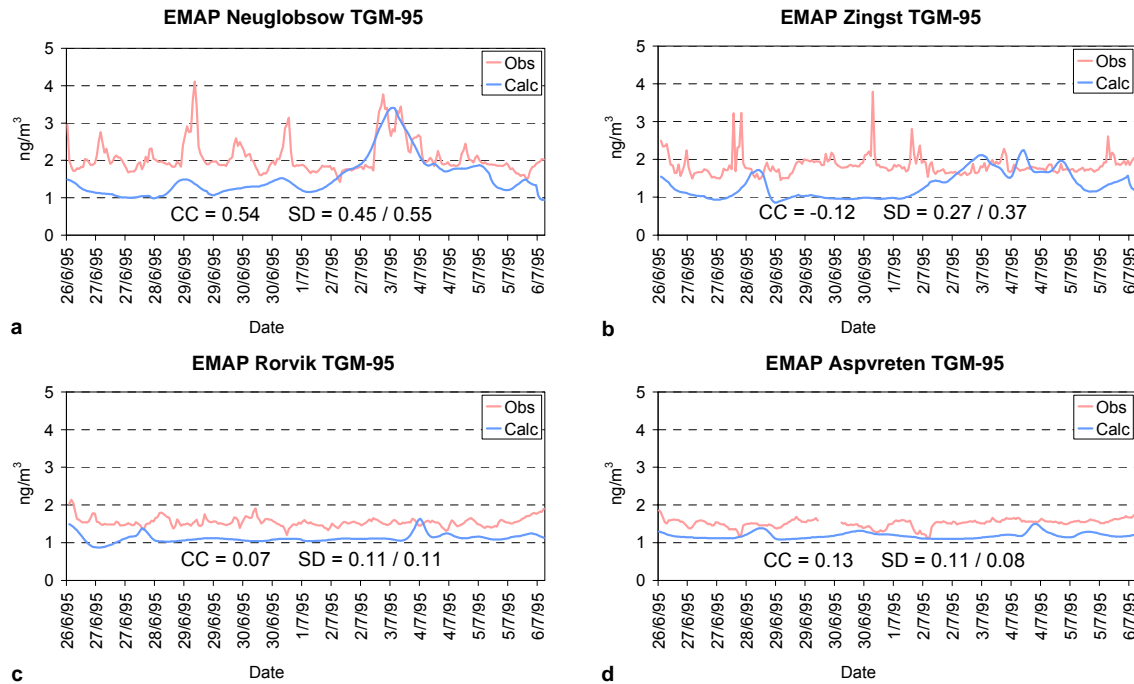


**Figure 6.31.** Modelled TGM concentrations by EMAP against observed ones during the 1995 episode:  
a - Neuglobsow; b - Zingst; c - Rorvik; d - Aspvreten stations

The second episode has been modelled for two German stations (Fig. 6.32 (a and b)). It is possible to mention a very similar shape of the modelling curves. All extremes coincide in time. In the case of Neuglobsow there is no agreement, while for Zingst one can find two periods when two peaks coincide in time. However, the correlation coefficients are somewhat low in both cases.

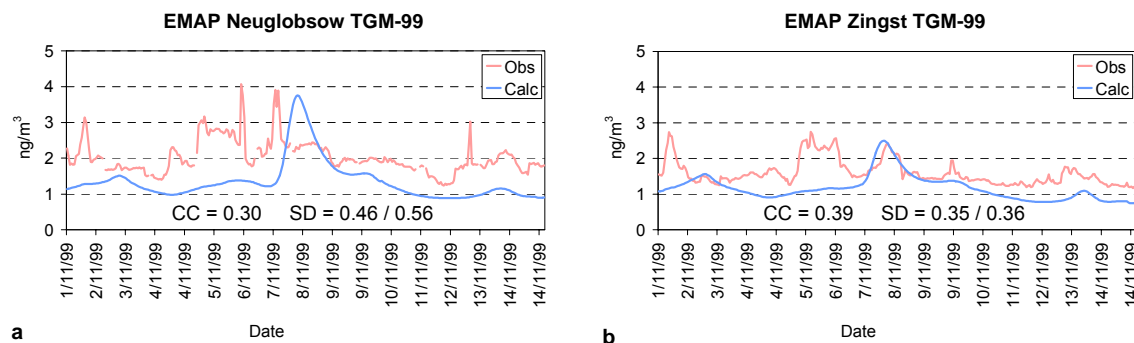


**Figure 6.32.** Modelled TGM concentrations by EMAP model against observed ones during the 1999 episode  
a - Neuglobsow; b - Zingst stations

The comparison of daily mean data for both episodes is shown in Fig. 6.33 (a-d). One can mention that in all cases the model underestimates the observations. However, for Neuglobsow-95 the model perfectly captures the peak of July 02.

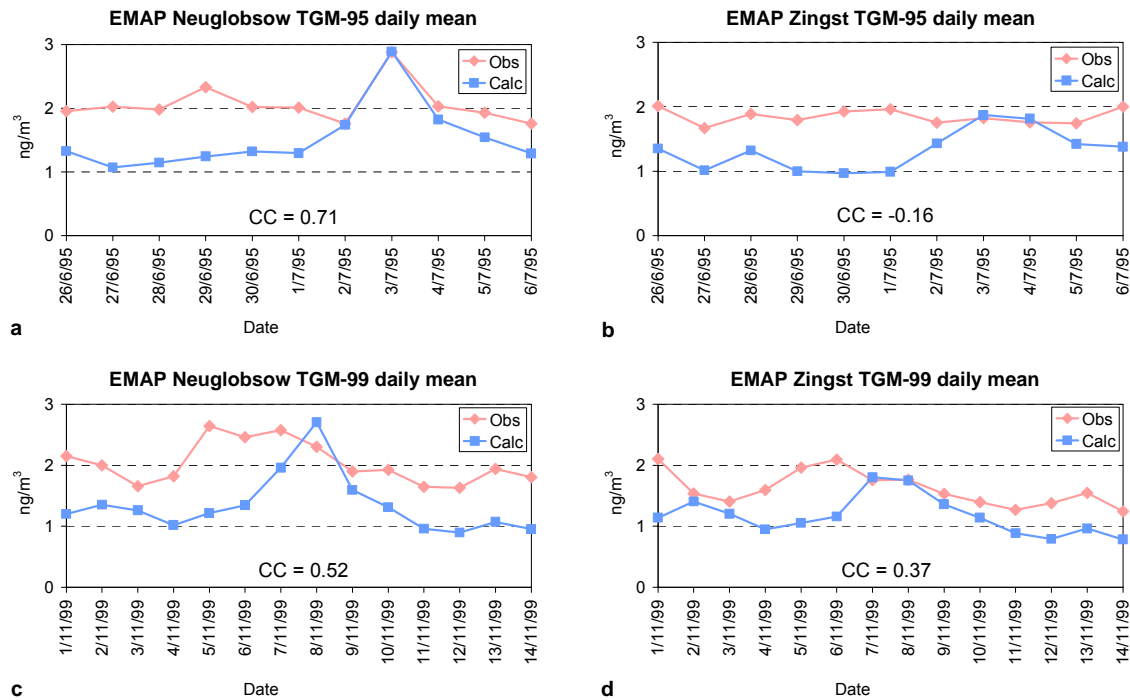


**Figure 6.33.** Comparison of daily mean values of EMAP modeled and observed concentrations for: a - Neuglobsow in 1995; b - Zingst in 1995; c - Neuglobsow in 1999; d - Zingst in 1999

Figs. 6.34 (a - d) demonstrate the comparison of RGM concentrations for three stations. One can see a very good agreement between the model and the observations at Neuglobsow and Aspvreten. At Roervik it is possible to find lack of coincidence for three individual samples (less than a half). The plot for all compared pairs of RGM concentrations calculated by EMAP is showed in Fig. 6.34d. The regression line ( $\text{CAL}=0.82 \cdot \text{OBS}$ ) is just a little bit lower than the theoretical one. Only few dots are out of the lines of the factor of 2.

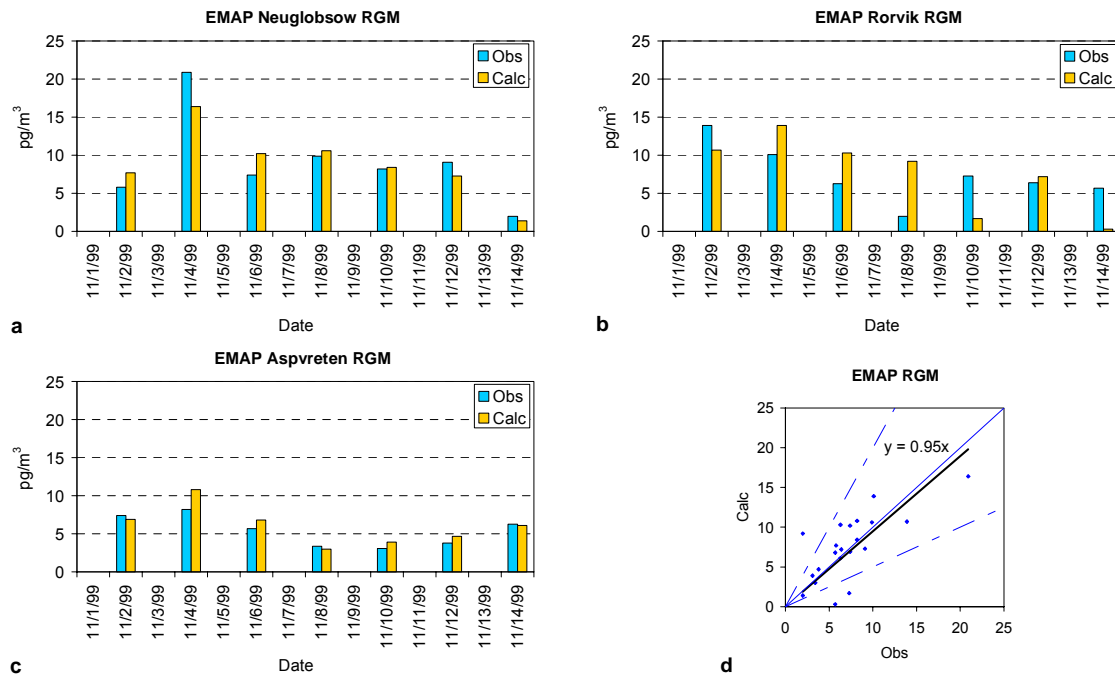


**Figure 6.34.** Modelled RGM concentrations by EMAP against observed ones during the 1999 episode: a – Neuglobsow; b – Roervik; c – Aspvetren; d – regression for all compared pairs

The comparison of the data for TPM is presented in Fig. 6.35 for four stations. Brief survey of the data in the figure shows that there is a satisfactory agreement between the modelling and observational results. The comparison of all “observation-calculation” pairs is showed in Fig. 6.35e. The regression line ( $CAL = 1.15 * OBS$ ) is very close to the theoretical “one-by-one” line. The correlation coefficient is very high (0.81). Most of the data are within the lines of the factor of 2.

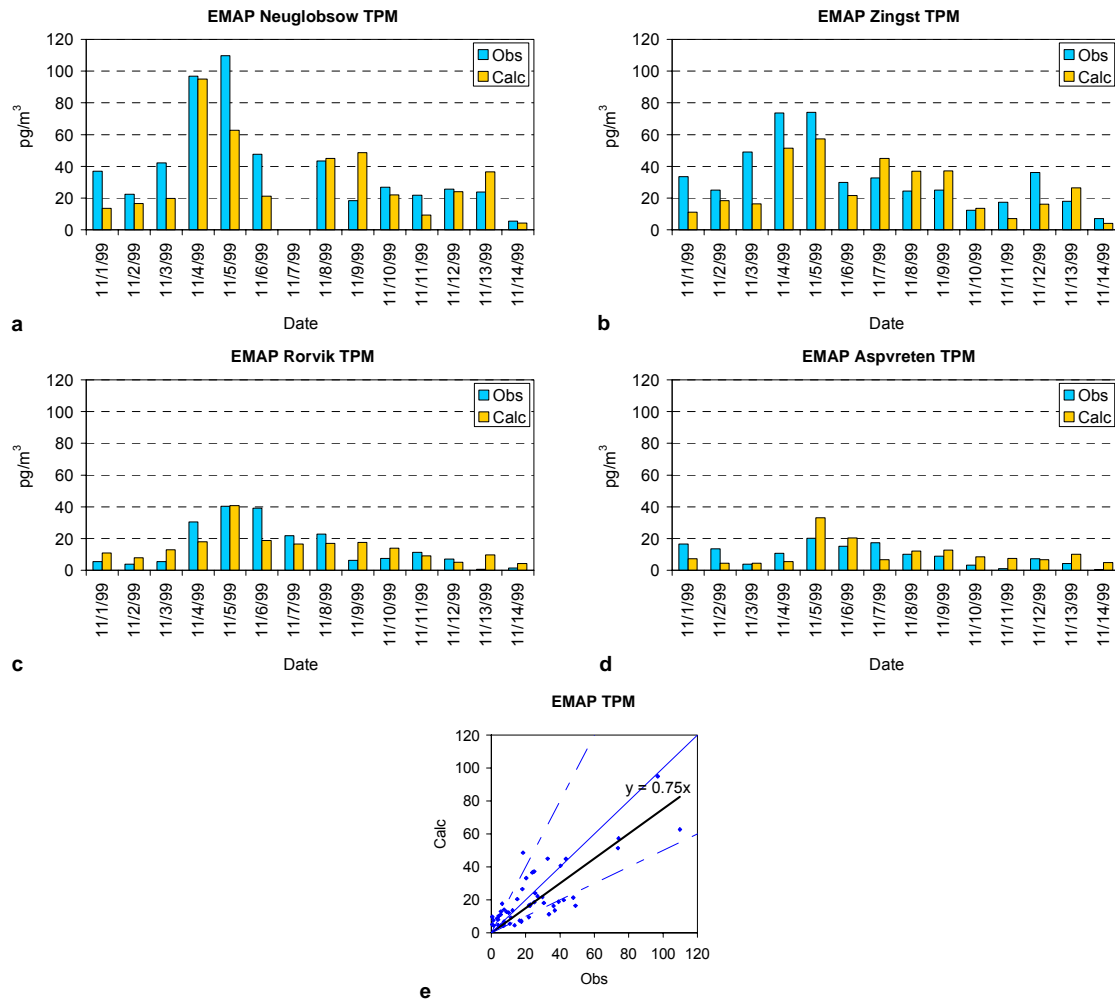


**Figure 6.35.** Modelled TPM concentrations by EMAP against observed ones during the 1999 episode: a - Neuglobsow; b - Zingst; c - Rorvik; d - Aspvreten; e - regression for all compared pairs

The statistical parameters, which characterize the EMAP results, are given in Table 6.7.

**Table 6.7.** Statistical parameters for the RGM and TPM results obtained by EMAP model

Parameter	RGM	TPM
CC	0.70	0.81
R <sub>bias</sub> , %	1	13
F <sub>2</sub> , %	86	62
F <sub>mean</sub>	1.6	1.9

It is obvious that the model can reproduce both RGM and TPM concentrations very well. Mean deviation factor is on the level of the factor of 2. The mean difference between calculated RGM and TPM concentration is practically negligible. The correlation in both cases is significant.

### COMPARISONS OF THE MODELLING RESULTS (SIMILARITIES AND DISTINCTIONS)

The results of statistical treatment show, that all the participating models are able (to some extent) to simulate mercury atmospheric transport during short episodes. One should keep in mind that this modelling experiment had several limitations. First, only anthropogenic emissions have been used for the regional models, and, the degree of reliability of the anthropogenic emission data is low. Moreover, information on any temporal variations in emissions, which can be important for short-term episodes, was not available for any of the sources in the inventory. In addition, the participating models are of regional or global character and they have not been designed for simulation of short-term variability of mercury concentrations. Nevertheless, it is instructive to evaluate performance of the models as they attempt to achieve this ambitious task.

Results of statistical treatments of TGM data for the first episode are shown in Table 7.1. The values, which are closest to the data of the observations, are highlighted in bold. First of all, one can see that all modelling results are within  $\pm 40\%$  of the mean observed values. There is an obvious regularity: all models underestimate the TGM concentrations at German stations and mainly overestimate them at Swedish stations. Standard deviation values show that practically in all cases the observational values vary in wider range than the modelled ones. For Neuglobsow – the most polluted station - the models demonstrate rather high correlation with the observations. It should be noted that usage of higher anthropogenic emission (UBA scenario) leads to better agreements with observations for ADOM and MSCE-Hg models.

The same statistical parameters for modelled TGM against observed TGM during the second episode (1999) are showed in Table 7.2. One can see that in this case the models as usual do not underestimate observations. A possible explanation of this fact is that real mercury emission was reduced between 1995 and 1999, while the models used the emission data of 1995 calculating concentrations for 1999. The models, which use MM5 meteorological processor (CMAQ, DEHM, HYSPLIT), demonstrate better correlation coefficients. However, the correlation coefficients are generally lower than for the first episode.

**Table 7.1.** Statistical parameters for TGM concentrations ( $\text{ng}/\text{m}^3$ ) during the first episode (from 12:00 26.06.1995 to 00:00 06.07.1995).

Station	Parameter	Obs	CMAQ	ADOM E <sub>1995</sub>	ADOM E <sub>1990</sub>	MSCE E <sub>1995</sub>	MSCE E <sub>1990</sub>	GRAHM	DEHM	HYSPLIT	EMAP
Neuglobsow	Arith. Mean	<b>2.10</b>	1.75	1.28	1.59	1.44	1.88	<b>1.91</b>	1.56	1.70	1.55
	SD	<b>0.45</b>	0.10	0.08	0.23	0.12	0.55	0.20	0.12	0.35	<b>0.55</b>
	Max	<b>4.11</b>	2.14	1.56	2.54	1.81	4.22	2.76	2.04	<b>3.97</b>	3.41
	Min	<b>1.42</b>	1.64	1.10	1.22	1.28	1.37	1.67	<b>1.46</b>	1.51	0.98
	CC		0.60	0.08	0.54	0.52	0.55	<b>0.62</b>	0.55	0.60	0.54
Zingst	Arith. Mean	<b>1.82</b>	1.72	1.28	1.54	1.43	1.71	<b>1.91</b>	1.52	1.58	1.31
	SD	<b>0.27</b>	0.03	0.08	0.24	0.05	0.26	<b>0.19</b>	0.06	0.09	0.37
	Max	<b>3.79</b>	1.80	1.58	2.70	1.55	2.57	<b>2.49</b>	1.73	1.91	2.25
	Min	<b>1.45</b>	1.68	1.09	1.19	1.32	1.36	1.65	<b>1.46</b>	1.51	0.86
	CC		0.05	0.04	0.43	-0.06	0.05	<b>0.08</b>	0.04	-0.03	-0.12
Roervik	Arith. Mean	<b>1.54</b>	1.70	1.29	1.35	1.42		1.77	1.49	<b>1.54</b>	1.11
	SD	<b>0.11</b>	0.02	0.10	0.10	0.03		0.15	0.03	0.04	<b>0.11</b>
	Max	<b>2.14</b>	1.74	1.58	1.58	1.48		<b>2.32</b>	1.60	1.77	1.64
	Min	<b>1.20</b>	1.65	<b>1.06</b>	1.10	1.36		1.57	1.44	1.51	0.87
	CC		0.09	-0.01	0.06	0.10		<b>0.34</b>	-0.05	0.25	0.07
Aspvreten	Arith. Mean	<b>1.51</b>	1.69	1.26	1.28	1.44		1.73	<b>1.49</b>	<b>1.53</b>	1.19
	SD	<b>0.11</b>	0.03	<b>0.09</b>	0.08	0.03		0.14	0.03	0.03	0.08
	Max	<b>1.86</b>	<b>1.75</b>	1.52	1.51	1.51		2.18	1.58	1.70	1.50
	Min	<b>1.10</b>	1.62	<b>1.09</b>	1.09	1.40		1.57	1.44	1.51	1.08
	CC		-0.05	0.17	0.19	-0.48		<b>0.28</b>	0.18	0.23	0.13

\* - the data of subsidiary character

**Table 7.2.** Statistical parameters for TGM concentrations (ng/m<sup>3</sup>) during the second episode (from 12:00 01.11.99 to 23:00 14.11.99)

Station	Parameter	Obs	CMAQ	ADOM E <sub>MOE</sub>	ADOM E <sub>UBA</sub>	MSCE	GRAHM	DEHM	HYSPLIT	EMAP
Neuglobsow	Ar.Mean	<b>2.03</b>	2.32	1.20	1.89	2.15	<b>2.09</b>	1.80	1.91	1.35
	SD	<b>0.46</b>	0.28	<b>0.43</b>	0.77	0.34	0.29	0.19	0.38	0.56
	Max	<b>4.07</b>	2.97	3.56	3.68	3.52	3.00	2.18	3.61	<b>3.76</b>
	Min	<b>1.24</b>	1.80	0.64	0.78	1.74	1.66	<b>1.46</b>	1.52	0.89
	CC		0.50	0.21	0.48	0.20	0.34	<b>0.56</b>	0.42	0.30
Zingst	Ar.Mean	<b>1.59</b>	2.13	1.07	1.45	2.11	1.93	<b>1.66</b>	1.85	1.17
	SD	<b>0.35</b>	0.27	0.22	0.38	0.22	0.25	0.16	0.30	<b>0.36</b>
	Max	<b>2.75</b>	2.73	1.61	2.83	<b>2.75</b>	2.65	2.10	3.26	2.50
	Min	<b>1.17</b>	1.74	0.67	0.76	1.76	1.63	<b>1.44</b>	1.51	0.75
	CC		0.65	0.24	0.69	0.22	0.54	<b>0.68</b>	0.44	0.39
Mace Head	Ar.Mean	<b>1.88</b>				<b>1.73</b>	1.71	1.47	1.60	
	SD	<b>0.08</b>				<b>0.09</b>	0.12	0.03	0.13	
	Max	<b>2.03</b>				1.98	1.93	1.51	<b>2.01</b>	
	Min	<b>1.66</b>				<b>1.57</b>	1.43	1.41	1.51	
	CC					-0.66	-0.70	<b>-0.50</b>	-0.66	

\* - the data of subsidiary character

One of the tasks of the study was to answer the question: to what extent can the models follow the concentration peaks measured at the monitoring stations? It was mentioned above that concentration peaks, which can be attributed to the influence of any emission sources, were measured only at Neuglobsow and Zingst stations. Nine rather short periods connected with elevated concentrations were singled out from the observed TGM concentrations and were compared with the corresponding calculation data. Such a comparison is shown in Table 7.3. The analysis of the table shows that practically in all cases the participating models follow the observational peaks, however, the calculated values are noticeably lower than the observed ones. As usual the models demonstrate only small elevations which coincide in time with the observational peaks. The only exception is the peak of July 03. Some models describe it rather satisfactory.

**Table 7.3.** Comparison of peak periods (TGM concentrations are averaged)

Station	Period	Observed and measured TGM concentrations, ng/m <sup>3</sup>								
		Obs	CMAQ	ADOM	MSCE	GRAHM	DEHM	HYSPLIT	EMAP	
Neuglobsow	23:00 28.06.95 - 07:00 29.06.95	<b>3.01</b>	1.74	1.29	1.42	<b>1.95</b>	1.50	1.58	1.44	
	02:00 01.07.95 - 06:00 01.07.95	<b>2.71</b>	1.79	1.36	1.39	<b>1.98</b>	1.54	1.63	1.49	
	01:00 03.07.95 - 17:00 03.07.95	<b>3.09</b>	1.99	1.25	1.73	2.38	1.89	2.56	<b>3.05</b>	
	04:00 05.11.99 - 11:00 06.11.99	<b>2.84</b>	<b>2.73</b>	1.21	2.61	2.40	2.08	2.44	1.29	
	03:00 07.11.99 - 13:00 07.11.99	<b>2.97</b>	<b>2.40</b>	1.18	1.88	2.19	1.77	1.87	1.33	
Zingst	01:00 28.06.95 - 08:00 28.06.95	<b>2.28</b>	1.77	1.27	1.44	<b>1.99</b>	1.49	1.52	1.14	
	23:00 30.06.95 - 02:00 01.07.95	<b>2.55</b>	1.68	1.34	1.41	<b>1.95</b>	1.49	1.51	0.99	
	12:00 05.11.99 - 11:00 06.11.99	<b>2.40</b>	2.62	1.12	<b>2.41</b>	2.42	2.02	2.28	1.12	
	19:00 07.11.99 - 05:00 08.11.99	<b>2.23</b>	<b>2.27</b>	1.24	2.01	1.97	1.75	1.71	2.31	

One should note an important regularity of the observed peaks: practically all of them take place during night-time or in the early morning. It is possible to hypothesize that most of these peaks are caused by natural reasons. Natural emission (and re-emission) during night-time, when atmospheric stability is highest, can lead to short-term elevated mercury concentrations in the lowest atmosphere. After sunrise atmospheric turbulence increases, and the concentration peaks disappear. Naturally, such peaks cannot be described by the models because they consider only anthropogenic emission. Nevertheless, the models simulate small nocturnal peaks, caused by a combination of anthropogenic emission and low atmospheric mixing. Such a hypothesis allows to believe that the modelling results could be much better if natural emission and re-emission would be taken into consideration.

Modelling RGM and TPM concentrations represents an especially difficult task. It is connected with a fact that our knowledge on physical-chemical properties and the atmospheric chemistry of RGM and TPM is very poor. Besides, as it was noted earlier, the uncertainty of the measurement data is also very high. Hence, it was not expected that the models would be able to closely match the observed concentrations.

Table 7.4 presents mean concentrations of RGM obtained by each model for each monitoring station. Besides, the table shows the ratio of the observed and calculated values. The ratio is obtained by dividing the greater value by the smaller one in each "observation-calculation" pair. First of all, one can mention that the mean calculated values vary within broad range for all stations. For Neuglobsow the models (but DEHM and EMAP) usually overestimate the RGM concentrations 2-4 times. For Swedish stations the range is even wider, and both overestimation and underestimation take place. The highest discrepancy is noted for Neuglobsow where the ratio reaches 2 orders of magnitude because relatively high RGM concentrations were measured during this "clean Atlantic" period. In this case the only exception is HYSPLIT model, which uses a prescribed constant in space and time background value of RGM concentration ( $5 \text{ pg/m}^3$ ). While the other models predict very low or zero RGM concentrations in clean Atlantic air masses, HYSPLIT gives the background value.

Table 7.4 confirms once more that our knowledge on RGM behaviour in the atmosphere is not sufficient. We know neither the chemical forms of RGM in emissions or in the atmosphere nor rates of their removal from the atmosphere. The Mace Head case suggests a possibility of RGM formed in the marine atmosphere. If we accept the idea of occurrence of RGM background then HYSPLIT model demonstrates the best result (averaged for all four stations) among the other models. On the other hand, EMAP model also demonstrates very good agreement for the three continental stations.

**Table 7.4.** Mean RGM concentrations ( $\text{pg/m}^3$ ) and ratio (R) of the observed and calculated values (the greater to the smaller)

Station Mod or Obs	Neuglobsow		Roervik		Aspvreten		Mace Head	
	$\text{pg/m}^3$	R	$\text{pg/m}^3$	R	$\text{pg/m}^3$	R	$\text{pg/m}^3$	R
Observations	<b>9.0</b>		<b>7.4</b>		<b>5.4</b>		<b>17.0</b>	
CMAQ	32.1	3.6	10.7	1.4	6.2	1.1	-	-
ADOM	23.6	2.6	1.9	3.9	1.4	3.9	-	-
MSCE-Hg	19.6	2.2	5.7	1.3	3.6	1.5	2.5	6.8
GRAHM	36.3	4.0	4.6	1.6	2.6	2.1	0.2	85.0
DEHM	3.5	2.6	0.9	8.2	0.4	13.5	0.9	18.9
HYSPLIT	12.9	1.4	7.8	1.1	7.1	1.3	13.9	<b>1.2</b>
EMAP	8.9	<b>1.0</b>	7.6	<b>1.0</b>	6.0	<b>1.1</b>	-	-

The general picture for the TPM comparison (Table 7.5) looks much more optimistic than for RGM. For practically all the samples the calculated mean concentrations differ from the observed ones by less than the factor of 2. Only GRAHM and CMAQ significantly overestimate the concentrations at the Swedish stations. The four models that simulated the TPM concentrations at Mace Head showed good agreement between the calculations and observations.

**Table 7.5.** Mean TPM concentrations ( $\text{pg}/\text{m}^3$ ) and ratio (R) of the observed and calculated values (the larger to the smaller)

Station Mod or Obs	Neuglobsow		Zingst		Roervik		Aspvreten		Mace Head	
	$\text{pg}/\text{m}^3$	R								
Observations	40.2		32.8		14.6		9.5		13.6	
CMAQ	73.2	1.8	61.0	1.9	45.4	3.1	45.6	4.8	-	
ADOM	31.2	1.3	18.8	1.7	15.3	1.0	11.6	1.2	-	
MSCE-Hg	31.6	1.3	34.3	1.0	14.1	1.0	10.6	1.1	13.1	1.0
GRAHM	61.5	1.5	42.5	1.3	40.3	2.8	52.0	5.5	14.1	<b>1.0</b>
DEHM	45.3	<b>1.1</b>	31.5	<b>1.0</b>	19.1	1.3	16.1	1.7	18.1	1.3
HYSPLIT	46.2	1.1	38.7	1.2	24.8	1.7	18.1	1.9	15.8	1.2
EMAP	32.2	1.2	26.0	1.3	14.5	<b>1.0</b>	10.4	<b>1.1</b>	-	

To evaluate the general ability of the different models to reproduce the observations of RGM and TPM, three statistical parameters mentioned above were used: Correlation Coefficient (CC), Factor Two Coverage ( $F_2$ ) and Mean Deviation Factor ( $F_{\text{mean}}$ ). The results of statistical treatment of the data obtained at all stations and calculated by all models are summarized in Table 7.6. The table allows us to compare the calculation results demonstrated by each model.

**Table 7.6.** Statistical data for RGM and TGM

Mercury species	Statistical parameter	CMAQ	ADOM	MSCE	GRAHM	DEHM	HYSPLIT	EMAP
RGM	CC	0.68	0.40	-0.01	0.26	0.12	0.10	0.70
	$F_2$ (%)	48	29	19	30	15	59	86
	$F_{\text{mean}}$	2.2	4.9	5.1	5.6	9.1	1.9	1.6
TPM	CC	0.77	0.81	0.70	0.51	0.78	0.83	0.81
	$F_2$ (%)	29	71	58	55	75	64	62
	$F_{\text{mean}}$	3.1	1.8	2.3	2.2	1.7	2.0	1.9

The analysis of the table demonstrates that only CMAQ and EMAP models can reproduce the observed RGM concentrations (at least on the level of the factor of 2.5 and with significant correlation). HYSPLIT gives rather good correspondence of the calculations and observations but correlation between the values is low. For the other models the mean factor exceeds 2 and can reach an order of magnitude. The correlation between calculations and observations for these models is also low.

It is obvious that for the TPM concentrations the models as a rule can reproduce the observed values. Practically in all cases more than half the calculation/observation ratios are within a factor of 2. Taking into account a considerable uncertainty of the measurements such agreement can be considered to be quite satisfactory. This good agreement for TPM concentrations points to the fact that the

participating models are able to simulate atmospheric transport and deposition of aerosol particles, which carry some mercury compounds within the solid matter. Although we know very little about the chemical nature of particulate mercury, the behaviour of mercury compounds themselves has no practical importance in this case because behaviour of a particle is not influenced by any trace constituents (e.g., mercury compounds) which may be present in the particle.

A separate consideration of the situation at Mace Head can help to reveal reasons for the difference between modelling of RGM and TPM. For example, the GRAHM model underpredicts the RGM observations at Mace Head station one-two orders of magnitude (see Figure 6.15). At the same time the model satisfactorily predicts TPM at this station (see Figure 6.16). This fact demonstrates that the model is capable of simulating air transport dynamics, and possible reasons for the disagreement revealed for RGM is in the treatment of RGM behaviour. Problems connected with model parameterisation for RGM are typical to a greater or smaller extent for all participating models. Obvious underestimation of RGM concentrations by both global models (GRAHM and DEHM) and regional model (MSCE-Hg) at Mace Head station suggests that processes that create mercury in this form may be significant in the oceanic atmosphere.

## Chapter 8

### NEW ASPECTS OF ATMOSPHERIC MERCURY DYNAMICS

The science of atmospheric cycling of mercury has developed tremendously over the last decade. A number of transformation processes of atmospheric mercury have been experimentally identified, including the ability of molecules (e.g. O<sub>3</sub>, Cl<sub>2</sub>) and radicals (e.g. OH, Cl, Br) to oxidise elemental mercury in the gaseous and aqueous phases. A general conclusion is that the gas-phase reactions are generally slow while those occurring in the aqueous phase may approach the diffusion-controlled limit. Despite this, the overall atmospheric oxidation rate is relatively slow due to the low solubility of Hg<sup>0</sup> in water. Moreover, a reversible redox balance is present in the aqueous phase involving reduction of divalent mercury by S(IV) complexes and possibly other reactants further lowering the net oxidation rate.

#### *New chemistry*

During recent years, some new information has been presented with relevance to atmospheric modelling. Some of the new information is preliminary and has thus not yet been implemented in current atmospheric modelling schemes. Below, a summary of some of the recent information on mercury chemistry is presented. In some cases, this information is included in some models and in other cases it represents new data which should be considered for inclusion in future versions of chemistry schemes in the models.

One important recent result is the revision of earlier proposed reaction mechanisms for reduction of aqueous Hg(II) by HO<sub>2</sub>, which suggested a rapid reaction converting dissolved Hg(II) to Hg<sup>0</sup> [Lin and Pehkonen, 1997]. It has recently been shown [Gårdfeldt and Jonsson, 2003] shown that this reaction will not proceed at all in aerated solutions (i.e. in the presence of oxygen) thus removing a major pathway for converting Hg(II) to Hg<sup>0</sup> in atmospheric water droplets. This new result will have a significant impact on modelling applications where the reaction involving HO<sub>2</sub> was included as a reduction pathway for aqueous phase Hg(II).

Recent findings of polar depletion of atmospheric mercury (first discovered by W.H. Schroeder and co-workers at Alert, Canada [Schroeder *et al.*, 1998]) have led to an increased interest in reactions between halogen species and elemental mercury. Although these reactions are mainly believed to be of importance under the specific conditions of Polar spring, they may also play some role in the atmospheric cycling of mercury in mid-latitude regions, and may be important in the marine atmosphere. The main candidates for oxidation reactions are bromine and chlorine atomic radicals as well as molecules (e.g. BrO, ClO).

The reactions of halogens and halogen compounds are treated differently in many models. The gas-phase oxidation of Hg<sup>0</sup> by halogen atoms (Cl, Br) and molecular halogens (Cl<sub>2</sub>, Br<sub>2</sub>) has recently been re-investigated in Canada by Ariya *et al.* [2002]. The upper-limit estimate for the room temperature (RT) Hg+Br<sub>2</sub> reaction was lowered in comparison to earlier studies. However, the potential importance of this reaction cannot be completely evaluated based on these results. The homogeneous Hg+Cl<sub>2</sub> reaction was found to be too slow to be important under atmospheric conditions ( $k = (2.6 \pm 0.2) \times 10^{-18} \text{ cm}^3 \text{ s}^{-1}$ ). The measured rates for the fast Hg+Cl and Hg+Br are very high and these reactions may be of relevance, at least under certain conditions (e.g. Br in polar spring).

OH radicals have been found to be capable of oxidising elemental mercury in both the gas [Sommar *et al.*, 2001], and aqueous phases [Gårdfeldt *et al.*, 2001]. In both cases, the reactions are sufficiently fast to influence the atmospheric cycling of mercury.

One important issue of atmospheric chemistry of mercury is the products of oxidation of gaseous  $\text{Hg}^0$ . In most experimental studies, the actual products have not been determined. For oxidation reactions involving halogens, the most likely product is  $\text{HgX}_2$  (g) species. This would imply a two-step reaction since most reactions occur via a first step where an intermediate  $\text{HgX}$  molecule is formed. This will however, most likely react further to  $\text{HgX}_2$ . For oxygen-containing oxidants such as OH or  $\text{O}_3$ , the reaction product is more uncertain.  $\text{HgO}$  would be a likely first step but the stability of this species in the gas phase is uncertain; indeed, it is likely that this compound would partition to particulate matter in the atmosphere. If formed as an intermediate,  $\text{Hg}(\text{OH})_2$  may be formed in the presence of water vapour. Again, this species has not been identified in the gas phase. Most modellers use the general assumption that oxidation of  $\text{Hg}^0$  yields  $\text{HgX}_2$  compounds such as  $\text{HgCl}_2$  for which physical and chemical properties are known. The current knowledge is not sufficient to recommend any other mechanisms.

### ***Sources and behaviour of atmospheric mercury species***

Notwithstanding the above considerations, compared to RGM and TPM, the emissions, distribution and transformations of elemental mercury ( $\text{Hg}^0$ ) appear to be relatively well characterised insofar as most models seem to be capable of simulating concentrations fairly accurately. To some extent, this can be explained by the relatively uniform global background concentration, which makes up the major part of  $\text{Hg}^0$  in the atmosphere. Emissions occurring within a modelling domain will, however, give rise to episodes with significantly increased concentrations. In most cases, these episodes can be reproduced by atmospheric models although there may be discrepancies in the predicted magnitude of any given concentration peak. It is not clear to what extent these discrepancies are due to inaccuracies in the emissions inventory or are due to inaccuracies in the fate and transport simulations in the models.

For TPM and RGM, uncertainties concerning emissions and atmospheric behaviour are much larger and the prospects for accurately modeling these species given the current state of knowledge are not as promising as for  $\text{Hg}^0$ . Perhaps surprisingly, relatively good agreements were obtained for TPM whereas RGM concentrations are often underpredicted by orders of magnitude. Part of the explanation for these difficulties may lie in the emissions inventories used as input to the models. Some discrepancies in emission inventory data has been noted in emission measurements at selected point sources [Munthe *et al.*, 2003]. In these studies, measured emissions of TPM are often insignificant or even under detection limits of the applied methods. This would suggest that current emission inventories overestimate TPM emissions. In contrast to this, the results of this model intercomparison exercise suggest that perhaps the emission inventories are somewhat correct, since the models were generally capable of reproducing measured ambient air concentrations with reasonable accuracy. One possible explanation is of course that the measured point source emissions of TPM are incorrect or non-representative. Another explanation is that RGM and TPM are not independent species once emitted to the atmosphere and that transformation of RGM to TPM occurs. Thus, point source emissions of RGM would lead to the formation of TPM in the plume. Although there is no direct experimental evidence for this, RGM is known to be easily adsorbed on most solid surfaces and is, by definition, also water-soluble. However, the solubility of particulate mercury, and that of RGM once it is absorbed to solid surfaces is uncertain. Further, the fate of dissolved  $\text{Hg}(\text{II})$  species once a droplet has evaporated is not certain. It should be noted that field measurement data

and trajectory analysis have shown that TPM is a very good tracer for air mass transport over source regions [Wängberg *et al.* 2001, 2003].

The atmospheric behaviour of RGM is the most uncertain of the mercury species. Emissions from point sources occur [e.g. Munthe *et al.*, 2003] as does formation via gas phase oxidation via OH radicals [Sommar *et al.*, 2001] and other reactants, as well as formation in the aqueous phase by ozone and other reactants. At the same time, RGM is reduced back to elemental mercury by dissolved S(IV) and potentially other compounds. The rates of all of these transformation reactions, as well as the concentrations of the many of the relevant reactants are somewhat uncertain. In Fig. 8.1, an example of time resolved RGM data is shown.

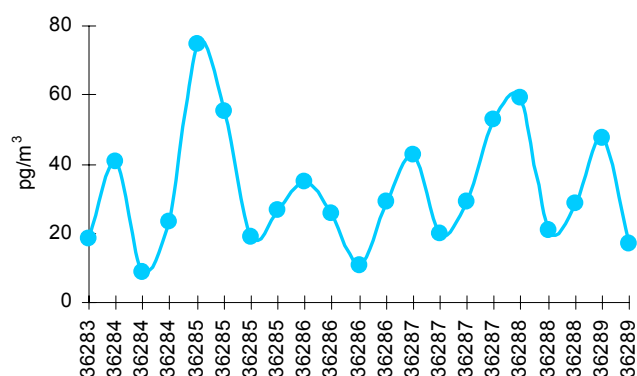


**Figure 8.1.** Atmospheric concentrations of RGM at Rörvik, SW Sweden ( $\text{pg Hg/m}^3$ ). 6 h average values obtained using annular KCl coated denuders

This data clearly shows the dynamical behaviour of RGM with dry deposition occurring during night (under conditions with a stable nocturnal boundary layer). In the morning with the break-up of the boundary layer RGM concentrations increase rapidly via mixing of air from the troposphere. The RGM can originate from both point source emissions and formation in gas and aqueous phase processes. In certain conditions (e.g. Marine Boundary Layer) formation of RGM from evaporation of aqueous aerosols has also been suggested [Hedgecock *et al.*, 2003].

## **SUMMARY, CONCLUSIONS AND RECOMMENDATIONS**

A broad cross-section of the regional, hemispheric and global models for mercury airborne transport, chemical transformations and deposition developed in Europe and North America took part in the second stage of the mercury model intercomparison study. The results allow for a general judgment of the performance of the participating models if applied to the simulation of short-term episodes with relatively high time resolution. The simulation of such episodes is a challenging task, in part because highly resolved (in time and space) information on meteorology and emissions were not available to the models.

Five regional scale models with a horizontal domain covering the European continent and its surrounding seas, hemispheric and global scale models participated in the intercomparison study. The models are designed for the assessment of mercury long-range atmospheric transport and deposition for time periods of a month or more, but three of them (CMAQ, ADOM and HYSPLIT) also have capabilities to simulate short-term episodes with basic time steps of one hour or less. Model predicted concentrations in ambient air were compared against mercury species observed at four monitoring stations in Central and Northern Europe and a station at the Irish west coast. The temporal resolution of measured total gaseous mercury concentrations (TGM), for comparative purposes, was averaged to 1 hour and 1 day. Reactive gaseous mercury (RGM) and total particulate mercury (TPM) were sampled during time periods of several hours.

A number of conclusions can be drawn from the essential part of the study, which was the simulation of the three most important species, i.e.. elemental and oxidized gaseous mercury and mercury associated with particles and their comparison against the observations mentioned above during two episodes of approximately two weeks each:

- In general, the results show that the models are able to reproduce adequately the measurement data. However, there are indications that further improvement of the modeling schemes and refinement of input data are needed. This intercomparison study allows us to evaluate chemistry transport models for atmospheric mercury, to reveal gaps in our knowledge, to identify how the models can be further improved.
- Results from all models show a relative good correlation between calculations and observations of TGM at the two German stations. The correlation coefficient value in this case can be as high as 0.69. For most of the models the mean TGM values lie within +/25% from the values observed in 1995 and 1999. However, all the models underestimated the mean values for 1995. At the Swedish stations and at the Irish west coast both observations and model predictions show a low variability and, naturally, a relative poor correlation, especially at the Irish station. At the same time the agreement between the mean values is much better ( $\pm 0.25 \text{ ng/m}^3$ ) than for German stations.
- The majority of participating models underestimate observed peak concentrations at the two Central European stations significantly most probably due to the fact that the model simulations included European anthropogenic mercury emissions for 1995 without possible re-emissions from contaminated soils in the vicinity of the main emission areas of Central Europe. Moreover, the inventory for 1995 may not contain all important mercury point sources in that area and the reduction of mercury emissions in Central Europe between 1990 and 1995 may be overestimated since test runs with two of the models indicate that the simulated peak concentrations show a better agreement with observations when the 1990 emission inventory is used.

- Model predicted TGM concentrations for the summer 1995 episode are generally lower than observed values, whereas models predictions are higher than observations during the two weeks of 1999. This is most probably due to the fact that mercury emissions in Europe have been further reduced from 1995 to 1999 but models have used the 1995 inventory for both episodes.
- Concentration values of gaseous elemental mercury at the inflow boundaries seem to be of importance for the participating regional scale models. There is evidence now from long-term measurements at the Irish station that average  $\text{Hg}^0$  concentrations are higher than the boundary concentrations used with the models. Besides, the long-term measurements also show a certain seasonal variability, which may have a significant effect on concentrations in the model domain at least at locations relatively far from major anthropogenic sources such as the two Swedish monitoring stations.
- Model simulations of reactive gaseous mercury (RGM) have shown that our knowledge about atmospheric physico-chemical processes of this species is still incomplete and hence sufficient parameterization schemes for RGM have not yet been incorporated into the models. For example, the models tended to significantly underestimate RGM concentrations observed at the Irish west coast indicating that an adequate parameterization of RGM emissions from the ocean and/or RGM formation in the marine atmosphere is missing. At all sites, in general, differences between model predictions and observations for RGM are large, exceeding an order of magnitude in some cases even for multi-hour averages. Some models show a tendency to overestimate concentrations (CMAQ, ADOM) and some tended to underestimate concentrations (MSCE-Hg, DEHM). The application of constant RGM background concentrations in space and time improves results from the HYSPLIT model to a certain extent, but as with uncertainties introduced into the Eulerian models by use of boundary concentrations, it is certain that this procedure is an oversimplification. In general, all of the regional models faced the difficulty of trying to account for the effect of re-emissions within the model domain and all emissions outside the model domain.
- Results of total particulate mercury (TPM) concentrations show that the observations at all monitoring sites are quite well reproduced by each of the models, i.e. within a factor of 2 in most of the cases with relatively high correlation coefficients up to 0.83 for the HYSPLIT model. Results from some models are in good agreement with observations even at the two Swedish sites, where the formation of secondary particles (e.g. by cloud evaporation processes) may be more important than direct emissions of particulate mercury. An explicit treatment of physical-chemical mercury processes in clouds is necessary to model TPM in an adequate way.

The results of the model comparison allow us to make the following recommendations:

- In general, all models have capabilities to describe the atmospheric pathways of transport and transformation of TGM and TPM from their emission sources through the atmosphere to deposition over spatial scales from some hundred kilometers to continental with time steps in the range of hours. These capabilities are recommended to be used (and are used now) for making predictions of mercury contamination and for estimating how a specific region is affected by mercury emissions in other areas.
- Models are recommended to be extended and to be further developed according to advancements in the knowledge of air-surface exchange of gaseous mercury species and of atmospheric processes of mercury. RGM appears to be the most sensitive species to limitations in our current understanding, since observed RGM is poorly reproduced by all models.

- Emission data bases are still a source of uncertainty both in the total amounts and spatial and temporal distribution of the most important mercury species. However, within the scope of this study, it is difficult to determine the importance of this factor in all cases. The fact that models were able to reproduce some peaks but not others may have been at least partially caused by unrealistic nature in the emission inventories. Uncertainty of the emission values can exceed 50% for individual grid cells. Decreasing trends in observations between 1995 to 1999 suggest that emissions were declined over this period in Europe. Hence, European inventories will have to be updated for 1999 and the following years on an annual basis to allow for consistent comparisons of model results and observations for that time period.
- There is an urgent need to assess the natural mercury emission and re-emission in Europe. For modeling purposes a spatial distribution pattern of the natural emission and re-emission should be obtained. It is also very important to get some idea about mercury speciation for the natural emission and re-emission.

## ***Acknowledgements***

The authors of the Report express their gratitude Dr. Trond Iversen for the data on soot concentrations in the atmosphere. Valuable contribution to the work was done by Meteorological Synthesizing Center "West" which provided the authors with information on ozone spatial distribution. We also would like to thank Dr. Ingvar Wängberg for preparation of the emission data and for fruitful discussion of the input data. Very useful suggestions and comments were done by Prof. David Lee on the stage of the result discussion and the text preparation. The authors are thankful to Mrs. Olga Rozovskaya for a huge technical work made for this report.

## REFERENCES

- Ariya, P. A., Khalizov, A. and Gidas, A. [2002] *Phys. Chem. Acta* . v.106, pp.7310-7320
- Axenfeld F., Munch J., and Pacyna J.M. [1991] Belastung von Nord- und Ostsee durch ökologisch gefährliche Stoffe am Beispiel atmosphärischer Quecksilberkomponenten. Teilprojekt: Europäische Test-Emissionsdatenbasis von Quecksilber-Komponenten für Modellrechnungen". Dornier, Report 104 02 726, 99 p.
- BC-EMEP [1994-1998] Bulgarian contribution to EMEP. Annual reports for 1994, 1995, 1996, 1997,1998, NIMH, EMEP/MSC-E, Sofia-Moscow.
- Berdowski J.J.M., Baas J., Bloos J.P.J., Visschedijk A.J.H., and Zandveld P.Y.J. [1997] The European Emission Inventory of Heavy Metals and Persistent Organic Pollutants for 1990. TNO Institute of Environmental Sciences, Energy Research and Process Innovation, UBA-FB report 104 02 672/03, Apeldoorn, 239 p.
- Bidleman T.F. [1988] Atmospheric Processes: Wet and Dry Deposition of Organic Compounds are Controlled by their Vapor-Particle Partitioning. . *Environ. Sci. Technol.*, v.22, pp.361-367.
- Binkowski F.S. [1999] Aerosols in Models-3 CMAQ, in Science algorithms of the EPA Models-3 Community Multiscale Air Quality (CMAQ) modeling system. D.W. Byun and J.K.S. Ching (Eds.) U.S. Environmental Protection Agency, U.S. Government Printing Office, Washington D.C., pp. 10-1 - 10-23, EPA-600/R-99/030.
- Binkowski F.S. and Shankar U. [1995] The regional particulate model: 1. Model description and preliminary results. *Geophysical Research*, v.100, pp.26191-26209.
- Bullock O.R. Jr. [2001] Development of the CMAQ Model for Atmospheric Mercury. Personal Communication: Poster presented at the NOAA Air Resources Laboratory Review, Research Triangle Park, NC, USA.
- Bullock O.R. Jr. and Brehme K.A. [2002] Atmospheric mercury simulation using the CMAQ model: formulation description and analysis of wet deposition results. *Atmos. Environ.*, v.36, pp.2135-2146.
- Byun D.W. and Ching J.K.S. [1999] Science algorithms of the EPA Models-3 Community Multiscale Air Quality (CMAQ) modeling system. U.S. Environmental Protection Agency, U.S. Government Printing Office, Washington D.C., EPA-600/R-99/030.
- Calhoun J.A. and Prestbo E. [2001] Kinetic study of the gas phase oxidation of elemental mercury by molecular chlorine. Report available from Frontier Geosciences, Inc., 414 Pontius Avenue N., Seattle, WA, USA, 98109.
- Chang J.S. [1990] Acidic Deposition: State of Science and Technology. Volume 1: Emissions, Atmospheric Processes, and Deposition. Irving, P.M. (Ed.), U.S. Govt. Printing Office: Washington D.C., Report 4.
- Christensen J.H. [1997] The Danish Eulerian Hemispheric Model – a three - dimensional air pollution model used for the Arctic. *Atmos. Environ.*, v.31, pp.4169 - 4191.
- Christensen J. [1999] An overview of modelling the Arctic mass budget of metals and sulphur: Emphasis on source apportionment of atmospheric burden and deposition. In "Modelling and Sources: A Workshop on Techniques and Associated Uncertainties in Quantifying the Origin and Long-Range Transport of Contaminants to the Arctic. Report and extended abstracts of the workshop Bergen, 14-16 June 1999".
- Christensen J. [2001] Modelling of Mercury with the Danish Eulerian Hemispheric Model. The international Workshop on Trends and Effects of Heavy Metals in the Arctic, McLean, Virginia, 18-22 June 2001.
- Cohen M., Commoner B., Bartlett P.W., Cooney P., Eisl H. [1997a] Exposure to Endocrine Disruptors from Long Range Air Transport of Pesticides. Center for the Biology of Natural Systems, Queens College, Flushing, NY, USA.
- Cohen M., Commoner B., Eisl H, Bartlett P., Dickar A., Hill C., Quigley J., and Rosenthal J. [1995] Quantitative Estimation of the Entry of Dioxins, Furans, and Hexachlorobenzene into the Great Lakes from Airborne and Waterborne Sources. Center for the Biology of Natural Systems, Queens College, Flushing, NY, USA.
- Cohen M., Commoner B., Eisl H, Bartlett P., Dickar A., Hill C., Quigley J., and Rosenthal J. [1997b] Development and Application of an Air Transport Model for Dioxins and Furans. *Organohalogen Compounds*, v.33, pp. 214-219.
- Cohen M., Draxler R.R., Artz R., Commoner B., Bartlett P., Cooney P., Couchot K., Dickar A., Eisl H., Hill C., Quigley J., Rosenthal J.E., Neimi D., Ratte D., Deslauriers M., Laurin R., Mathewson-Brake L., McDonald J.

- [2002] Modeling the Atmospheric Fate and Transport of PCDD/F to the Great Lakes. *Environmental Science and Technology*. v.36, pp.4831-4845.
- Commoner B., Richardson J., Cohen M., Flack S., Bartlett P.W., Cooney P., Couchot K., Eisl H., and Hill C. [1998] Dioxin Sources, Air Transport, and Contamination in Dairy Feed Crops and Milk. Center for the Biology of Natural Systems, Queens College, Flushing, NY, USA.
- Commoner B., Bartlett P., Eisl H., and Couchot K. [2000] Long Range Air Transport of Dioxin from North American Sources to Ecologically Vulnerable Receptors in Nunavit, Arctic Canada. Center for the Biology of Natural Systems, Queens College, Flushing, NY, USA (available at <http://www.cec.org> and <http://www.cbns.qc.edu>).
- Draxler R.R. [1999] HYSPLIT\_4 User's Guide. NOAA Technical Memorandum # ERL ARL-230. NOAA Air Resources Laboratory, Silver Spring, MD, USA.
- Draxler R.R. [2000] Meteorological Factors of Ozone Predictability at Houston, Texas. *Air Waste Manage. Assoc.*, v.50, pp.259-271.
- Draxler R.R. and Hess G.D. [1997] Description of the HYSPLIT\_4 Modeling System. NOAA Technical Memorandum # ERL ARL-224. NOAA Air Resources Laboratory, Silver Spring, MD, USA.
- Draxler R.R. and Hess G.D. [1998] An Overview of the HYSPLIT\_4 Modelling System for Trajectories, Dispersion and Deposition. *Australian Meteorological Magazine*, v.47, pp.295-308.
- Draxler R.R., Jean M., Hicks B., Randerson D. [1997] Emergency Preparedness – Regional Specialised Meteorological Centres at Washington and Montreal. *Radiation Protection Dosimetry*, v.73, pp.27-30.
- Draxler R.R., McQueen J.T., Stunder B.J.B. [1994] An evaluation of air pollutant exposures due to the 1991 Kuwait oil fires using a Lagrangian model. *Atmos. Environ.*, v.28, pp.2197-2210.
- Ebinghaus, R., Jennings, S.G., Schroeder, W.H., Berg, T., Donaghy, T., Guentzel, J., Kenny, C., Kock, H.H., Kvietskus, K., Landing, W., Munthe, J., Prestbo, E.M., Schneeberger, D., Slemr, F., Sommar, J., Urba, A., Wallschläger, D., Xiao, Z. [1999] International field intercomparison measurements of atmospheric mercury species at Mace Head, Ireland, *Atmos. Environ.*, v.33, pp.3063-3073.
- Ebinghaus R., Kock H.H., Coggins A.M., Spain T.G., Jennings S.G., Temme Ch. [2002] Long-term measurements of atmospheric mercury at Mace Head, Irish west coast between 1995 and 2001. *Atmos. Environ.*, v.36, pp.5267-5276.
- Ebinghaus R. and Schmolke S.R. [2000] Spatial and temporal variability of atmospheric mercury concentrations in northwestern and central Europe, Proceedings of the NIMD Forum 1999, National Institute for Minamata Disease, Minamata, Japan, pp.173-197.
- Ebinghaus R., Tripathi R.M., Wallschläger D., and Lindberg S.E. [1999] Natural and Anthropogenic Mercury Sources and Their Impact on the Air-Surface Exchange of Mercury on Regional and Global Scales. In: R. Ebinghaus, R.R. Turner, L.D. de Lacerda, O.Vasiliev, and W.Salomons (Eds.), *Mercury Contaminated Sites. Characterization, Risk Assessment and Remediation*. Springer, pp. 3-50.
- EPRI [2000] Assessment of Mercury Emissions. Transport, Fate and Cycling for the Continental United States: Model Structure and Evaluation. Palo Alto, CA, USA. EPRI Report Number 1000522.
- Finlayson-Pitts B.J. and Pitts J.N., Jr. [1999] *Chemistry of the Upper and Lower Atmosphere*. Academic Press, New York, 969 p.
- Gårdfeldt, K. and Johnsson, M. [2002] Submitted to *J. Phys. Chem. Part A*.
- Gårdfeldt, K., Sommar, J., Strömberg, D. and Feng, X. [2001] *Atmos. Environ.* v.35, pp.3039-3047.
- Grell G.A., Dudhia J. and Stauffer D.R. [1995] A Description of the Fifth-Generation Penn State/NCAR Mesoscale Model (MM5) Mesoscale and Microscale Meteorology Division. National Center for Atmospheric Research. Boulder, Colorado, NCAR/TN-398+STR. NCAR Technical Note. June 1995, pp. 122.
- Gusev A., Ilyin I., Peterson G., van Pul A., Syrakov D. [2000] Long-range transport model intercomparison studies. EMEP/MSC-E Technical Note 2/2000, Moscow.
- Gustin M.S., Lindberg S., Marsik F., Casimir A., Ebinghaus R., Edwards G., Hubble-Fitzgerald C., Kemp R., Kock H., Leonard T., London J., Majewski M., Montecinos C., Owens J., Pilote M., Somar J., Turner R., Vette A., Wallschläger D., Xiao Z., and Zhang H. [1999] Nevada STORMS project: Measurement of mercury emissions from naturally enriched surfaces. *JGR*, v.104, No D17, pp. 21831-21844.
- Hall B. [1995] The gas phase oxidation of elemental mercury by ozone. *Water, Air and Soil Pollution*, v.80, pp.301-315.

- Hedgecock I., N. Pirrone, Sprovieri, Pesenti E. [2003] Reactive Gaseous Mercury in the Marine Boundary Layer: Modeling and Experimental Evidence of its Formation in the Mediterranean *Atmospheric Environment*. In press.
- Hicks B.B., Baldocchi D.D., Meyers T.P., Hosker R.P., and Matt D.R. [1987] A Preliminary Multiple Resistance Routine for Deriving Dry Deposition Velocities from Measured Quantities. *Water, Air, Soil Pollut.* v.36, pp.311-330.
- Hidy G.M. [1986] Definition and Characterization of Suspended Particles in Ambient Air. In: *Aerosols: Research, Risk Assessment and Control Strategies*, Si Duk Lee, et al., (Eds.) Lewis Publishers: Chelsea, MI, USA, pp.19-41.
- Junge C.E. [1977] Basic Considerations About Trace Constituents in the Atmosphere as Related to the Fate of Global Pollutants. In: *Fate of Pollutants in the Air and Water Environments*. Suffet I.H. (Ed.), John Wiley & Sons: New York, pp.7-22.
- Kämäri J., Joki-Heiskala P., Christensen J., Degerman E., Derome J., Hoff R. and Kahkonen A.-M. [1998] Acidifying Pollutants, Arctic Haze, and Acidification in the Arctic, Chapter 9 in: *AMAP Assessment Report: Arctic Pollution Issues*. Arctic Monitoring and Assessment Programme (AMAP) Eds: S. Wilson, J. Murray and H. Huntington.
- Larson S.E., Edson J.B., Hummelshøj P, Jensen N.O., de Leeuw G., Mestayer P.G. [1995] Dry Deposition of Particles to Ocean Surfaces. *Ophelia*, v.42, pp.193-204.
- Lin C.-J. and Pehkonen S.O. [1997] Aqueous free radical chemistry of mercury in the presence of iron oxides and ambient aerosol. *Atmos. Environ.*, v.31, pp.4125-4137.
- Lin C.-J. and Pehkonen S.O. [1998] Oxidation of elemental mercury by aqueous chlorine (HOCl/OCl<sup>-</sup>): Implication for tropospheric mercury chemistry. *Journal of Geophysical Research*, v.103, pp.28093-28201.
- Lin C.-J. and Pehkonen S.O. [1999] The chemistry of atmospheric mercury: a review. *Atmos. Environ.*, v.33, pp.2067-2079.
- Lindqvist O. and Rodhe H. [1985] Atmospheric mercury - a review. *Tellus*, v.37B, pp.136-159.
- Loon Van L., Mader E., and Scott S.L. [2000] Reduction of the aqueous mercuric ion by sulfite: UV spectrum of HgSO<sub>3</sub> and its intramolecular redox reaction. *Journal of Physical Chemistry*, v.A 104, pp.1621-1626.
- Lu Y. and Khalil M.A.K. [1991] Tropospheric OH: Model Calculations of Spatial, Temporal, and Secular Variations. *Chemosphere*, v.23, pp.397-444.
- Lu, J.Y., Schroeder, W.H., Berg, T., Munthe, J., Schneeberger, D., Schaedlich, F. [1998] A device for sampling and determination of total particulate mercury in ambient air, *Anal. Chem.* v. 70, No. 11, pp.2403-2408.
- McQueen J.T., Draxler R.R. [1994] Evaluation of Model Back-Trajectories of the Kuwait Oil Fires Smoke Plume Using Digital Satellite Data. *Atmos. Environ.*, v.28, pp.2159-2174.
- Munthe J. [1992] Aqueous oxidation of elemental Hg by O<sub>3</sub>. *Atmos. Environ.*, v.26A, pp.1461-1468.
- Munthe, J., Wängberg, I., Iverfeldt, Å. Lindqvist, O., Strömberg, D., Sommar, D., Gärdfeldt, K., Petersen, G., Ebinghaus, R, Prestbo, Larjava, K. and Siemens, V. [2003] Distribution of atmospheric mercury species in Northern Europe: Final Results from the MOE Project. *Atmos. Environ.* In press.
- Munthe, J., I.Wängberg, N.Pirrone, A.Iverfeldt, R.Ferrara, P.Costa, R.Ebinghaus, X.Feng,K.Gardfelt, G.Keeler, E.Lanzillotta. S.E.Lindberg, J.Lu, Y.Mamane, E.Nucaro, E.Prestbo, S.R.Schmolke, W.H.Schroeder, J.Sommer, F.Sprovieri, R.K.Stevens, W.Stratton, G.Tuncel, A.Urba; [2001] Intercomparison of methods for sampling and analysis of atmospheric mercury species. *Atmos. Environ.*, v. 35/17, pp.3007-3017.
- Petersen G., Munthe J., Pleijel K., Bloxam R., and Kumar A.V. [1998] A comprehensive Eulerian modelling framework for airborne mercury species: development and testing of the tropospheric chemistry module (TCM) *Atmos. Environ.* v.32., pp.829-843.
- Pacyna E.G. and Pacyna J.M. [2002] Global emission of mercury from anthropogenic sources in 1995. *Water, Air and Soil Pollution*, v.137, No.1, pp.149-165.
- Pacyna E. G., Pacyna J. M., and Pirrone N. [2001] European emissions of atmospheric mercury from anthropogenic sources in 1995. *Atmos. Environ.*, v.35, pp.2987-2996.
- Pehkonen S. O. and Lin C.-J. [1998] Aqueous photochemistry of mercury with organic acids. *Journal of the Air & Waste Management Association*, v.48, pp.144-150.
- Petersen G., Bloxam R., Wong S., Munthe J., Krüger O., Schmolke S.R., Kumar A.V. [2001] A comprehensive Eulerian modelling framework for airborne mercury species: Model development and applications in Europe.

- Atmos. Environ.*, v.35, pp.3063-3074.
- Petersen G., Munthe J., Pleijel K., Bloxam R. and Kumar A. V. [1998] A comprehensive Eulerian modelling framework for airborne mercury species: Development and testing of the tropospheric chemistry module (TCM) *Atmos. Environ.*, v.32, pp.829-843.
- Pleijel K. and Munthe J. [1995] Modelling the atmospheric mercury cycle - chemistry in fog droplets. *Atmos. Environ.*, v.29, pp.1441-1457.
- Pleim J.E. and Xiu A. [1995] Development and testing of a surface flux and planetary boundary layer model for application in mesoscale models. *Journal of Applied Meteorology*, v.34, pp.16-32.
- Rolph G.D., Draxler R.R., and DePena R.G. [1992] Modeling Sulfur Concentrations and Depositions in the United States During ANATEX. *Atmos. Environ.*, v.26, pp.73-93.
- Rolph G.D., Draxler R.R., and DePena R.G. [1993] The Use of Model-Derived and Observed Precipitation in Long-Term Sulfur Concentration and Deposition Modeling. *Atmos. Environ.*, v.27, pp.2017-2037.
- Sanemasa I. [1975] The solubility of elemental mercury vapor in water. *Bulletin of the Chemical Society of Japan*, v.48, pp.1795-1798.
- Schmolke S., Schroeder W.H. Munthe J. Kock H.H., Schneeberger D. and Ebinghaus R. [1999] Simultaneous measurements of Total Gaseous Mercury at four sites on a 800 km transect: Spatial distribution and short time variability of Total Gaseous Mercury over Central Europe. *Atmos. Environ.*, v.33, pp.1725 - 1733.
- Schroeder, W. H., Anlauf, K. G., Barrie, L. A., Lu, J. Y., Steffen, A., Schneeberger, D. R., and Berg, T. [1998] 'Arctic springtime depletion of mercury', *Nature*, v.394, pp. 331-332.
- Schroeder, W.H., Keeler, G., Kock, H., Roussel, P., Schneeberger, D. and Schaedich, F. [1995b] International field intercomparison of atmospheric mercury measurement methods, *Water Air Soil Pollut.*, v.80, pp.611-620.
- Seigneur C., Abeck H., Chia G., Reinhard M., Bloom N.S., Prestbo E., and Saxena P. [1998] Mercury adsorption to elemental carbon (soot) particles and atmospheric particulate matter. *Atmos. Environ.*, v.32, pp.2649-2657.
- Slinn A.A. and Slinn W.G.N. [1980] Predictions for Particle Deposition on Natural Waters. *Atmos. Environ.*, v.14, pp.1013-1016.
- Smith R. M. and Martell A.E. [1976] *Critical Stability Constants*. Vol. 4: Inorganic Complexes. Plenum, New York, 257 p.
- Sommar J., Gårdfeldt K., Strömberg D., Feng X. [2001] A kinetic study of the gas-phase reaction between hydroxyl radical and atomic mercury. *Atmos. Environ.*, v.35, pp.3049-3054.
- Stein A.F., Lamb D., and Draxler R.R. [2000] Incorporation of detailed chemistry into a three-dimensional Lagrangian-Eulerian hybrid model: application to regional tropospheric ozone. *Atmos. Environ.*, v.34, pp.4361-4372.
- Syrakov D. [1995] On a PC-oriented Eulerian Multi-Level Model for Long-Term Calculations of the Regional Sulphur Deposition. In: Gryning S.E. and Schiermeier F.A. (Eds.), *Air Pollution Modelling and its Application XI* 21, Plenum Press, N.Y. and London, pp. 645-646.
- Syrakov D. [1996] On the TRAP advection scheme - Description, tests and applications. In: Geernaert G., A.Walloe-Hansen and Z.Zlatev (Eds.), *Regional Modelling of Air Pollution in Europe*. Proceedings of the first REMAPE Workshop, Copenhagen, Denmark, September 1996, National Environmental Research Institute, Denmark, pp. 141-152.
- Syrakov D. and Galperin M. [1997a] A model for airborne poly-dispersive particle transport and deposition, Proc. of 22nd NATO/CCMS International Technical Meeting on Air Pollution Modelling and its Application, 2-6 June 1997, Clermont-Ferrand, France, pp.111-118.
- Syrakov D. and Galperin M. [1997b] On a new Bott-type advection scheme and its further improvement. In: H. Hass and I.J. Ackermann (Eds.) Proc. of the first GLOREAM Workshop, Aachen, Germany, September 1997, Ford Forschungszentrum Aachen, pp. 103-109.
- Syrakov D. and Prodanova M. [1997] Bulgarian Long-range Transport Models - Simulation of ETEX First Release. In: K.Nodop (Ed.) Proc. of ETEX Symposium on Long-range Atmospheric Transport, Model. Verification and Emergency Response, 13-16 May 1997, Vienna (Austria), Office for Official Publications of the European Communities, Luxembourg, ISBN 92-828-0669-3, pp.141-144.

- Syrakov D. and Yordanov D. [1997] Parameterization of SL Diffusion Processes Accounting for Surface Source Action. In: Proc. of 22nd NATO/CCMS International Technical Meeting on Air Pollution Modelling and its Application, 2-6 June 1997, Clermont-Ferrand, France, pp.111-118.
- Tokos J.J.S., Hall B., Calhoun J.A., and Prestbo E.M. [1998] Homogeneous gas-phase reaction of  $\text{Hg}^0$  with  $\text{H}_2\text{O}_2$ ,  $\text{O}_3$ ,  $\text{CH}_3\text{I}$ , and  $(\text{CH}_3)_2\text{S}$ : Implications for atmospheric Hg cycling. *Atmos. Environ.*, v.32, pp.823-827.
- UNEP [2002] Chemicals: Global Mercury Assessment. Geneva, Switzerland, 258 p. [<http://www.chem.unep.ch>].
- Vestreng V., and Klein H. [2002] Emission data reported to UNECE/EMEP. MSC-W Status Report, Note 1/2002, Oslo, Norway, 101 p.
- Walcek C.J., Brost R.A., Chang J.S. and Wesely M.L. [1986]  $\text{SO}_2$ , Sulfate and  $\text{HNO}_3$  Deposition Velocities Computed using regional Landuse and Meteorological Data. *Atmos. Env.*, v.20, pp.949-964.
- Wängberg I, Munthe J., Ebinghaus R., Gärdfeldt K. and J.Sommar [2002] Distribution of TPM in Northern Europe. *Sci. Tot. Environ.* in press.
- Wängberg I, Munthe J., Pirrone N., Iverfeldt Å., Bahlman E., Costa P., Ebinghaus R., Feng X., Ferrara R., Gärdfeldt K., Kock H., Lanzillotta E., Mamane Y., Mas F., Melamed E., Nucaro E. Osnat Y., Prestbo E., Sommar J., Spain G., Sprovieri F., Tuncel G. [2001] Atmospheric Mercury Distribution In Northern Europe and In the Mediterranean Region. *Atmos. Environ.* v. 35/37, pp.3007-3017.
- Wesely M. [1989] Parameterization of Surface Resistances to Gaseous Dry Deposition in Regional-Scale Numerical Models. *Atmos. Environ.*, v.23, pp.1293-1304.
- Whitby K.T. [1975] Modeling of Atmospheric Aerosol Size Distributions, A Progress Report on EPA Research Grant No. R800971. Rep. 253, Particle Technology Laboratory, Univ. Of Minnesota, Minneapolis. (As cited in Prospero, J.M. *et al.*, The Atmospheric Aerosol System: An Overview. *Rev. Geophys. Space Phys.* 1983, v.21, pp.1607-1629]
- Williams R.M. [1982] A Model for the Dry Deposition of Particles to Natural Water Surfaces. *Atmos. Environ.*, v.16, pp.1933-1938.
- Xiao Z.F., Munthe J., Stromberg D., and Lindqvist O. [1994] Photochemical behavior of inorganic mercury compounds in aqueous solution. In Mercury as a Global Pollutant - Integration and Synthesis. C.J.Watras and J.W.Huckabee (Eds.), Lewis Publishers, pp. 581-592.
- Yordanov D., Syrakov D., and Djolov G. [1983] A barotropic planetary boundary layer. *Boundary Layer Meteorology*, v.25, pp.363-373.